Lunar Wave Analyses – Template and Appendices 2024-11-28

Dr. G. Innes   ginnes88@gmail.com

Since the first known recording of the lunar wave phenomenon in 2012, there have been over 30 posted videos on the Internet. The phenomenon consists of a pair of fleeting transparent wave-like disturbances seen crossing the face of the Moon or a bright planet such as Jupiter or Saturn.

The purpose of this study is to extract data from all of the currently available videos and recreate the 3-dimensional situation of each observation. With the aid of additional data from on-line astronomical sources and the framework of two theoretical models, it is possible to estimate factors such as the wave travel direction, altitude, speed and probable cause.

Due to the time required to analyze dozens of videos in detail, the results based on this template will be added incrementally as they become available. Future updates will also occur as new findings come to light. For example, the term "vortex" is sometimes used instead of "wave" to specify the structure of rapidly spinning air that causes particular optical distortions.

The title of each section consists of the date of observation followed by the name or pseudonym of the observer, which in all known cases was an amateur astronomer. A list is presented alphabetically by observer in the Table below.

To research the lunar wave phenomenon, it has been necessary to develop a working knowledge in many diverse areas and link the various aspects to form a coherent picture of what is happening when the waves are detected. These areas include astronomy, digital videography (including Schlieren photography), image enhancement, graphical editing, geometry, trigonometry, calculus, cartography (map-making), optics, fluid mechanics and vortices, aircraft design and operation, air traffic control, meteorology (weather phenomena), plasma physics and lightning.

To handle these complexities, a toolbox has been developed to enable a deeper understanding and detailed interpretation of the recorded events. The protocols and theoretical derivations for each part of the analysis are presented in Appendices A to H at the end of this document:

> APPENDIX A – Analyzing a Lunar Wave Video
> APPENDIX B – Image Differencing and Image Matching
> APPENDIX C – Moon Tilt and Orbital Position
> APPENDIX D – Stretched Angle-of-View
> APPENDIX E – Refractive Index Models for Image Shift
> APPENDIX F – Detailed Lighting Analysis
> APPENDIX G – Aircraft Wake Analysis
> APPENDIX H – Celestial Barkhausen Analysis

A) This Appendix is the master protocol which outlines the scope of the analysis, drawing upon the specialized material in the other Appendices.

B) A method to enhance the wave motion in a still photograph is outlined using the difference between two consecutive video frames. The resulting frame is then matched to a reference image of the Moon from an astronomical data source, as part of recreating the celestial scene.

C) The Moon is constantly changing orientation relative to an Earth-based observer as it moves across the sky. Formulas are derived to provide the correct tilt, azimuth (compass heading) and altitude at the known time of observation, thus allowing the observer's sky view to be recreated accurately.

D) The telescope or camera will generally be pointing at an angle above the horizon when the waves are spotted. The circular telescope field of view appears stretched into an ellipse where it passes through the horizontal wave layer. The stretch changes the angle of the wavefront from that seen through the telescope. A formula to account for this is derived.

E) All known lunar wave sightings have been by optical means. Details of where the light rays travel during a sighting are explained.

F) The Moon or a bright planet background may not be the only light source during a sighting. Other possible sources are considered, leading to two theoretical models for the most likely cases.

G) In the first model, Appendix G, it is noted that most people (including amateur astronomers) reside within sight of aircraft service routes. At nighttime, the powerful landing lights may herald the nearby passing of an aircraft. The wingtip vortices and hot gas plumes of aircraft wakes are predicted to cause waves parallel to the airways and which drift with the prevailing wind.

H) In the second model, Appendix H, the waves are triggered magnetically by celestial alignments. The resulting upper atmosphere plasma discharge may possibly be detected as a brief flash of light. It would also create a ring vortex at a lower altitude due to sudden upward displacement of a column of superheated gas. Under limited circumstances, the ring vortex may appear as a double wave.

The two proposed models must be tested for applicability in a given case. The atmosphere is affected by hot exhausts from turbofan engines, the cooled (lower pressure) air in the center of a wingtip vortex and by energies in the magnetosphere and beyond. It is possible both models are correct, with the first explaining the predominant lunar wave mechanism in the high-traffic airways near major metropolitan centers and the second being more relevant elsewhere.

Disclaimer

The notes accompanying each reference analyzed below are those of Dr. Graeme Innes. They represent his summary of the data found in each video recording as of the date of this publication, which may differ from the observations and opinions of other analysts looking at the same videos.

Technical Note

A number of the lunar wave videos are available in 1080p resolution from the Crrow777 archive: https://archive.org/download/Crrow777_archive/. This author has found downloading from the archive is preferred using a Google Chrome browser. Viewing videos in Quicktime is also preferred, which allows frame-by-frame playback by tapping the arrow keys on a standard keyboard. To enable Quicktime to open the file, each video was re-processed using VLC. Choose "convert/stream" and then "keep original track" for both video and audio format choices before saving as a new file.

Observer	Date of Observation	Time of Observation (* = estimated)	Location of Observation (* = estimated)	Body(s) involved
Clark	2017-07-09	*	Lexington*, Kentucky, USA	Moon (+aircraft out of frame)
	Title: Lunar Wave 7-9-17, Filmed at 200fps URL: https://www.youtube.com/watch?v=N68RdBt7Qc4 Video time code: 0:00 to 0:08, Posted: 9 July 2017			
CRROW	2012-09-26	20:22 PDT (03:22 UT)	San Diego, California, USA	Moon
	Title: The first Lunar Wave from Sept 2012 URL: https://youtu.be/_3axPn65MGM?si=cd1HxgAep9woWlxk Video time code: 0:22 to 0.38, Posted: 13 November 2013			
CRROW	2014-03-09	23:47 PST (07:47 UT)	San Diego, California, USA	Moon
	Title: 9 Lunar Waves Filmed – Game Change URL: https://www.youtube.com/watch?v=0mi0w8bLtUM Video time code: 9:24 to 9:38, Posted: 9 October 2017			
CRROW	2014-03-14a	21:33 PST (05:33 UT)	San Diego, California, USA	Moon
	Title: 9 Lunar Waves Filmed – Game Change URL: https://www.youtube.com/watch?v=0mi0w8bLtUM Video time code: 10:23 to 10:29, Posted: 9 October 2017			
CRROW	2014-03-14b	21:39 PST (05:39 UT)	San Diego, California, USA	Moon
	Title: 9 Lunar Waves Filmed – Game Change URL: https://www.youtube.com/watch?v=0mi0w8bLtUM Video time code: 11:12 to 11:18, Posted: 9 October 2017			
CRROW	2014-04-14	22:46 PDT (05:46 UT)	San Diego, California, USA	Lunar eclipse
	Title: Lunar Wave Filmed During Eclipse -Historic! URL: https://youtu.be/4CCJxF7nIcM?si=hcZy2z-JrrhPJPPP Video time code: 1:12 to 1:20, brightened 1:39 to 1:50, Posted: 20 April 2014			
DeFranco	2024-10-03	*	*USA	Moon
	Title: Moon Wave REAL Footage!!! URL: https://rumble.com/v5h9a8b-moon-wave-real-footage.html?start=71 Video time code: 01:18 to 01:27, Posted: 3 October 2024			
De Jong	2020-03-09	21:19 CET (20:19 UT)	*Germany	Moon
	Title: Lunar Wave Mystery solved! #4k (**also:** Lunar wavE in Frame subtract view (no audio)) URL: https://www.youtube.com/watch?v=7qBxYlvvjxQ (**also:** https://www.youtube.com/watch?v=1pwyQu4HNSk) Video time code: 00:11 to 00:18, Posted: 10 March 2020 (**also:** 00:14 to 00:21, Posted: 27 May 2021)			
Dinos	2023-04-27	20:45 CET (19:45 UT)	Larissa, Greece	Moon
	Title: Lunar Wave (27 April 2023) URL: https://www.youtube.com/watch?v=DUJzNe3yOpo Video time code:0:02 to 0:06, Posted: 27 April 2023			
DLU	2019-01-17	*	*United Kingdom	Moon
	Title: Lunar Wave 2019 – I'm NOT Imagining It! URL: https://www.youtube.com/watch?v=lu4Mg2wXmz0&t=2s Video time code: 0:30 to 0.47, Posted: 13 June 2019			
DOTT	2013-07-19	*	Los Angeles*, California, USA	Moon
	Title: Moon close-up with 10" Meade LX200 URL: https://www.youtube.com/watch?v=QunIJHbNuhM Video time code: 1:24 to 1:31, Posted: 19 July 2013			

Gregory	2023-07-25	*	Fresno*, California, USA	Moon
	Title: 7/25/2023 Lunar Wave on the Moon URL: https://www.youtube.com/watch?v=lpGBgkDmsAY Video time code: 00:33 to 1:27, Posted: 29 July 2023			
Gustav	2014-07-07	22:00 CET (21:00 UT)	*Germany	Moon
	Title: 9 Lunar Waves Filmed – Game Change URL: https://www.youtube.com/watch?v=0mi0w8bLtUM Video time code: 5:59 to 6:23, Posted: 9 October 2017			
Hannon	2013-06-15	20:30 EDT (00:30 UT)*	Terryville, Connecticut, USA	Moon
	Title: 010 Moonscapes We use a 10 inch telescope for the first time URL: https://www.youtube.com/watch?v=T_2sOBISBHc Video time code: 3:11 to 3:16, Posted: 16 June 2013			
Jayling	2018-12-19	17:23 EST (22:23 UT)	Warren*, Ohio, USA	Moon (+ possible aircraft)
	Title: Waves Ripple Across the Moon, A Little Bit of a Lunar Wave, 5:18pm to 5:35pm December 19, 2018 NE Ohio (eastern sky) URL: https://youtu.be/XIKAJK1sNSg?si=SxXENF_SmgJ9kEJH Video time code: 5:18 to 5:21, Posted: 19 Dec 2018			
McKeon	2017-04-08	03:05 GMT (02:05 UT)	Dublin, Ireland	Jupiter + 2 moons
	Title: Atmospheric wave passing Jupiter twice. URL: https://youtu.be/axaHyog_1Ow?si=K5373Wf3-75n0ChD Video time code: 0:02 to 0:21, Posted: 22 April 2019			
Ojos	2016-06-17	*	Paterson*, New Jersey, USA	Moon
	Title: 49 - MUST WATCH LUNAR WAVE of the Ð M?♣ ▌♥NÐ June-17-2016 URL: https://youtu.be/qr6J3C9bvW4?si=KU7Npm5UyFK0OCWP Video time code: 0:01 to 0:06, Posted: 17 June 2016			
Parker	2016-05-13	22:22 EDT (02:22 UT)	*North Carolina, USA	Moon
	Title: Lunar Wave May 13 2016, 22_22p.m. EST URL: https://www.youtube.com/watch?v=kcQSP9YLXi4 Video time code: 0:08 to 0:34, Posted: 14 May 2016			
P&K	2019-01-22	21:40 EST (02:40 UT)	Miami, Florida, USA	Moon
	Title: Scanning The Moon Surface LIVE! URL: https://youtu.be/ypfhfLAIdAc?t=3319 Video time code: 54:18 to 54:30, Posted: 22 January 2019			
R205M	2014-11-09	23:36:38 EST (04:36 UT)	Newark*, New Jersey, USA	Moon
	Title: LUNAR WAVE CAUGHT AS PREDICTED URL: https://youtu.be/4zwmXDyF6zE?si=5vTgUV733O3jEhE- Video time code: 0:40 to 0:42, Posted: 23 Sept 2015			
R205M	2015-05-02	21:33:44 (01:33 UT)	Newark*, New Jersey, USA	Moon
	Title: LUNAR WAVE CAUGHT AS PREDICTED URL: https://youtu.be/4zwmXDyF6zE?si=5vTgUV733O3jEhE- Video time code: 2:02 to 2:09, Posted: 23 Sept 2015			
R205M	2015-07-	*	Newark*, New Jersey, USA	Moon
	Title: LUNAR WAVE CAUGHT AS PREDICTED URL: https://youtu.be/4zwmXDyF6zE?si=5vTgUV733O3jEhE- Video time code: 4:50 to 4:53, Posted: 23 Sept 2015			
R205M	2015-08-01	22:31:22 (02:31 UT)	Newark*, New Jersey, USA	Moon
	Title: LUNAR WAVE CAUGHT AS PREDICTED URL: https://youtu.be/4zwmXDyF6zE?si=5vTgUV733O3jEhE- Video time code: 5:17 to 5:23, Posted: 23 Sept 2015			
R205M	2015-09-20	19:35:27 (23:35 UT)	Newark*, New Jersey, USA	Moon
	Title: LUNAR WAVE CAUGHT AS PREDICTED URL: https://youtu.be/4zwmXDyF6zE?si=5vTgUV733O3jEhE- Video time code: 8:04 to 8:13, Posted: 23 Sept 2015			
R205M	2016-04-20	*	Newark*, New Jersey, USA	Moon
	Title: lunar wave # 6 (energy shock)4-20-2016 and ufos off the moon URL: https://www.youtube.com/watch?v=Ky-q2ybKvc8 Video time code: 3:19 to 3:27, Posted: 24 April 2016			

R205M	2016-10-12	19:37:36 EDT (23:37 UT)	Newark*, New Jersey, USA	Moon
	Title: the moon energy wave # 7 last one I've filmed, but never posted before URL: https://www.youtube.com/watch?v=VBoPomemeuA Video time code: 0:04 to 0:16, Posted: 8 June 2018			
Randy	2015-03-27	21:20 CST (03:20 UT)	Houston, Texas, USA	Moon
	Title: 12th Lunar Wave Timing Predicted & Filmed March 27 in Houston URL: https://youtu.be/BVF8xZ5naKM Video time code: 2:53 to 3:41, Posted: 28 March 2015			
Rakete	2018-08-19	*	*Germany	Moon
	Title: Lunar Wave 2018 URL: https://www.youtube.com/watch?v=6GRK6aTJt2o Video time code: 0:30 to about 1:10, Posted: 20 August 2018			
TBS	2016-02-13	19:05 EST (00:05 UT)	Tampa, Florida, USA	Moon
	Title: LUNAR PULSE caught LIVE! - Possible Lunar Anomaly Evidence in HD URL: https://www.youtube.com/watch?v=Ep2W56zuT3U Video time code: 0:11 to 0:14, Posted: 16 Feb 2016			
TBS	2016-02-17	21:40 EST (02:40 UT)	Tampa, Florida, USA	Moon
	Title: 2ND LUNAR PULSE or WAVE - Captured Live on Moon TV - Feb 17th – 7_40pm URL: https://www.youtube.com/watch?v=qejYOsrWoXw Video time code: 0:22 to 0:24, Posted: 18 Feb 2016			
TBS	2018-05-23	20:47 EDT (12:47 UT)	Tampa, Florida, USA	Jupiter-Io
	Title: Capture of the Double Space Pulsewave passing Jupiter LIVE! URL: https://www.youtube.com/live/EaRTY69Hkb8 Video time code: 20:22 to 20:24, Posted: 23 May 2018			
TBS	2019-09-02	00:00:51 (04:00 UT)	Tampa, Florida, USA	Saturn-ring
	Title: SATURN 'WAVE' - Possible Plasma Double Layer Refraction URL: https://www.youtube.com/watch?v=OxiJS4pYVG4 Video time code: 0:08 to 0:09, Posted: 2 Sept 2019			
TBS	2020-06-16	00:50:02 EDT (04:50 UT)	Tampa, Florida, USA	Jupiter-redspot
	Title: LIVE 4K - Jupiter and Saturn - JUPITER WAVE number 2! URL: https://www.youtube.com/live/IzXroCOcmzg Video time code: 38:36 to 38:42, Posted: 16 June 2020			
TBS	2022-10-09	20:23:49 EDT (00:23 UT)	Tampa, Florida, USA	Moon
	Title: Lunar Wave 2022 - Captured LIVE 10.09.22 (Please READ the Description) URL: https://www.youtube.com/watch?v=Prl5yYHKHic Video time code:0:08 to 0:15 (0:24 to 0:49 zoomed in), Posted: October 2022			
TLO	2016-08-23	00:42 EDT (04:42 UT)	Cincinnati*, Ohio, USA	Moon
	Title: Defending My Lunar Wave!!!!!!! URL: https://www.youtube.com/watch?v=jfq5_HiXrDc Video time code:1:24 to 2:09, Posted: 1 October 2016			
WegE	2015-01-02	17:40 CET (16:40 UT)	Berlin, Germany	Moon
	Title: 10 Lunar Waves Filmed To Date & What We Know URL: https://www.youtube.com/watch?v=xUGxysKSGEM Video time code: 0:46 to 1:25, Posted: 9 October 2017			

Observer Details (* = estimated location)

Clark	Brennan Clark, Lexington*, KY	McKeon	John McKeon, Dublin, Ireland
CRROW	CRROW777, San Diego, CA	Ojos	Abriendo Ojos 360, Paterson*, NJ
DeFranco	Jay DeFranco, *USA	Parker	Chris Parker, Raleigh*, NC
De Jong	Jan de Jong, *Germany	P&K	Paul&Keith, Miami, FL + PA
Dinos	Sky-Watcher Dinos, Larissa, Greece	R205M	Richard205Maria, Newark*, NJ
DLU	Deceptive Little Universe, *UK	Randy	Randy, Houston, TX
DOTT	Defender Of The Town, Los Angeles*, CA	Rakete	Rudi Rakete, *Germany
Gregory	Daren Gregory, Fresno*, CA	TBS	Take Back Space, Tampa, FL
Gustav	Gustav, Berlin*, Germany	TLO	They Lie Ohio, Cincinnati*, OH
Hannon	James Hannon, Terryville, CT	WegE	Weg der Erkenntnis, Berlin, Germany
Jayling	Jayling - Ohio Skies, Warren*, OH			

2013-06-15 Hannon

Observer: James Hannon
Video Title: "010 Moonscapes We use a 10 inch telescope for the first time"
URL: https://www.youtube.com/watch?v=T_2sOBISBHc
Video time code: **3:11 to 3:16**, Posted: 16 June 2013

Location: Terryville, Connecticut, USA, 41.6782° N, 73.0109° W, Elevation 1383 m (4540 ft)
Date of observation: 15 June 2013
Time of observation: about 8:30 pm EDT (00:30 UT, 16 June 2013)
Equipment: 10 inch F4 Celestron Meade telescope, 3x Barlow lens, C9 Tech Logitech camera

General Observations

- there is no record of the exact time of observation, only the date
- the video starts around sunset, as blue skylight is visible in the lunar shadows
- the waves appear at about the same time as the sun sinks below the horizon (2nd contact), at about 8:30 pm (see the spreadsheet summary at the end of this section)
- darker skies occur after the waves pass (no blue visible 30 minutes afterwards)
- the colour in the video frame contrasts with the grey-scale Goddard reference image, which does not include local atmospheric filtering of the light
- the live audio commentary by Mr. Hannon indicates he did not notice the waves at the time
- since there was no second camera, no triangulation data is available to determine the true altitude or actual wave speed and separation
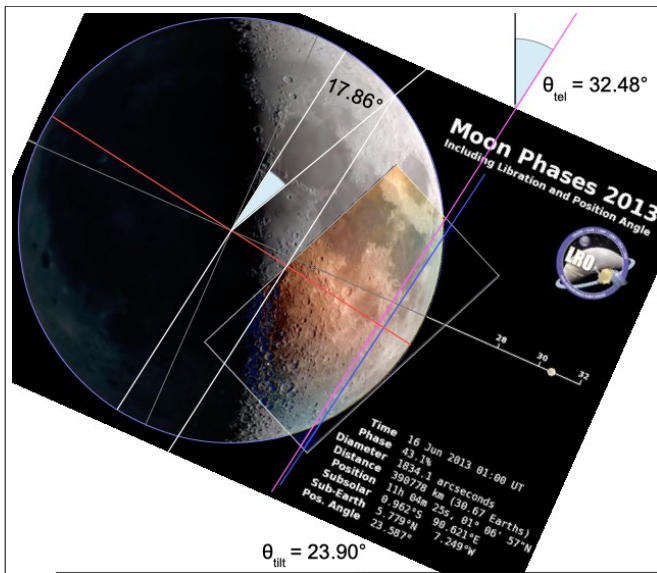
Fig. 1 Final orientation of the video frame and waves #1 (magenta) and #2 (blue), matched to the Goddard reference image and tilted +23.9 degrees to indicate the horizon of the observer.	Fig. 2 Stretched field-of-view where the telescope view passes through the wave layer. The small ring vortex size indicates the Barkhausen model does not accurately explain this sighting.
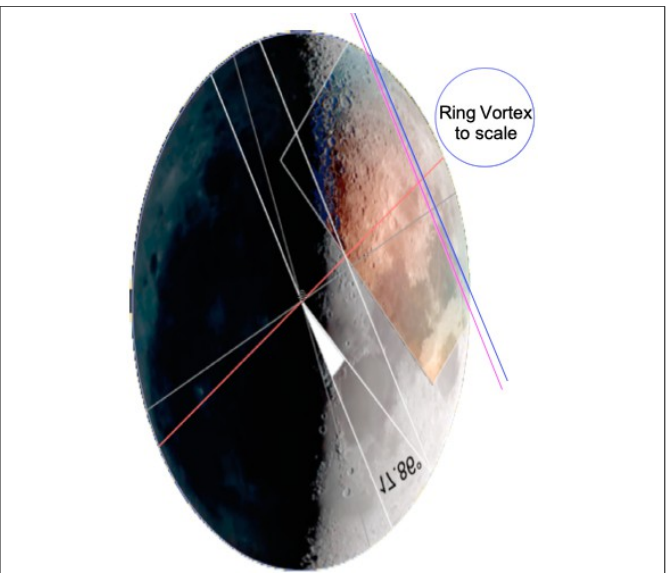
Basic Wave Analysis

- referring to Fig. 1, the video frame covers 34.7% of the lunar diameter
- the waves are spaced 1.67 seconds apart (40±1 frames at 24 frames per second)(±2.5%)

- wave #1 transits 34.7% of lunar diameter in 2.00 seconds (48±1 frames at 24 fps)(±2.1%)
- transits 100% of lunar diameter in 5.77 seconds
- wave #2 transits 34.7% of lunar diameter in 2.00 seconds (48±1 frames at 24 fps)(±2.1%)
- transits 100% of lunar diameter in 5.77 seconds
- the second wave appears to move at the same speed as the first

- average transit of 100% of lunar diameter in 5.77 seconds
- total elapsed time 7.44 seconds from 1st wave initiation to 2nd wave termination

Aircraft Wake Model

- from Fig. 5, the jetstream speed at the 300mb level (about 30,000 ft) was about 26 m/s (58 mph) from a compass direction of about 315 degrees
- this is consistent with calculations for a wave separation d_{wsep} = 40 m (130 ft), appearing to drift at 22 m/s (49 mph) out of the compass direction 293 degrees at 29,100 ft
- wind speed data for d_{wsep} = 20 m (65 ft) at an altitude of 14,600 ft at the time of observation was not available, but may also be consistent with calculated wave movement at this altitude

- the intersection of the two wavefronts points in the direction of New York city, Fig. 3, indicating the direction of aircraft travel
- the location and compass direction of several nearby air traffic routes, Fig. 4, is consistent with the wavefront (aircraft wake) orientation
- the wake calculations indicate that a generating aircraft passed by the Moon about 29 seconds before the first wave was observed, i.e., well outside the telescope field-of-view
- the observations are consistent with the wingtip (or flap) vortices generated by an aircraft approaching a New York city area airport with compass heading 193 degrees

Celestial Barkhausen Model

- the sunset serves as the most probable magnetic alignment for producing a Barkhausen pulse
- none of the major moons of Jupiter or Saturn were conjunct or transiting the parent planet at the time of observation, Figs 6 and 7
- the wave travel direction of 113° is nearly opposite both the sunset (303° WNW) and Jupiter (296° WNW), possibly pointing towards the source of the pulse, Fig. 3
- for a ring vortex at 10,000 m (33,000 ft) altitude viewed at an angle $\varphi = 39°$, the angle-of-separation $\alpha_{wsep} = 0.14718$ degrees gives a ring diameter of 45 m (148 ft)
- the ring drift speed is calculated as 24 m/s (55 mph), consistent with the jetstream data
- the curvature of the ring does not match the straightness of the waves, meaning the ring vortex model is not a good explanation for this sighting, Fig. 2
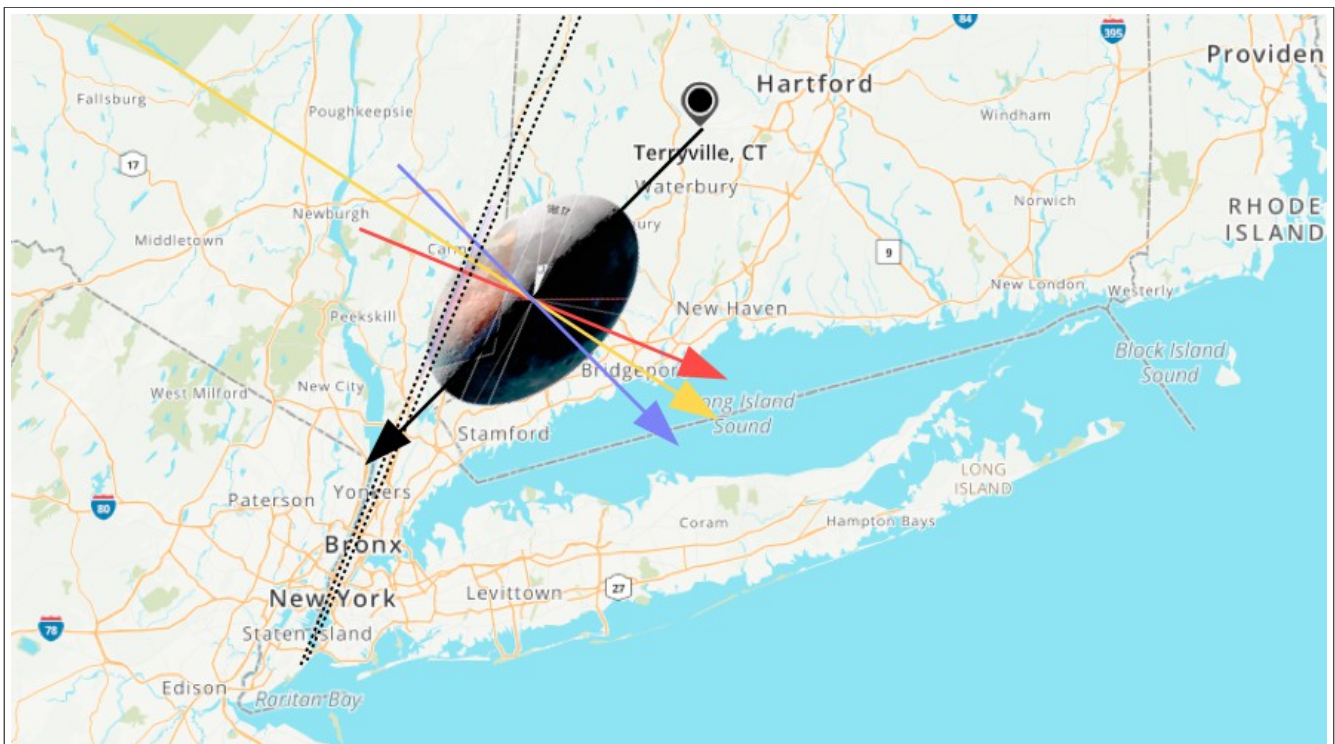
Fig. 3 Map orientation showing the wavefronts (dotted black lines), Moon heading (black arrow and ellipse), wave travel direction (red arrow), sunlight direction (yellow) and jetstream direction (blue). (Map: https://www.mapquest.com/us/connecticut/terryville-ct-282023621).
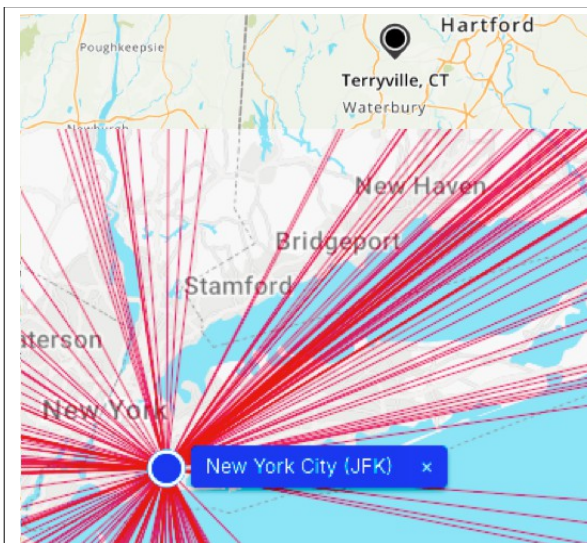

Fig. 4 JFK airport traffic routes in the Terryville CT area. The map distance between Terryville and New York city is about 100 km (62 miles)
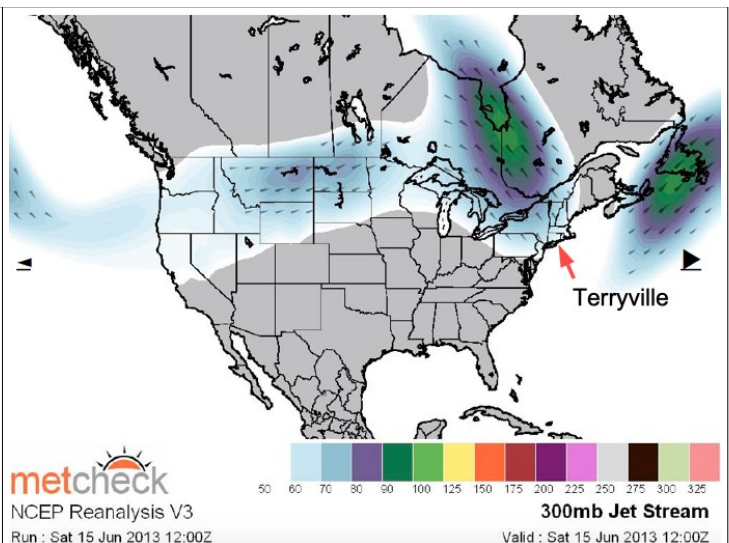(Data: https://www.flightconnections.com/flights-from-new-york-city-jfk).

Fig. 5 Jetstream data for North America around the time of the Terryville sighting (indicated by the red arrow). The 300 mb (millibar) pressure is between 27,000 and 32,000 ft altitude (8,200 to 9,600 m) (Data: https://www.metcheck.com/WEATHER/jetstream_archive.asp and https://www.noaa.gov/jetstream/upper-air-charts/constant-pressure-charts-300-mb).
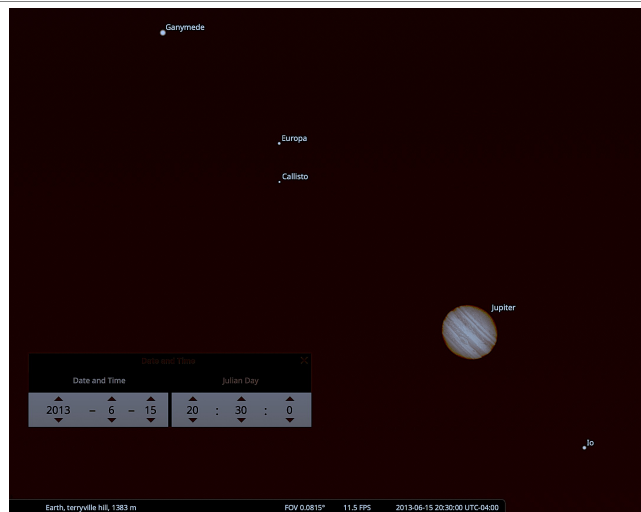
Fig. 6 Re-created view of Jupiter as seen from Terryville CT. None of the major moons were conjunct or transiting Jupiter. (Source: Stellarium.org)	Fig. 7 Re-created view of Saturn as seen from Terryville CT. None of the major moons were conjunct or transiting Saturn. (Source: Stellarium.org)
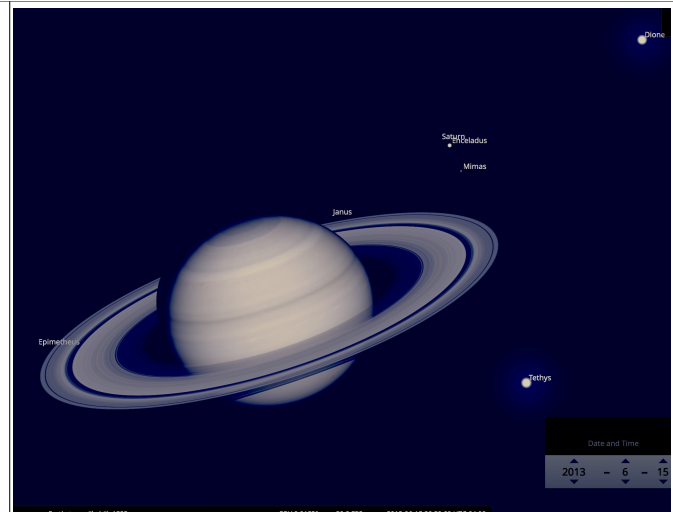
Concluding Remarks

- the most probable cause for the waves in this case is the passing of an aircraft in one of the world's busiest airways, even though no aircraft was detected in the narrow field-of-view of the telescope and no commentary about aircraft or the waves was made by the observer
- New York airspace is at the western side of the North Atlantic Organised Track System (NAT-OTS), which handles about 10,000 transatlantic flights per week at peak times (2024 data, https://aviationweek.com/air-transport/airports-networks/analysis-record-transatlantic-summer-awaits)
- the straightness of the waves strongly indicates an aircraft generated origin, not a high-altitude ring vortex.

Observer:	**James Hannon, 2013-06-15**	

VIDEO

Video Title:	010 Moonscapes We use a 10 inch telescope for the first time
URL:	https://www.youtube.com/watch?v=T_2sOBISBHc
Video time code mm:ss:*fr* (start, end):	03:12:*06* 03:16:*00*
Posted:	16 June 2013

PLACE + TIME

Location + elevation (m, ft):	Terryville, Connecticut, USA 1,383 m 4,537 ft
Latitude φ_{lat} + longitude:	41.6782° -73.0109°
Date of observation + UT date:	15 June 2013 16 June 2013
Time of observation + UT + UT offset (hrs):	20:30 00:30 UT 4 hours
Equipment:	10 inch F4 Celestron Meade telescope, 3x Barlow lens, C9 Tech Logitech camera

MOON DATA

TimeAndDate URL:	https://www.timeanddate.com/moon/@4844084?month=6&year=2013		
Moonrise + UT + heading θ_{Moon}:	11:53	15:53 UT	86°
Moonset + UT + heading θ_{Moon}:	00:26	04:26 UT	270°
Meridian + UT + altitude φ_{mer}:	18:14	22:14 UT	49°
Time from meridian (min, hr, θ_{rot}, deg/hour):	136 min	2.27 hrs	32.85° 14.492°/hr
Altitude φ + heading θ_{Moon}:	39°	225°	
Tilt angle θ_{tilt} (Eqn A.5):	23.90°	$\theta_{tilt} = \operatorname{asin}(\cos\varphi_{lat}\,\sin\theta_{rot})$ 57.29578	
Goddard reference URL:	https://svs.gsfc.nasa.gov/4000/		
Ref image UT time + date:	01:00:00 16 June 2013		
Moon distance (km, miles):	390,778 km 242,818 miles		
Moon diameter (arcsec, deg):	1834.1 0.50947°		

SUN DATA

TimeAndDate URL:	https://www.timeanddate.com/sun/@4844084?month=6&year=2013	
Sunrise + UT + heading:	05:17	09:17 UT 57°
Sunset + UT + heading:	20:28	00:28 UT 303°

JUPITER DATA

Almanac URL:	https://www.almanac.com/astronomy/planets-rise-and-set/CT/Terryville/2013-06-15			
Jupiter rise + UT + θ_{rot} + heading (Eqn C.16e):	05:33	09:33 UT	-113°	58°	$\theta_{Jup} = -\operatorname{asin}[\sin(\varphi_{mer}+\varphi_{lat})\sin\theta_{rot}/\cos\varphi]$
Jupiter set + UT + θ_{rot} + heading (Eqn C.16h):	20:37	00:37 UT	113°	302°	$\theta_{Jup} = 360° - \operatorname{asin}[\sin(\varphi_{mer}+\varphi_{lat})\sin\theta_{rot}/\cos\varphi]$
Meridian + UT + altitude φ_{mer}:	13:05	17:05 UT	72°		
Time from meridian (min, hr, θ_{rot}):	445 min	7.42 hrs	111°	$\varphi = \operatorname{asin}[\cos\theta_{rot}\sin(\varphi_{mer}+\varphi_{lat})\cos\varphi - \cos(\varphi_{mer}+\varphi_{lat})\sin\varphi_{lat}]$ (Eqn C.11)
Altitude φ + heading θ_{Jup} of observation:	1°	301°	$\theta_{Jup} = 360° - \operatorname{asin}[\sin(\varphi_{mer}+\varphi_{lat})\sin\theta_{rot}/\cos\varphi]$ (Eqn C.16h)

SATURN DATA

Almanac URL:	https://www.almanac.com/astronomy/planets-rise-and-set/CT/Terryville/2013-06-15			
Saturn rise + UT + θ_{rot} + heading (Eqn C.16b):	16:06	20:06 UT	-81°	104°	$\theta_{Sat} = 180° + \operatorname{asin}[\sin(\varphi_{mer}+\varphi_{lat})\sin\theta_{rot}/\cos\varphi]$
Saturn set + UT + θ_{rot} + heading (Eqn C.16c):	02:52	06:52 UT	81°	256°	$\theta_{Sat} = 180° - \operatorname{asin}[\sin(\varphi_{mer}+\varphi_{lat})\sin\theta_{rot}/\cos\varphi]$
Meridian + UT + altitude φ_{mer}:	21:29	01:29 UT	38°		
Time from meridian (min, hr, θ_{rot}):	-59 min	-0.98 hrs	-15°	$\varphi = \operatorname{asin}[\cos\theta_{rot}\sin(\varphi_{mer}+\varphi_{lat})\cos\varphi - \cos(\varphi_{mer}+\varphi_{lat})\sin\varphi_{lat}]$ (Eqn C.11)
Altitude φ + heading θ_{Jup} of observation:	36°	162°	$\theta_{Jup} = 180° + \operatorname{asin}[\sin(\varphi_{mer}+\varphi_{lat})\sin\theta_{rot}/\cos\varphi]$ (Eqn C.16b)

WIND DATA

Metcheck URL (300mb level):	https://www.metcheck.com/WEATHER/jetstream_archive.asp
Open-Meteo URL:	https://open-meteo.com/en/docs/historical-weather-api#start_date=2013-06-15&end_date=2013-06-15&hourly=wind_speed_100m,wind_direction_100m&location_mode=csv_coordinates&csv_coordinates=41.6782%2C%B0+N,+73.0109%2C%B0+W&timezone=America%2F New_York
Jetstream (m/s, km/h, mph, knots, θ):	26 m/s 93 km/h 58 mph 50 knots 315°
Wind @100m (m/s, km/h, mph, kt, θ):	1 m/s 4 km/h 3 mph 2 knots 195°

WAVE DATA FROM VIDEO

t_{1init}, t_{1term} (video mm:ss:*frames*):	03:12:*07*	03:14:*07*		11527	7	11520	11647	7	11640
t_{2init}, t_{2term} (video mm:ss:*frames*):	03:13:*23*	03:15:*23*		11603	23	11580	11723	23	11700
Frame rate (frames/second):	24 fps				16	60		16	60
Frame to Moon diameter (θ_a, θ_b, θ_{geo1}):	261.42°	243.56°	17.86°	$\theta_{geo1} = \theta_a - \theta_b$	1.67			1.67
(θ_a, θ_b, θ_{geo2}):	0.00°	0.00°	0.00°	$\theta_{geo2} = \theta_a - \theta_b$				
Frame to Moon diameter coverage C_{geo} (%):	34.67%	$C_{geo} = (1 - \sin\theta_{geo1})/2$ (Eqn A.3i)						
t_{1frame} (*fr*, ss), t_{1Moon} (ss) (Eqns A.1, A.2):	48 frames	2.00 sec	5.77 sec	$t_{1frame} = t_{1term} - t_{1init}$, $t_{1Moon} = t_{1frame}/C_{geo}$				
t_{2frame} (*fr*, ss), t_{2Moon} (ss) (Eqns A.1, A.2):	48 frames	2.00 sec	5.77 sec	$t_{2frame} = t_{2term} - t_{2init}$, $t_{2Moon} = t_{2frame}/C_{geo}$				
t_{1wsep}, t_{2wsep} (*fr*, *fr*, ss, ss) (Eqn A.4):	40 frames	40 frames	1.67 sec	1.67 sec	$t_{1wsep} = t_{2init} - t_{1init}$, $t_{2wsep} = t_{2term} - t_{1term}$			
Total elapsed time ($t_{1Moon} + t_{2wsep}$):	7.44 sec	$t_{1Moon} + t_{2wsep}$						

CONVERSION TO MAP

H, x_{new}, y_{new}, H_{new}, θ_{new} (Appendix B.21):	17.10 cm	-2.82 cm	-6.51 cm	7.09 cm	246.58°	$H_{new} = (x^2 + y^2)^{1/2}$, $\theta_{new} = 180° + \operatorname{atan}(y/x)$
V, x_{new}, y_{new}, V_{new}, C_{VS} (Appendix B.24):	10.17 cm	3.97 cm	-1.72 cm	4.33 cm	1.0254057	$C_{VS} = (V_{new}/H_{new})/(V/H)$
H_{frame}, V_{frame}, H_{newfr}, V_{newfr} (Appendix B.25):	19.58 cm	11.05 cm	8.12 cm	4.70 cm	$H_{newfr} = H_{frame}(H_{new}/H)$, $V_{newfr} = V_{frame}(V_{new}/V)$
θ_{1wvid}, θ_{2wvid}, $\theta_{1wvidVS}$, $\theta_{2wvidVS}$ (Appendix B.28):	14.49°	13.63°	14.84°	13.96°	$\theta_{wvidVS} = \operatorname{atan}[C_{VS}\tan\theta_{wvid}]$
($\theta_{1wvidVS} + \theta_{frame}$), ($\theta_{2wvidVS} + \theta_{frame}$):	261.42°	260.54°	$\theta_{wvidVS} + \theta_{frame}$		
θ_{frame}, θ_{tilt}, θ_{1tel}, θ_{2tel} (Eqn A.6):	246.58°	23.90°	32.48°	33.36°	$\theta_{tel} = -90° - \theta_{wvidVS} + (360° - \theta_{frame}) + \theta_{tilt}$
θ_{wvidVS} average, θ_{tel} average (degrees):	14.40°	32.92°	$\theta_{wvidVS} = (\theta_{1wvidVS} + \theta_{2wvidVS})/2$, $\theta_{tel} = (\theta_{1tel} + \theta_{2tel})/2$
θ_{1wave}, θ_{2wave} (degrees) (Eqn A.8):	21.83°	22.50°	$\theta_{1wave} = \operatorname{atan}(\sin\varphi\,\tan\theta_{1tel})$, $\theta_{2wave} = \operatorname{atan}(\sin\varphi\,\tan\theta_{2tel})$
θ_{wake} average, θ_{wave} (degrees):	22.17°	0.67340°	$\theta_{wave} = (\theta_{1wave} + \theta_{2wave})/2$, $\theta_{wake} = \theta_{2wave} - \theta_{1wave}$
$-\theta_{wave}$ average (degrees):	-22.17°	(vertically flipped, relative to vertical axis)		
$\theta_{wtravel} = -90 - \theta_{wave}$ (degrees):	-112.17°	(without Moon compass heading, relative to vertical axis)		
$\theta_{wtravel} = \theta_{Moon} - 90 - \theta_{wave}$ (degrees):	112.83°	(includes Moon compass heading)		
$180 + \theta_{wtravel}$ (degrees):	292.83°	(compass direction of apparent source of waves)		
α_{1wsep}, α_{2wsep} (degrees) (Eqn A.12):	0.14718°	0.14718°	$\alpha_{1wsep} = \alpha(t_{1wsep}/t_{1Moon})$, $\alpha_{2wsep} = \alpha(t_{2wsep}/t_{2Moon})$
α_{wsep} average (degrees) (Eqn A.13):	0.14718°	$\alpha_{wsep} = \alpha(t_{1wsep}/t_{1Moon} + t_{2wsep}/t_{2Moon})/2$
$\alpha_{wstretch}$ (degrees) (Eqn A.14):	0.16237°	$\alpha_{wstretch} = \alpha_{wsep}[\sin^2(\theta_{wave})/\sin^2\varphi + \cos^2(\theta_{wave})]^{1/2}$

AIRCRAFT WAKE ANALYSIS

	d_{wsep} = 20m (65 ft)		d_{wsep} = 40m (130 ft)		d_{wsep} = 60m (200 ft)		
Distance to waves L (km, miles) (Eqn A.15):	7.06 km	4.39 miles	14.12 km	8.77 miles	21.17 km	13.16 miles	$L = d_{wsep}/\tan(\alpha_{wstretch})$
Wave altitude h (m, ft) (Eqn A.16):	4,441 m	14,572 ft	8,883 m	29,143 ft	13,324 m	43,715 ft	$h = L\sin\varphi$
Map distance L_{map} (km, miles) (Eqn A.17):	5.48 km	3.41 miles	10.97 km	6.82 miles	16.45 km	10.22 miles	$L_{map} = L\cos\varphi$
#1 Wave speed v_1 (m/s, km/h) (Eqn A.10):	11 m/s	39 km/h	22 m/s	78 km/h	33 m/s	117 km/h	$v_1 = L\tan(\alpha_{1wsep})/t_{1wsep}$
(mph, knots):	24 mph	21 knots	49 mph	42 knots	73 mph	63 knots	
#2 Wave speed v_2 (m/s, km/h) (Eqn A.10):	11 m/s	39 km/h	22 m/s	78 km/h	33 m/s	117 km/h	$v_2 = L\tan(\alpha_{2wsep})/t_{2wsep}$
(mph, knots):	24 mph	21 knots	49 mph	42 knots	73 mph	63 knots	
Average wave speed v_{avg} (m/s, km/h):	11 m/s	39 km/h	22 m/s	78 km/h	33 m/s	117 km/h	$v_{avg} = (v_1 + v_2)/2$
(mph, knots):	24 mph	21 knots	49 mph	42 knots	73 mph	63 knots	
Wake position x (aircraft lengths) (Eqn A.18):	57	$x = [0.0445/\tan(\theta_{wake}/2)]^2$					
Wake age t_{pass} (at 2 lengths/sec) (Eqn A.19):	29 sec	$t_{pass} = x/2$					

RING VORTEX ANALYSIS

Altitude h = 10km (33,000 ft)

Distance to ring L (km, miles) (Eqn A.17):	15.89 km	9.87 miles	$L = h/\sin\varphi$	
Map distance L_{map} (km, miles) (Eqn A.18):	12.35 km	7.67 miles	$L_{map} = L\cos\varphi$	
Ring diameter d_{wsep} (m, ft) (Eqn A.19):	45 m	148 ft	$d_{wsep} = L\tan(\alpha_{wstretch})$	
$\alpha_{wsep}/\alpha_{Moon}$ (%), $(\alpha_{wsep}/\alpha_{Moon})\sin\varphi$ (%):	28.89%	18.18%	$\alpha_{wsep}/\alpha_{Moon}$, $(\alpha_{wsep}/\alpha_{Moon})\sin\varphi$	
Moon r, ring x, ring y (x level with horizon):	13.27 cm	3.83 cm	2.41 cm	
v_1 (m/s, km/h, mph, knots) (Eqn A.10):	24 m/s	88 km/h	55 mph	48 knots	$v_1 = L\tan(\alpha_{1wsep})/t_{1wsep}$
v_2 (m/s, km/h, mph, knots) (Eqn A.10):	24 m/s	88 km/h	55 mph	48 knots	$v_2 = L\tan(\alpha_{2wsep})/t_{2wsep}$
Average speed v_{avg} (m/s, km/h, mph, knots):	24 m/s	88 km/h	55 mph	48 knots	$v_{avg} = (v_1 + v_2)/2$

APPENDIX A – Analyzing a Lunar Wave Video

The lunar wave phenomenon consists of a pair of nearly straight transparent disturbances or waves crossing the face of the Moon or bright planet, as seen by the subtle shifting of background craters or objects in the wave travel direction. The optical effect is similar to a pair of cylindrical lenses moving across the sky, characterized by an inverted image effect rippling along the lunar rim.

The lunar transit times have varied between 2.1 and 160 seconds, with a time between waves of 0.7 to 40 seconds. The earliest known video recording was made by Crrow777 and titled "The first Lunar Wave from Sept 2012", which is believed to be the origin of the term "lunar wave".

The analysis of a lunar wave recording begins by recreating the celestial scene based on the known date, time and location of observation. With additional information obtained from astronomical data sources and the aid of two theoretical frameworks, the most probable explanation for the waves can be determined.

The task of measuring wave orientation, speed and altitude accurately requires a thorough understanding of the 3-dimensional situation. The procedures below assume the observer was in a northern hemisphere location. Similar procedures apply for an observer in the southern hemisphere, who will see the Moon rotated 180 degrees compared with the northern observer.

A list of procedures is presented and a few mathematical formulas are derived below to enable the true wave travel direction to be determined from the video recording. A graphical approach is used to determine critical angles, which should provide an overall accuracy of better than ±3.6° (±1% of a full circle).

It is assumed that the lunar wave recordings were obtained by a single telescope (or camera with telephoto lens) closely tracking the Moon over periods of several hours per night, in the hope of capturing something unusual such as an unidentified flying object (UFO) or a wave event.

Ideally, a second wide-angle camera would simultaneously video record the general vicinity of the Moon, including an audio track. The second recording would allow verification of the direction, timing and sound of any aircraft appearing to pass near the Moon. Since this camera would operate at nighttime, possibly a time-lapse function could be used to increase sensitivity, so distant aircraft navigation lights could be detected. Alternatively, faint images can be enhanced by post-processing with software, such as iMovie, to improve contrast and exposure settings.
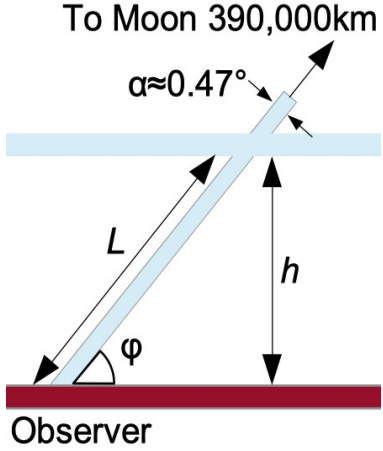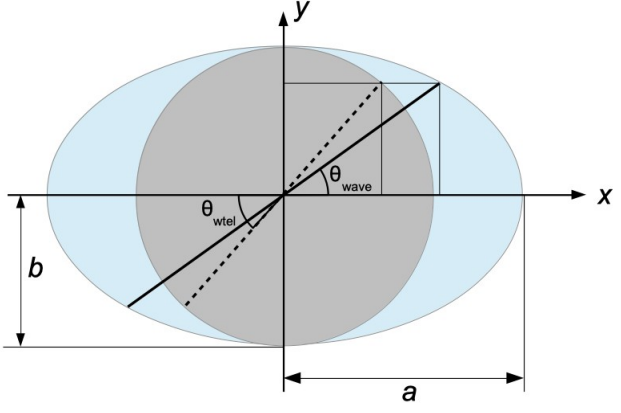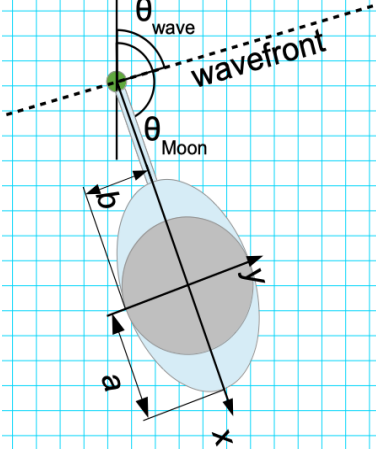
The clocks of the two cameras should be closely synchronized for accurate comparison of recorded events.

Geometry

For purposes of defining geometric variables, Fig. A.1 shows the field-of-view angle α of the observer looking at the distant Moon, which appears at an altitude angle φ above the horizon. Many amateur telescopes have a field-of-view similar to the size of the Moon, which averages $\alpha = 0.47$ degrees. Also shown are the distance L of the wave layer from the camera and the altitude of the waves $h = L\sin\varphi$.

Fig. A.2 shows a cross-section of the field-of-view of the observer cutting through the horizontal layer in which the waves appear to travel. The circle is what is seen looking through the telescope, but in the plane of the wave layer, the field-of-view appears as an ellipse.

Fig. A.3 shows the final map orientation (directly above the observer) of the elliptical field-of-view, allowing θ_{wave} to be known. Note that, in this view, the ellipse x-axis is pointing away from the observer and will appear to point vertically in the telescope view.

Fig. A.1 Elevation view showing the field-of-view angle $\alpha \approx 0.47°$ of an observer, the Moon altitude angle φ, the wave layer distance from the camera L and the wave altitude $h = L\sin\varphi$.

Fig. A.2 A cross-section of the field-of-view comparing the telescope image (circle and dotted wavefront) with the elliptical shape and true wavefront orientation as seen in the wave layer.

Fig. A.3 The final map orientation of the elliptical shape and true wavefront seen in the wave layer, yielding θ_{wave}.

Fig. A.4 Video still frame with the wavefront highlighted by a superimposed line (Video: James Hannon, https://www.youtube.com/watch?v=T_2sOBISBHc, video time code 3:12).

When the lunar wave recording is analyzed, a methodical process is followed to obtain the desired data:
  a) Obtain one or more still frames of the waves from the video recording and enhance as needed.
  b) Determine the raw wave angle θ_{wvid} from each still frame (overlay a line for clarity, Fig. A.4).

c) Obtain the angle-of-view α, which measures the apparent diameter of the Moon, for the hour of observation from an astronomical data source (eg., Goddard Space Flight Center, https://svs.gsfc.nasa.gov/gallery/moonphase/). Note: one degree is 3600 arcseconds.

d) Superimpose the scaled and rotated video still frame onto the reference Moon image (also from Goddard) for the hour of observation and align the images as exactly as possible, Fig. A.5.

e) From a series of lines superimposed on the reference image and by counting video frames (at a known frame rate per second), determine the wave transit times and the wave separation time.

f) Determine the video frame rotation angle θ_{frame} from item **d)** (Appendix B).

g) Obtain the Moon azimuth (compass heading) θ_{Moon} and altitude φ at the time of observation from an astronomical data source (eg., https://www.timeanddate.com/moon/, Fig. A.7).

h) Determine the actual tilt of the Moon θ_{tilt} relative to the horizon (Appendix C).

i) Calculate the true wavefront angle θ_{wave} using the circle-to-ellipse conversion formula.

j) Create an accurate map with arrows showing compass directions θ_{Moon} and $\theta_{wtravel}$.

k) Add arrows indicating wind direction at a higher altitude, etc., based on weather records (eg., https://open-meteo.com/en/docs/historical-weather-api).

l) Correlate the separation distance of the waves with aircraft wake calculations (Appendix G).

m) Correlate the wavefront observations with the diameter of a ring vortex (Appendix H). The azimuth of celestial alignments (conjunctions, eclipses, etc.) should also be noted.

Detailed Procedures

In the list of procedures above, each item requires a more detailed explanation. There are 3 angles (θ_{wvid}, θ_{frame}, θ_{tilt}) required to get the correct tilt of the Moon relative to the horizon at the time of observation, thus the correct telescope wavefront angle θ_{tel}. There is then a conversion to find the true wavefront angle θ_{wave} in Fig. A.3. The compass direction of travel $\theta_{wtravel}$ is orthogonal to θ_{wave} and is in the range from zero to 360 degrees (measured clockwise from true north).

For item a), a computer screen capture of a single frame from the paused digital video recording is used. The choice of frame will require the wave to be seen distorting the background features at two or more points. These points should be as far apart as possible in the frame to get an accurate angle relative to the screen. Enhancing the frame with image filters, such as edge detection or applying frame differencing, Appendix B, may assist in making the wave clearer.

For item b), using a graphical editor, import the still frame and overlay a line passing through the two (or more) points identified in item **a)** to highlight the full wavefront, Fig. A.4. The graphical software can calculate the angle of the line, θ_{1wvid}, for the first wave. Repeat the procedure for the second wave to obtain θ_{2wvid}. Export this image, or create a new screen capture, with appropriate labeling.

For item c), the Moon undergoes a monthly series of wobbling and tilting motions known as libration, during which it also appears to change size. The apparent Moon size α for each hour of each year is published on-line, along with a reference image that already takes the libration angles into account. It shows accurately the lighting and placements of craters and other features. There are two versions, one for observers in the northern hemisphere and one for observers in the southern hemisphere.

With this tool, it is necessary to know the time of observation in Universal Time (UT). Converting the local time to UT may be done with an on-line calculator (eg., https://dateful.com/convert/utc).

13

For item d), it will be necessary to use graphics software to superimpose a video still frame onto the reference image of the Moon for the time of observation, Appendix B. This will typically involve adjusting the size of the still frame, possibly flipping the image horizontally and/or vertically, and rotating the image to obtain the closest match possible. Every telescope and camera configuration will be different and some may involve a mirror or prism or other arrangement that inverts the recorded image, which must be corrected for a proper match.

In some cases, the frame may be distorted such that, while some features align well, the curvature of the lunar rim does not match that of the reference image. It will be necessary to stretch the frame so that the rims match, Appendix B. This means the angles of the lines from item **b)** will also change and must be corrected after the stretch is performed. An example of the final result is in Fig. A.5.
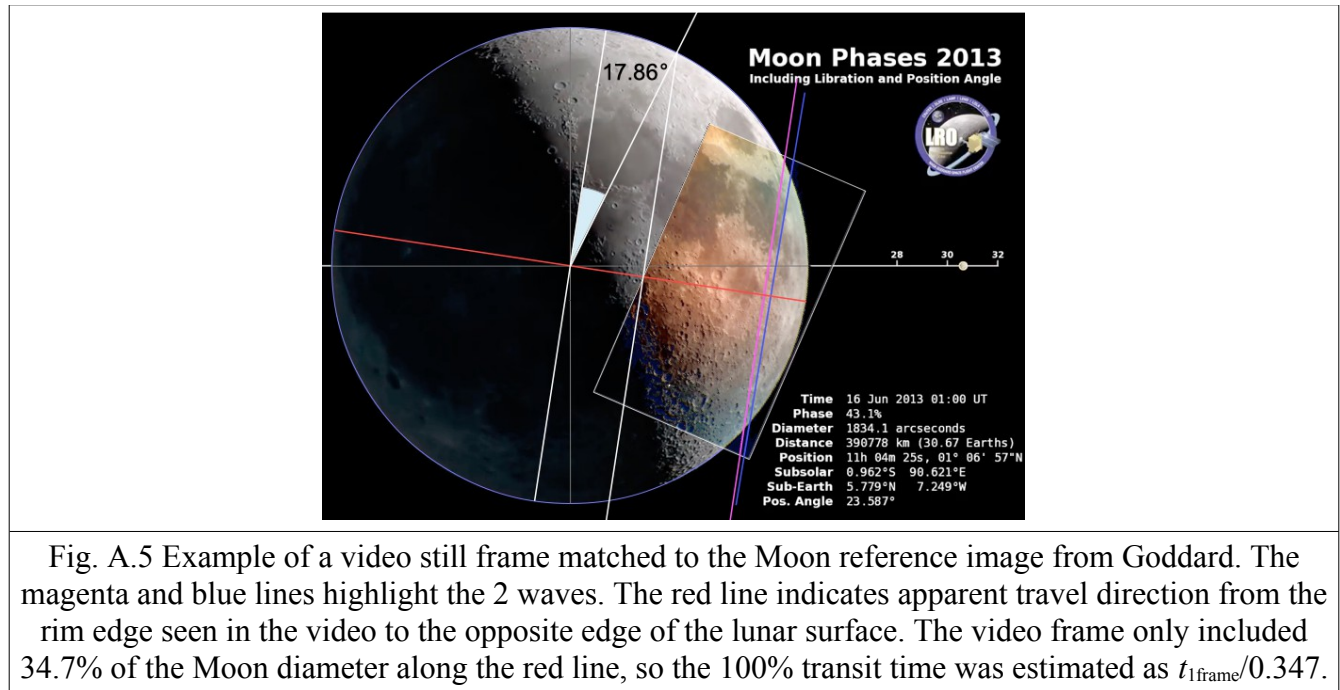
Fig. A.5 Example of a video still frame matched to the Moon reference image from Goddard. The magenta and blue lines highlight the 2 waves. The red line indicates apparent travel direction from the rim edge seen in the video to the opposite edge of the lunar surface. The video frame only included 34.7% of the Moon diameter along the red line, so the 100% transit time was estimated as $t_{1frame}/0.347$.

For item e), by superimposing a series of lines onto the reference image of the Moon, the lunar rim, the center of the disc, the video frame outline and the apparent wave travel direction can be indicated. The exact geometry applied will vary for each case, due to unique camera/telescope orientations and fields-of-view.

The procedure recreates where and when each of the two waves appears (initiates) and disappears (terminates) at opposite places on the lunar rim. This ensures that the angle-of-view α is matched to that of the Moon at the time of observation, since the video frame will often have a smaller view field.

The transit time across the video frame for the first wave may be calculated as:

$$t_{1frame} = t_{1term} - t_{1init} \qquad [A.1]$$

where t_{1init} and t_{1term} are the video time codes (to the nearest frame number) of wave initiation and termination seen in the video frame, respectively. The times for the second wave are t_{2init} and t_{2term}.

Slightly different speeds and sometimes directions have been observed for the two waves, which may be findings of scientific interest.

Since the video frame may not cover the full lunar diameter, a geometric correction C_{geo} must be determined and applied to get the transit time from rim to lunar rim:

$$t_{1Moon} = t_{1frame}/C_{geo} \qquad \text{[A.2]}$$

Two angles θ_{geo1} and θ_{geo2} may be defined to determine the parts of the lunar disc not covered by the frame. These may lie on just one side of the frame if it includes part of the rim, or on either side if no part of the rim is in frame. The advantage of using angles is independence of scale, because the lunar diameter is not explicitly needed in the calculations. Alternatively, the scaled distances may be used.

There are 4 scenarios, Fig. A.6, each with a different formula:
    i) the frame extent includes part of the lunar rim, but not the center of the disc,
$$C_{geo} = [1 - \sin(\theta_{geo1})]/2 \qquad \text{[A.3.}i\text{]}$$
    ii) the frame extent includes part of the rim and also the center of the disc,
$$C_{geo} = [1 + \sin(\theta_{geo1})]/2 \qquad \text{[A.3.}ii\text{]}$$
    iii) the frame extent does not include the rim, but includes the center of the disc,
$$C_{geo} = [\sin(\theta_{geo2}) + \sin(\theta_{geo1})]/2 \qquad \text{[A.3.}iii\text{]}$$
    iv) the frame extent includes neither part of the rim nor the center of the disc.
$$C_{geo} = [\sin(\theta_{geo2}) - \sin(\theta_{geo1})]/2 \qquad \text{[A.3.}iv\text{]}$$

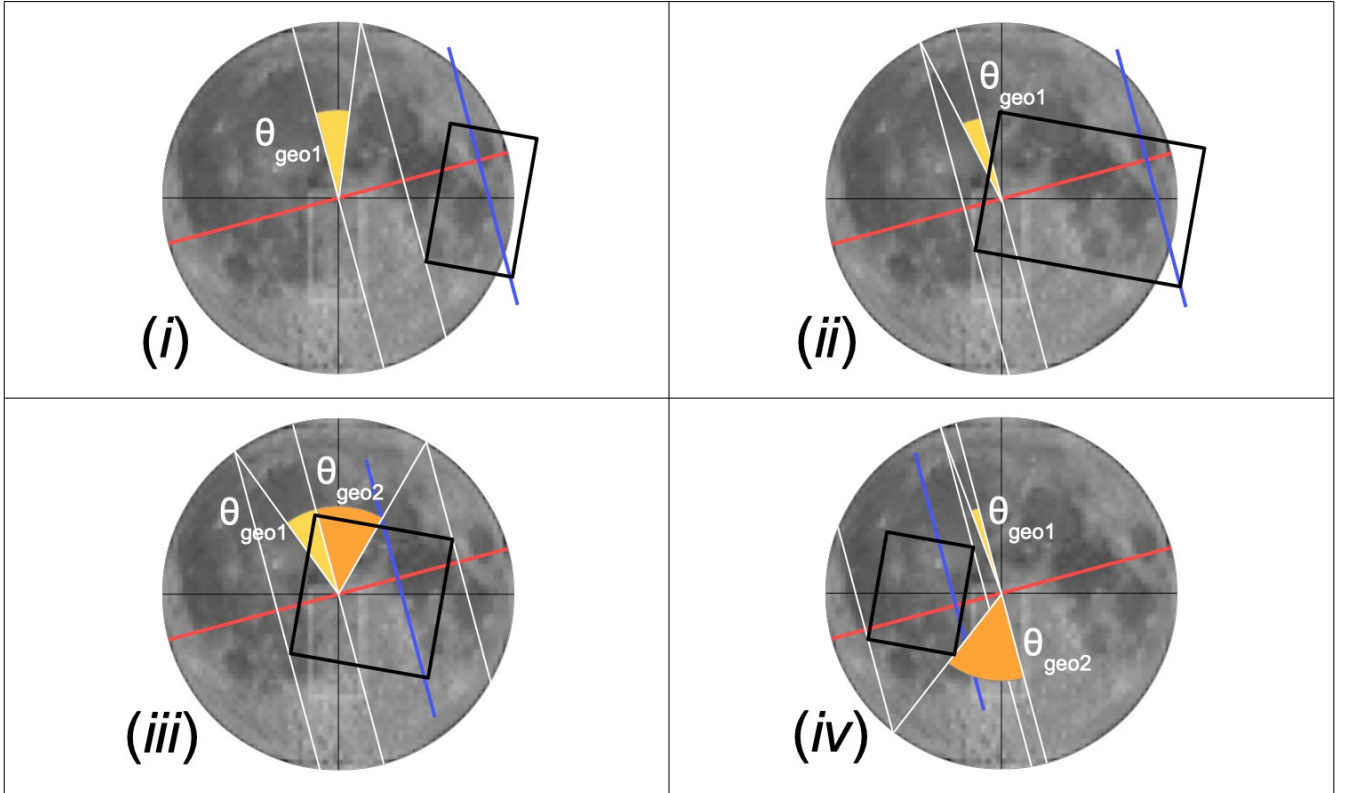Fig. A.6 Four scenarios to determine frame coverage of the lunar diameter using θ_{geo1} and θ_{geo2}. The wavefront is blue, parallel lines are white, wave travel direction is red and the video frame is black.

For the type *i*) example in Fig. A.5, the video frame covers $C_{geo} = [1 - \sin(17.86°)]/2 = 0.3467$ or 34.67% of the lunar diameter. Wave #1 transits the frame in 2.00 seconds (48±1 frames at 24 frames per second). Dividing by 0.3467, the wave transits 100% of the lunar diameter in 5.77 seconds. Note that this is merely the velocity component orthogonal to the wavefront and does not include any axial component.

The time of separation t_{1wsep} between the two waves is:

$$t_{1wsep} = t_{2init} - t_{1init} \qquad [A.4]$$

where a common reference point is used to mark the passing of each wave. If the camera was panning during the passage of the waves, careful review of the available video frames may be required to find a suitable reference point. A second alternative $t_{2wsep} = t_{2term} - t_{1term}$ is defined in Figs. A.14 and A.15 below.

For item f), the rotation of the video still frame θ_{vframe} in item **d)** can be obtained from the graphics software. Note that the reference image of the Moon is usually kept exactly the same as supplied by Goddard. In some cases, it may be known that the camera frame was already oriented closely with the horizon (e.g., using an azimuthal telescope mount or a handheld camera). The Goddard reference image may then be rotated to match the frame, particularly if the exact time of observation is not known.

For item g), a tilt angle θ_{tilt} due to Earth's rotation at the time of observation must be determined. This rotation constantly changes the observer's orientation (the horizon) relative to the Moon minute by minute, and so knowing the exact time of the observation becomes important.

To calculate θ_{tilt}, it is necessary to know the Moon position relative to the meridian (due south for an observer in the northern hemisphere). The meridian is the mid-sky location where $\theta_{tilt} = 0$, so the moon appears in the sky with no difference in tilt from the published reference image of item **e)**.
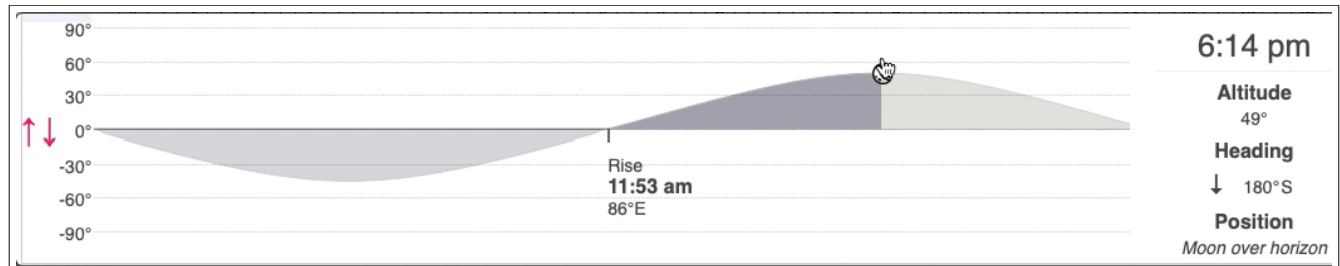

Fig. A.7 An on-line finder showing Moon altitude φ and heading θ_{Moon} for Terryville, CT, 15 June 2013. The due south time shown here is $t_{mer} = 6{:}14$ pm (heading $\theta_{Moon} = 180°S$, altitude $\varphi_{mer} = 49°$).
(Data: https://www.timeanddate.com/moon/@4844084?month=6&year=2013)

The time when the Moon is on the meridian t_{mer} for a given date and location may be found from an astronomical data source, Fig. A.7. Similarly, the heading angle θ_{Moon} and the altitude angle φ of the Moon above (or below) the horizon may also be found for the time of observation.

For item h), the Earth rotates at the rate of 1 degree every 4 minutes (15°/hour) and the Moon appears to move at a similar rate (14.492°/hour) from the east (moonrise) to the west (moonset). From Fig. A.8 and Appendix C, the frame tilt angle θ_{tilt} required to orient accurately the Goddard reference relative to

the horizon may be related to both the Earth's rotation θ_{rot} and latitude of observation φ_{lat}:

$$\theta_{tilt} = asin(cos\varphi_{lat}sin\theta_{rot}) \qquad [A.5]$$

For the example in Fig. A.9, $\varphi_{lat} = 41.6782°$ for Terryville CT, $\theta_{rot} = 14.492°(2.27hr) = 32.85°$ past due south at local time 20:30. Eqn [A.5] gives the tilt as $\theta_{tilt} = 23.90°$ in the clockwise direction, since the Moon had already passed the meridian on that day.
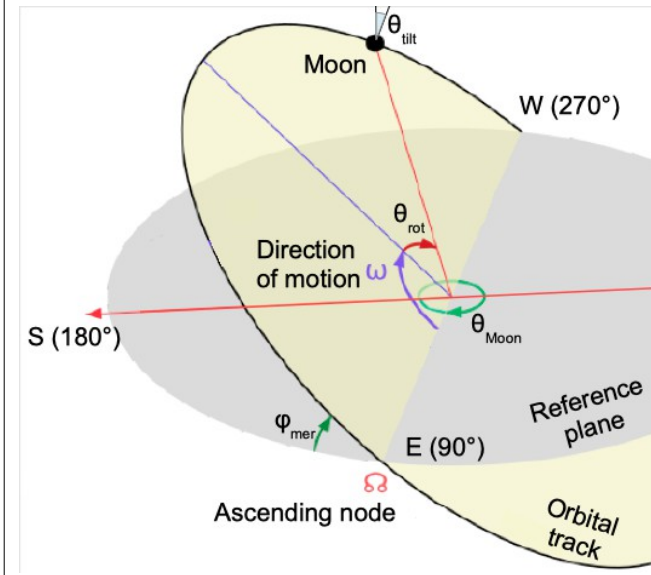

Fig. A.8 An observer sees the tilt of the Moon θ_{tilt} change with time as the Earth rotates. (Source: https://en.wikipedia.org/wiki/Orbital_node)	Fig. A.9 Final orientation of the reference image and wavefront relative to the observer's horizon. The wavefront telescope angle is $\theta_{tel} = 32.48°$.
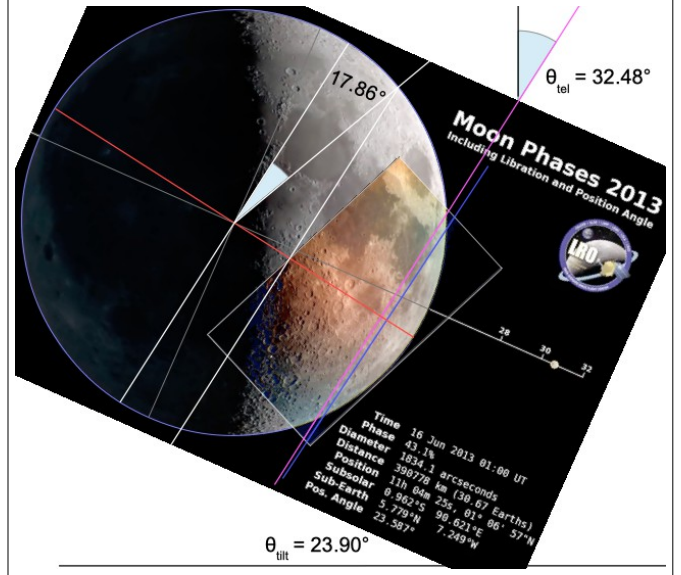
The total tilt angle of the wavefront relative to the horizon θ_{tel}, as seen through the telescope becomes:

$$\theta_{tel} = -90° - \theta_{video} + (360° - \theta_{vframe}) + \theta_{tilt} \qquad [A.6]$$

where θ_{tilt} and θ_{tel} are taken as clockwise and θ_{video} and θ_{vframe} taken as counterclockwise (due to the graphics software convention). Also due to the different convention, θ_{tel} is measured from the vertical, hence the offset of −90 degrees. The second offset of 360 degrees guarantees θ_{tel} is positive. Eqn [A.6] may be satisfied using graphical software to apply and display all of the correct rotations to the images. Rotating the image of Fig. A.5 by angle θ_{tilt}, the resulting angle θ_{tel} may be measured from Fig. A.9.

For item i), to determine the true wavefront compass angle θ_{wave}, there is a formula to convert the circle of Fig. A.2 to an ellipse, so the true wavefront orientation can be known. By definition, an ellipse is the curve that follows the formula:

$$1 = X^2 + Y^2 \qquad [A.7]$$

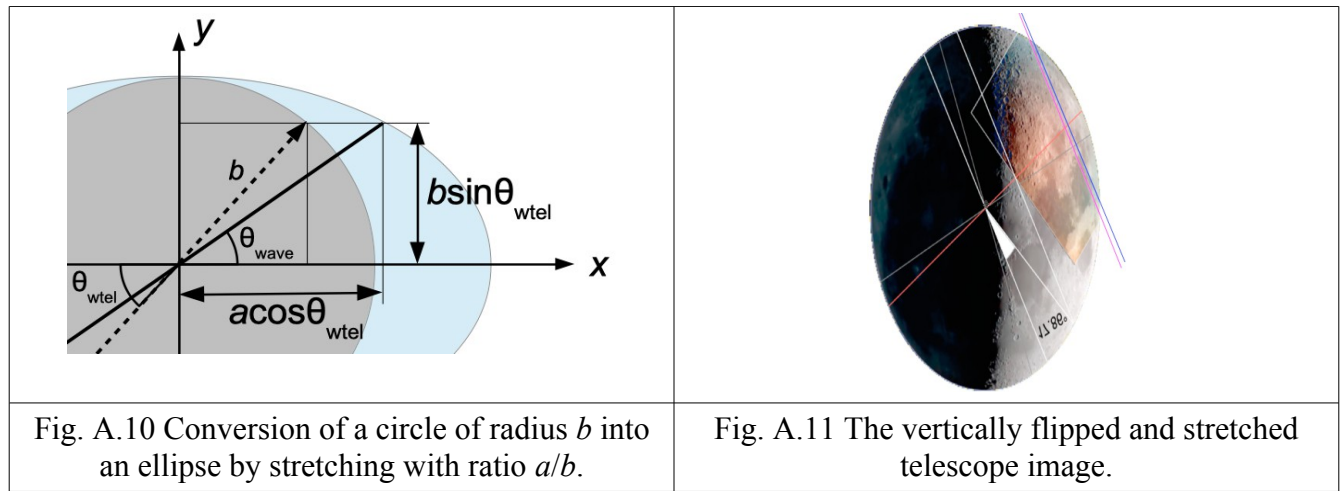where the *x-y* graph coordinates are scaled to $X = x/a$ and $Y = y/b$ and the ellipse semi-axial lengths are *a* and *b*, Fig. A.10. For the current purposes, the semi-axis *a* is $\alpha/2sin\varphi$ and *b* is $\alpha/2$, hence $b/a = sin\varphi$.

To convert the telescope wavefront angle θ_{tel}, the relation $\tan\theta = y/x$ is used. When stretching the x-axis to make the circle into an ellipse, it extends that axis by a factor a/b, while not changing the y-axis. The conversion becomes:

$$\theta_{wave} = \text{atan}[(b/a)(y/x)]$$
$$= \text{atan}[\sin\varphi\ \tan\theta_{tel}] \qquad\qquad [A.8]$$

Note that this formula will give an angle in the range $-90° < \theta_{wave} < 90°$ with most calculators or computers. The compass direction of the wave travel will be at a 90° angle (orthogonal) to this, in the range $0° < \theta_{wtravel} < 360°$. The correct travel direction may be determined from knowledge of the Moon heading θ_{Moon} of item **g)**, and from the wave motion in the video recording.

From $\theta_{tel} = 32.48$ degrees in Fig. A.9, with $\varphi = 39$ degrees at the time of observation, the true wavefront angle from Eqn [A.8] is $\theta_{wave} = 21.83$ degrees relative to the line-of-sight towards the Moon.

Fig. A.10 Conversion of a circle of radius b into an ellipse by stretching with ratio a/b.	Fig. A.11 The vertically flipped and stretched telescope image.

For items j) and k), since Fig. A.9 shows objects in the sky as viewed from underneath, the image must be vertically inverted (vertically flipped) to show the field-of-view as seen looking down from directly above the observer. Note that the graphics software may consider the image as rotated +180 degrees after this operation, which affects the final rotation below.

To account for the circle-to-ellipse conversion of item **i)**, the graphics software can be used to change the aspect ratio of the image, Fig. A.11, by applying a vertical stretch factor $a/b = 1/\sin\varphi$ (the x-axis of the ellipse is vertical as seen by the observer, Fig. A.3).

Superimposing this onto the Moon azimuth of 225 degrees (SW) for the time of observation, the graphics software reports the wavefront lies at a 67.17 degree angle. Note that the image rotation is 225 degrees clockwise, which is opposite to the convention in most graphics software. Here, specifying -45 degrees (+180 – 225 degrees) gave the correct result, with the sunlit portion of the image facing west and the label "17.86" pointing towards the observer's position.

The wave travel direction is orthogonal to the wavefront, giving a compass direction $\theta_{wtravel} = 112.83$ degrees, Fig. A.12. The wavefront is shown as a dotted black line and the travel direction as a red arrow. The Moon heading is indicated by a black arrow, the direction of sunlight by a yellow arrow and
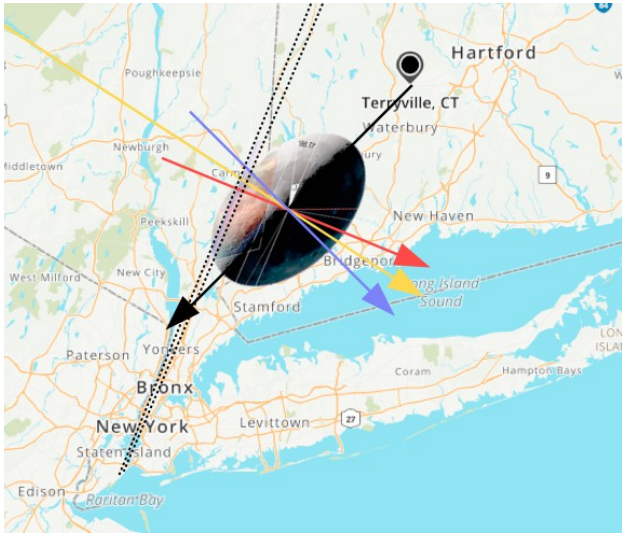
wind direction by a blue arrow.

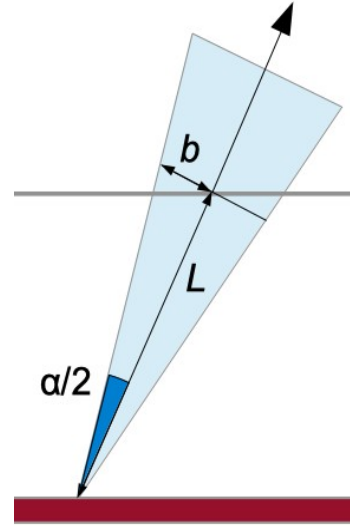| Fig. A.12 Map showing wavefronts (dotted black lines), wave travel direction (red arrow), Moon (black), Sun (yellow) and wind (blue). | Fig. A.13 Triangular relation of b and L to angle $\alpha/2$ within the observer's field-of-view (not to scale). |

Items l) and m) - Wave Distance, Altitude and Speed

With the assumption the two waves in the wave layer are separated by a horizontal length d_{wsep}, the wave distance from the camera L, altitude $h = L\sin\varphi$ and ground (map) distance $L_{map} = L\cos\varphi$ can be calculated. Particular values of d_{wsep} are specified for the aircraft wake analysis (item **l** below) and a particular altitude h for the ring vortex analysis (item **m** below).

From Fig. A.13 and taking the length $b \approx d_{wsep}/2$, the distance L is related to the angle-of-view α_{wsep} by $\tan(\alpha_{wsep}/2) = b/L$. For small values of α_{wsep}, the relationship can be written:

$$\tan\alpha_{wsep} = 2b/L \qquad\qquad [A.9]$$

Note that the angle α_{wsep} is different from the apparent size α of the Moon, Figs A.14 and A.15. It may be related to α by considering the speed v_1 of the first wave:

$$v_1 = 2b_1/t_{1wsep} = L\tan(\alpha_{1wsep})/t_{1wsep} \qquad\qquad [A.10]$$

where the separation time t_{1wsep} from Eqn [A.4] is measured between wave initiations, Fig. A.14. Note that this is only the velocity component orthogonal to the wavefront and does not include any axial component.

Alternatively, the speed of the second wave can be used to obtain t_{2wsep}, measured between wave terminations, Fig. A.15. The second measurement may be slightly different from the first if the waves travel at different speeds. The first wave also has an apparent speed across the face of the Moon:

$$v_1 = L\tan(\alpha)/t_{1Moon} \qquad\qquad [A.11]$$

Equating Eqns [A.10] and [A.11] and using the small angle approximation $\tan\alpha \approx \alpha$, the angles-of-view are related by the ratio of the measured times:

$$\alpha_{1wsep} = \alpha\, t_{1wsep}/t_{1Moon} \qquad\qquad [A.12]$$

A similar relationship can also be derived using the speed of the second wave, thus $\alpha_{2wsep} = \alpha\, t_{2wsep}/t_{2Moon}$. If the wave speeds are not identical (within the margin of error), the average wave separation angle-of-view α_{wsep} may be taken:

$$\alpha_{wsep} = \alpha(t_{1wsep}/t_{1Moon} + t_{2wsep}/t_{2Moon})/2 \qquad\qquad [A.13]$$

From Fig. A.13, the wave separation d_{wsep} is roughly equal to $2b$ in the layer of the waves. However, the horizontal wave layer is at an angle φ to the line-of-sight, so the circular telescope field-of-view takes on an elliptical shape when the wave layer is seen from above, Figs A.2 and A.10.

The waves will be oriented at an angle θ_{wave} relative to the ellipse axes, Fig. A.10, so the true separation distance d_{wsep} will be seen over an elliptically stretched angle-of-view $\alpha_{wstretch}$:

$$\alpha_{wstretch} = \alpha_{wsep}[\sin^2\theta_{wave}/\sin^2\varphi + \cos^2\theta_{wave}]^{1/2} \qquad\qquad [A.14]$$

where θ_{wave} is from Eqn [A.8]. A derivation of Eqn [A.14] as a function of φ and θ_{wave} is in Appendix D.

Fig. A.14 Definitions of the Moon angular size α and separation α_{1wsep} for wave initiations.	A.15 Definitions of the Moon angular size α and separation α_{2wsep} for wave terminations.

Item l) - Aircraft Wake Analysis

For the purpose of aircraft wake calculations, Appendix G, 3 scenarios are considered based on the typical range of flap-spans and wingspans of commercial-size aircraft. The wave or vortex separation is taken as:

1) $d_{wsep} = 20$ m (65 ft) for smaller aircraft flap-spans
2) $d_{wsep} = 40$ m (130 ft) for smaller wingspans and larger aircraft flap-spans, and
3) $d_{wsep} = 60$ m (200 ft) for larger aircraft wingspans

From Eqns [A.9] and [A.14] the length L, altitude h and map distance L_{map} for each scenario become:

$$L = d_{wsep}/\tan(\alpha_{wstretch}) \qquad\qquad [A.15]$$
$$h = L\sin\varphi \qquad\qquad [A.16]$$
$$L_{map} = L\cos\varphi \qquad\qquad [A.17]$$

Each resulting altitude allows wind direction and speed data from meteorological records to be compared with the observed drift direction and speed of the wavefronts. This allows the probable altitude of the waves to be estimated and possibly the aircraft size causing the waves.

From Eqns [G.2] and [G.3] in Appendix G, the small angle between the two vortices θ_{wake} allows estimation of their distance x from the generating aircraft (in aircraft lengths):

$$x = [0.0445/\tan(\theta_{wake}/2)]^2 \qquad\qquad [A.18]$$

This distance may be equated to time since passing t_{pass}, to estimate the age of that portion of the wake:

$$t_{pass} = x/2 \qquad\qquad [A.19]$$

Since the wake spreads slowly with time, the direction of aircraft travel is towards where the two vortex axes intersect. From this information, the likely map position of the aircraft at the moment of observation can be determined. An airport of interest may possibly be identified as well.

Item m) - Ring Vortex Analysis

For the purpose of calculating the ring vortex diameter d_{wsep}, Appendix H, the altitude for the base of an upper atmosphere plasma discharge is assumed to be $h = 10,000$ m (33,000 ft). Eqns [A.15] to [A.17] are rearranged to get:

$$L = h/\sin\varphi \qquad\qquad [A.20]$$
$$d_{wsep} = L\tan(\alpha_{wstretch}) \qquad\qquad [A.21]$$
$$L_{map} = L\cos\varphi \qquad\qquad [A.22]$$

The scaled ring is then superimposed onto a stretched video frame of the waves for comparison. A mismatch of curvature would indicate the ring model is not accurate for that particular sighting.

In addition, the probable celestial trigger is determined from the known azimuths of key magnetically active bodies at the time of observation: the Sun, Jupiter and Saturn (and possibly the Moon during an eclipse). The probable triggering body would be that closest to the direction from which the waves appeared, assuming it was near or above the horizon at the time.

Spreadsheet Summary

A summary of the data and results of the Equations for each case are expressed in spreadsheet format at the end of each study. This assures completeness of each analysis and accuracy of all calculations.

APPENDIX B – Image Differencing and Image Matching

One method of enhancing the visibility of a moving lunar wave is to take the difference between two consecutive frames of the video recording. The shift of the background image as the wave moves past it will enable the differencing to highlight the position of the wave. The resulting frame is then matched to the image published by the Goddard Space Flight Center, to give context to the sighting.

While software, such as OpenCV, can enhance the waves by performing frame subtraction for an entire video, the example below uses the iMovie software found on Macintosh computers to process just two consecutive frames. True frame subtraction results in 0 value (black) for unchanged pixels, while the iMovie differencing method gives a mid-grayscale value because a positive and a negative image are added, not subtracted. Further manipulation is required to obtain blackening of the unchanged pixels.

The procedure for each wave is:
1) screen capture two consecutive frames, where the wave span across the video frame is greatest
2) import the frames into iMovie
3) place one of the frames (say, #1) into the movie editing area
4) select "fit" under the cropping menu to prevent the zoom effect
5) select "negative" under the clip filter menu to invert the image
6) export as movie #1, choosing a high resolution (720 pixels or more)

7) import movie #1 into iMovie
8) remove the clip currently in the editing area
9) place frame #2 into the editing area and select "fit", followed by the new movie #1
10) highlight both clips and insert a cross-dissolve between them
11) stretch out the cross-dissolve to perhaps 3 seconds using the precision editor
12) export as movie #2

13) in Quicktime, play movie #2 frame-by-frame (with the keyboard arrow keys) in the cross-dissolve section and choose the best frame where the images nearly cancel each other
14) screen capture the best image as frame #3
15) screen capture the opening image of movie #2 as frame #4 (keep identically aligned with #3)
16) import frame #3 into a photo editor and adjust the image brightness and contrast to make the difference (the wave) as clear as practical, Fig. B.1
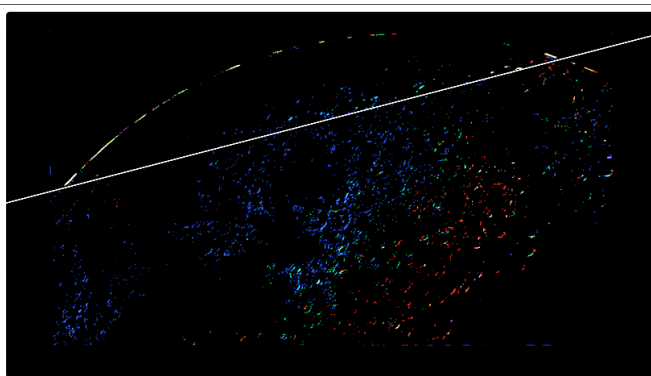

| Fig. B.1 Enhanced differencing image with overlaid line (Video: James Hannon). | Fig. B.2 The final (cropped) image with the wave highlighted by the same precisely overlaid line. |

Once frame #3 is enhanced, import it into a graphical editor to overlay a line to highlight the wavefront. Finally, insert frame #4 in place of frame #3. The overlaid line is now precisely placed on the desired video frame, Fig. B.2. Screen capture as frame #5 and crop as needed.

Image Matching Method

A simple method to obtain an accurate match between the video frame and the Goddard reference image is documented below, using the Hannon 2013 video example.

17) Superimpose a horizontal line (H) and a vertical line (V) onto the video frame.

18) Scale and position each line so the endpoints lie on well-spaced recognizable landmarks (points, craters, edges), Fig. B.3.

19) Calculate the ratio V/H of the line lengths.

20) Copy H, move to the Goddard reference image, rescale and rotate to match the same end point landmarks as for the video frame.

21) Note the length and rotation of the new line $H_{new} = (x^2 + y^2)^{1/2}$, $\theta_{new} = atan(y/x)$. If $x<0$ add 180°. If $y<0$ and $x>0$ add 360°.

22) Copy V, move to the Goddard reference image, rescale and rotate to match the same end point landmarks as the video.

23) For best accuracy, apply the rotation angle of item 21) to keep V_{new} orthogonal (90°) to H_{new}.

24) Calculate V_{new}/H_{new} and the Vertical Stretch factor $C_{VS} = (V_{new}/H_{new})/(V/H)$.

25) Re-scale a copy of the video frame so that $H_{newfr} = H_{frame}(H_{new}/H)$ and $V_{newfr} = V_{frame}(V_{new}/V)$.

26) Rotate the rescaled frame by the angle noted in item 21)

27) Superimpose the adjusted frame onto the reference image, Fig. B.4, applying minor corrections if needed, for a perfect match.

28) Correct the wave angles using $\theta_{wvidVS} = atan[C_{VS}tan(\theta_{wvid})]$, similar to Eqn [A.8].
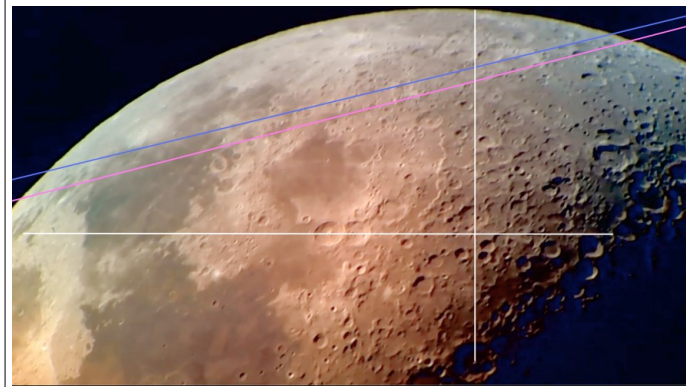

Fig. B.3 Video frame cross-hair lines (white) with endpoints positioned at landmark features. The magenta line marks the angle of the first wave, the blue line the second wave.
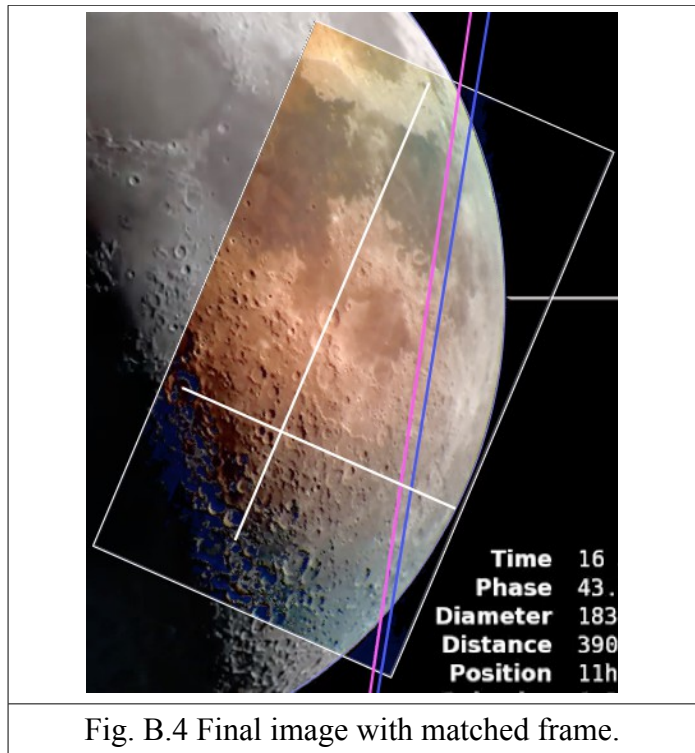

Fig. B.4 Final image with matched frame.

APPENDIX C – Moon Tilt and Orbital Position

Formulas are derived for the apparent tilt of the Moon θ_{tilt} of Eqn [A.5] in Appendix A and for the azimuth (compass) angle θ_{Moon} and altitude angle φ seen by the observer at latitude φ_{lat} in terms of the angular position θ_{rot} on the orbital track.

The only angle that must be supplied by an astronomical data source is the altitude angle φ_{mer} at the meridian (local north-south longitude) position. This enables rapid spreadsheet calculations with minimal need to use complex and time-consuming software, such as Stellarium. The same formulas can be applied to other planetary bodies, such as Jupiter and Saturn, as verified at the end of this Appendix.

The illustrations show a northern hemisphere viewpoint where the meridian lies due south ($\theta_{Moon} = 180°$) and φ_{lat} and φ_{mer} are positive. The derived formulas are also applicable to the southern hemisphere where the meridian lies due north, expressing φ_{lat} and φ_{mer} as negative values.

Views of the Moon's orbit are represented in Figs. C.1 and C.2, showing an arbitrary position on the equatorial orbital plane in 3 dimensions and edge-on. The Earth's spin axis is shown as a dotted-and-dashed line, which is perpendicular to the orbital plane.

Technically, the Moon's position as it moves across the sky follows a helical track with variable pitch. Since that pitch is quite fine, over a few hours of movement the track may be closely approximated by a circle lying in a plane.
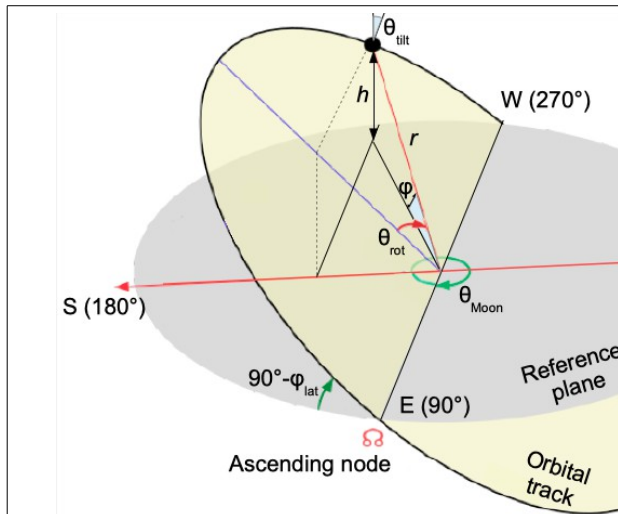

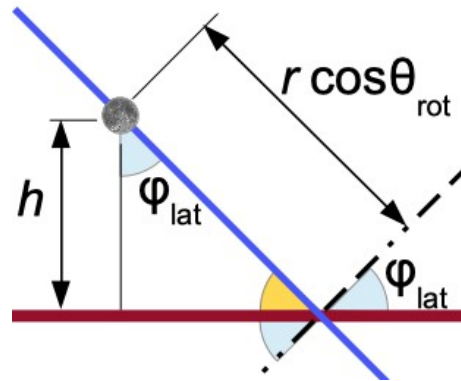| Fig. C.1 Moon at an arbitrary location along the equatorial orbital track, seen from latitude φ_{lat}.	Fig. C.2 Edge-on view of the orbital track (blue) showing relationships between h, r, θ_{rot} and φ_{lat}.

Moon Tilt Relative to the Horizon

From Fig. C.2, the apparent height of the Moon above the reference plane is:

$$h = (r \cos\theta_{rot})\cos\varphi_{lat} \qquad\qquad [C.1]$$

where θ_{rot} is the rotation angle of the Earth, relative to the meridian. In this simplified model, the height is positive over the range $-90° < \theta_{rot} < 90°$ and negative (below the horizon) otherwise.

While Earth's rotation is 24 hours per turn, or 15 degrees per hour, the Moon also moves 1 orbit per 29.53 days (708.72 hours), or 0.5080 degrees per hour in the same direction. Thus, the angle is related to clock time t (in hours) from the meridian position by:

$$\theta_{rot} = 14.4920°(t) \qquad\qquad [C.2]$$

All other bodies in the solar system are much more distant, hence appear to change position relative to the background star field much more slowly. Over a period of a few hours, the applicable formula becomes:

$$\theta_{rot} = 15°(t) \qquad\qquad [C.3]$$

The time t may be determined by taking the difference between the time of observation t_{obs} and the time of the Moon's transit of the meridian t_{mer} from an online data source (eg., https://www.timeanddate.com/moon/):

$$t = t_{obs} - t_{mer} \qquad\qquad [C.4]$$

A negative time means the Moon had not yet reached the meridian (mid-sky position) on the day the observation was made, thus the rotation will be a negative angle.

Fig. C.3 The tilt of the Moon changes relative to the observer's horizon as the Earth rotates.	Fig. C.4 Detail showing the local tilt angle θ_{tilt} of the orbital track (blue) as seen by the observer.
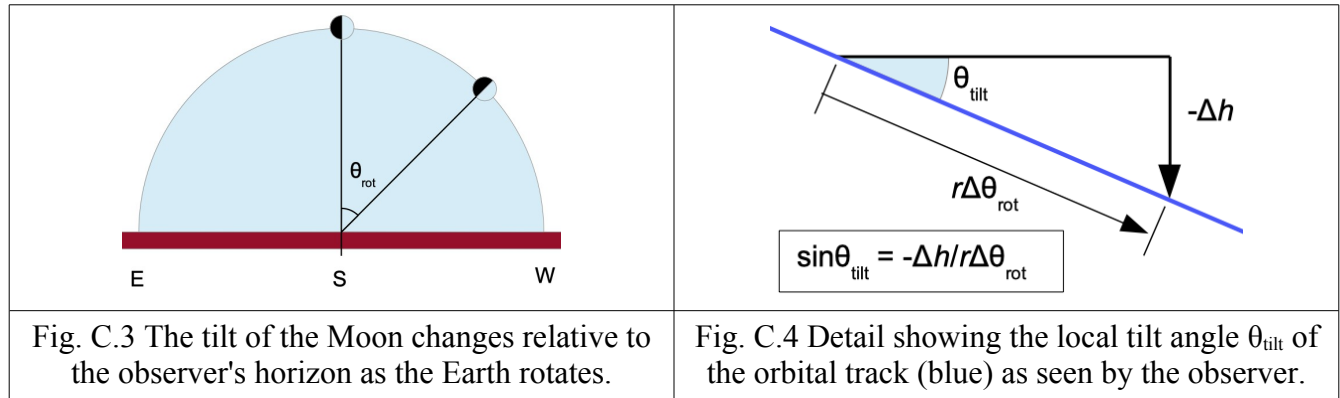
From Figs. C.3 and C.4, the tilt angle of the Moon as seen from the reference plane of the observer is the local slope of the orbital plane. Applying differential calculus, this is:

$$
\begin{aligned}
\sin\theta_{tilt} &= -dh/dr\theta_{rot} \\
&= -d(r\cos\theta_{rot})\cos\varphi_{lat}/rd\theta_{rot} \\
&= -\cos\varphi_{lat}(d\cos\theta_{rot}/d\theta_{rot}) \\
&= \cos\varphi_{lat}\sin\theta_{rot}
\end{aligned}
$$

$$\theta_{tilt} = asin(\cos\varphi_{lat}\sin\theta_{rot}) \qquad\qquad [C.5]$$

For $\theta_{rot} = -90°$ (east), the tilt $\theta_{tilt} = -(90° - \varphi_{lat})$. For $\theta_{rot} = +90°$ (west), the tilt $\theta_{tilt} = +(90° - \varphi_{lat})$. For $\theta_{rot} = 0°$ (meridian), the tilt is zero.

Moonrise and Moonset Azimuth Angles

From the general scenarios of Figs C.5 and C.6, the Moon does not rise exactly in the east or set exactly in the west. This is due to the Moon position not lying exactly on the equatorial plane at the time of observation. The orbital track as the Moon moves across the sky will appear to lie below or above the equator, causing the moonrise and moonset to be offset by a distance ε from true east and west, Figs C.7 and C.8. In both scenarios, the relationship of ε to the orbital radius seen by the observer r_{obs} and angles φ_{lat} and φ_{mer} is:

$$\varepsilon = r_{obs}\sin(\varphi_{mer}+\varphi_{lat}-90°)/\cos\varphi_{lat}$$
$$= -r_{obs}\cos(\varphi_{mer}+\varphi_{lat})/\cos\varphi_{lat} \qquad\qquad [C.6]$$
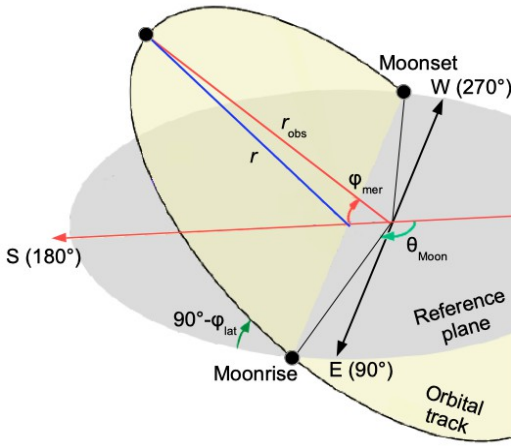
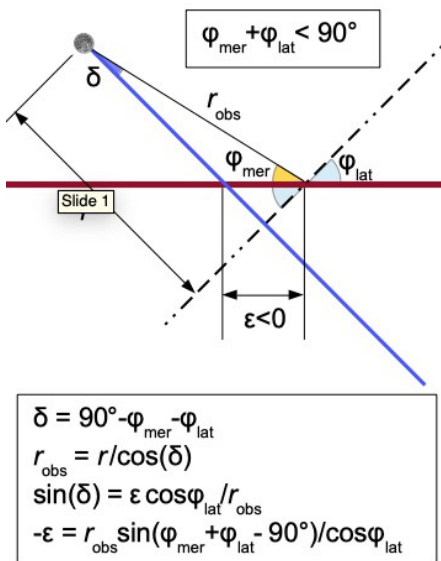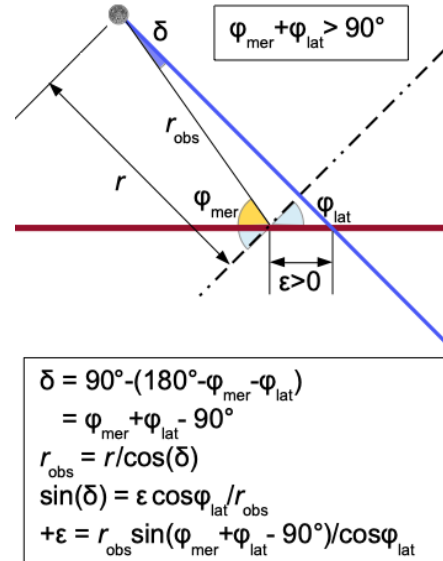|	
Fig. C.5 General view of the orbital track with apparent position below the equator. Moonrise and moonset are shifted southwards.	Fig. C.6 General view of the orbital track with apparent position above the equator. Moonrise and moonset are shifted northwards.
Fig. C.7 Edge-on view of the orbital track (blue) with apparent position below the equator. The Moon is at due south with altitude $\varphi_{mer}<\varphi_{lat}$.	Fig. C.8 Edge-on view of the orbital track (blue) with apparent position above the equator. The Moon is at due south with altitude $\varphi_{mer}>\varphi_{lat}$.
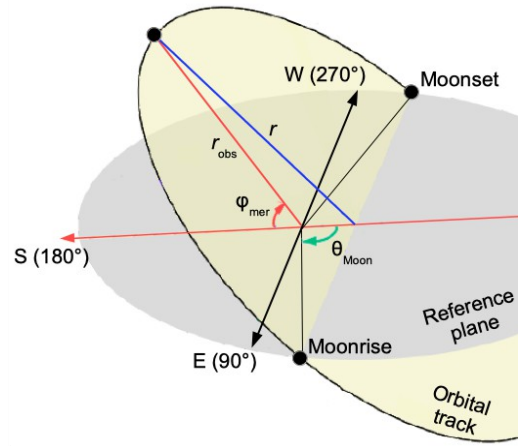
where the equivalence $\sin(\varphi-90°) = -\cos(\varphi)$ was used.

From the situation depicted in Fig. C.7, where $\varphi_{mer}+\varphi_{lat} < 90$ degrees, $\sin(\varphi_{mer}+\varphi_{lat}-90°)$ is negative and thus Eqn [C.6] yields a negative value.

In this model, the moonrise θ_{Mrise} and moonset θ_{Mset} azimuths are symmetrical about due south ($\theta_{Moon} = 180°$). Using trigonometry and the offset ε, the differences from the nominal east-west headings are:

$$\theta_{Mrise} = 90° - \mathrm{asin}(\varepsilon/r_{obs}) \qquad [C.7]$$
$$\theta_{Mset} = 270° + \mathrm{asin}(\varepsilon/r_{obs}) \qquad [C.8]$$

where the sign of ε from Eqn [C.6] accounts for the shift of the orbital plane north or south of the equator. These Equations are valid for $\varepsilon/r_{obs} \leq 1$, which is away from the polar regions as shown below. More general equations for the Moon angle θ_{Moon} at any position along the orbital track are also presented below, linking the position to the angle of rotation θ_{rot}.

Moon Altitude Angle

A formula is derived for the angle of the Moon above the horizon φ calculated in terms of the rotation angle φ_{rot} (or clock time), latitude φ_{lat} and due south altitude angle φ_{mer}. From Figs C.7 and C.8, noting that $\cos(\varphi-90°) = \sin(\varphi)$, the actual radius r is related to the observer's radius r_{obs} of the orbital track by:

$$r = r_{obs}\cos(\varphi_{mer}+\varphi_{lat}-90°)$$
$$= r_{obs}\sin(\varphi_{mer}+\varphi_{lat}) \qquad [C.9]$$

From Figs C.9 to C.12, using trigonometry and substituting Eqns [C.6] and [C.9], the altitude h becomes:

$$h = (r\cos\theta_{rot} + \varepsilon\sin\varphi_{lat})\cos\varphi_{lat}$$
$$= r_{obs}[\cos\theta_{rot}\sin(\varphi_{mer}+\varphi_{lat})\cos\varphi_{lat} + \sin(\varphi_{mer}+\varphi_{lat}-90°)\sin\varphi_{lat}] \qquad [C.10]$$

From the definition $h = r_{obs}\sin\varphi$ and noting that $\sin(\varphi-90°) = -\cos(\varphi)$, the altitude angle is:

$$\varphi = \mathrm{asin}(h/r_{obs})$$
$$= \mathrm{asin}[\cos\theta_{rot}\sin(\varphi_{mer}+\varphi_{lat})\cos\varphi_{lat} - \cos(\varphi_{mer}+\varphi_{lat})\sin\varphi_{lat}] \qquad [C.11]$$

The altitude angle and the radius r_{obs} are labelled with a gray font and indicated with a dashed line in Figs C.11 and C.12 since they are out-of-plane.

Polar Latitude Limit

The form of Eqns [C.7] and [C.8] fails for $\varepsilon/r_{obs} > 1$. This occurs for far northern and southern latitudes, especially where the orbital plane appears shifted towards the polar region of interest. The Moon (or other body) will appear above the horizon at all times, so there is no moonrise or moonset.

Instead, from Eqn [C.11] there is a calculation for the minimum altitude angle φ_0 of the orbital plane above the horizon (i.e., at the northernmost position $\theta_{rot} = 180°$):

$$\varphi_0 = \text{asin}[-\sin(\varphi_{mer}+\varphi_{lat})\cos\varphi_{lat} - \cos(\varphi_{mer}+\varphi_{lat})\sin\varphi_{lat}] \qquad [C.12]$$

For the limiting case $\varphi_0 = 0°$ (on the horizon), $[\sin(\varphi_{mer}+\varphi_{lat})\cos\varphi_{lat} + \cos(\varphi_{mer}+\varphi_{lat})\sin\varphi_{lat}] = 0$, or:

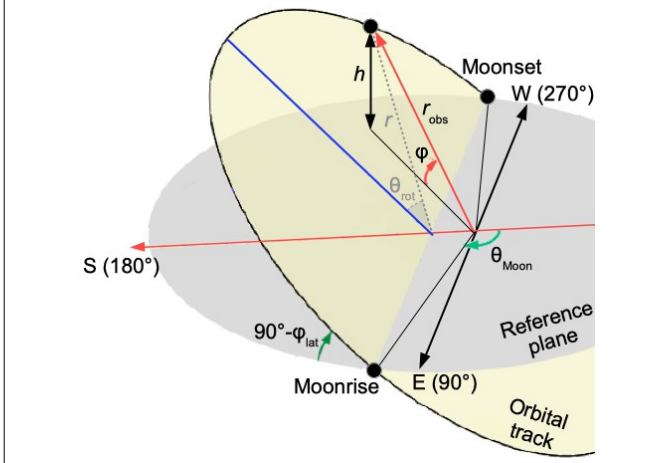$$\tan(\varphi_{mer}+\varphi_{lat}) + \tan\varphi_{lat} = 0 \qquad [C.13]$$

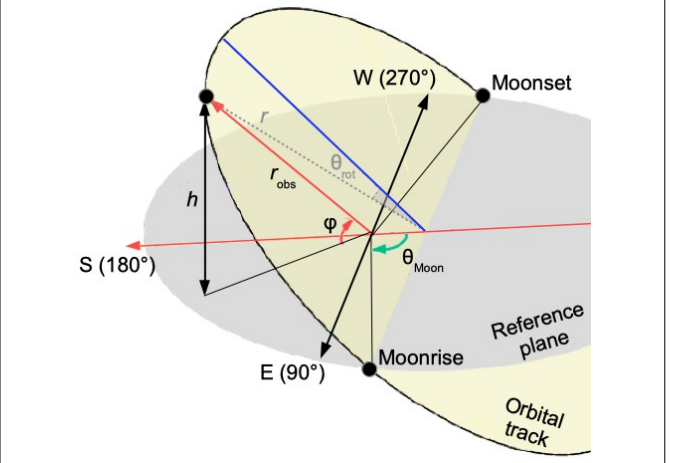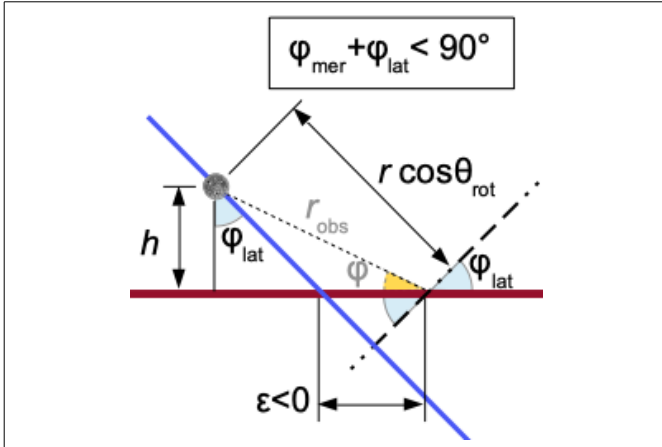| Fig. C.9 General view of the Moon at an arbitrary position along the orbital track with apparent position below the equator.	Fig. C.10 General view of the Moon at an arbitrary position along the orbital track with apparent position above the equator.

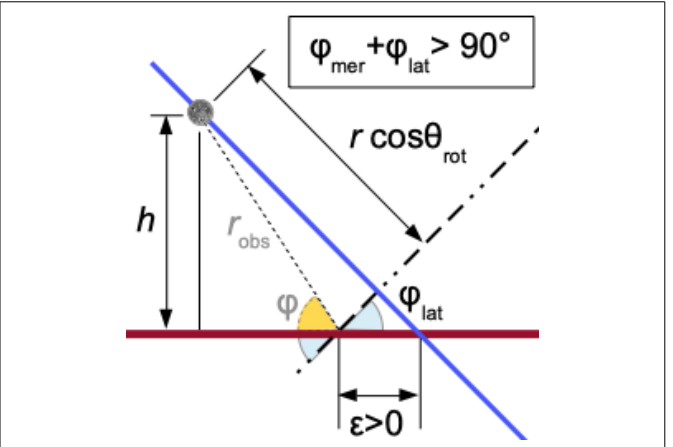| Fig. C.11 Edge-on view of the Moon at an arbitrary position along the orbital track (blue) with apparent position below the equator.	Fig. C.12 Edge-on view of the Moon at an arbitrary position along the orbital track (blue) with apparent position above the equator.

For a classic example, the 23.7° tilt of Earth's axis causes the apparent position of the sun's orbital plane to be farthest north of the equator at the summer solstice. Using $\varphi_{mer} = (90°-\varphi_{lat})+23.7°$ the arctic circle latitude is calculated as $\varphi_{lat} = \text{atan}[-\tan(113.7°)] = 66.3°$ (N).

For the antarctic circle and taking $\varphi_{mer} = -(90°-\varphi_{lat})-23.7°$, the latitude may be calculated as $\varphi_{lat} = \text{atan}[-\tan(-113.7°)] = -66.3°$ (S). This confirms the accuracy of the current model.

General Moon Azimuth Angle

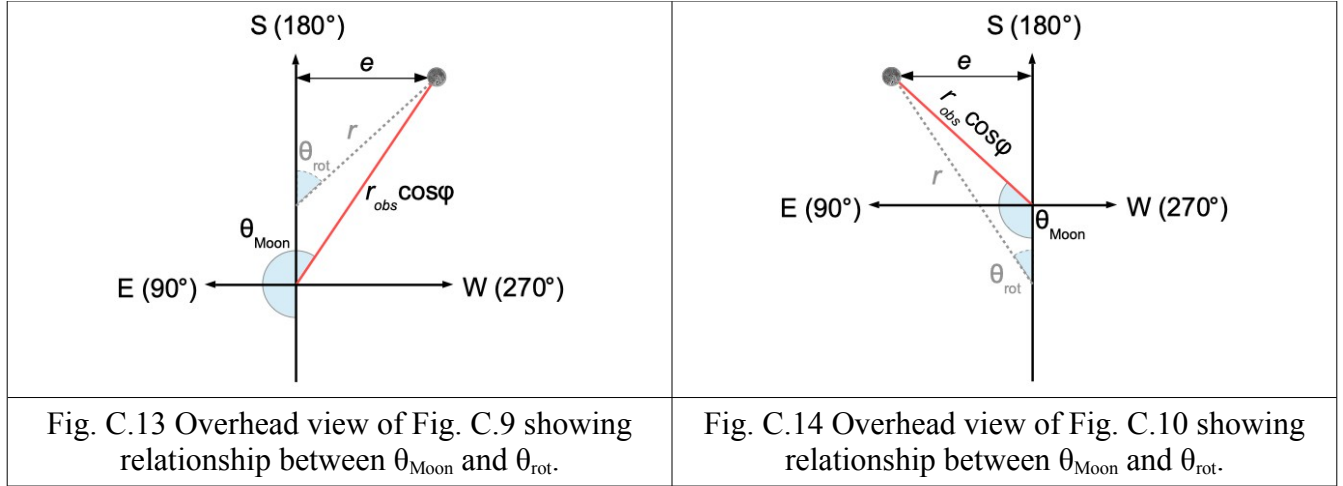A formula is derived for the general azimuth angle θ_{Moon} at any point along the orbital track in terms of θ_{rot} (clock time), altitude φ, latitude φ_{lat} and due south altitude angle φ_{mer}. From Figs. C.13 and C.14, the distance e allows equating of the two angles:

$$e = (r_{obs}\cos\varphi)\sin(\theta_{Moon}-180°) \qquad [C.14]$$
$$\text{and} \quad e = r\sin\theta_{rot} \qquad [C.15]$$

where θ_{rot} and r are labelled with a gray font and indicated with a dashed line since they are out-of-plane. Substituting Eqn [C.9], the Moon azimuth angle is related to the other angles by:

$$\sin(\theta_{Moon}-180°) = r\sin\theta_{rot}/r_{obs}\cos\varphi$$
$$= \sin(\varphi_{mer}+\varphi_{lat})\sin\theta_{rot}/\cos\varphi \qquad [C.16]$$

Fig. C.13 Overhead view of Fig. C.9 showing relationship between θ_{Moon} and θ_{rot}.	Fig. C.14 Overhead view of Fig. C.10 showing relationship between θ_{Moon} and θ_{rot}.

Since the sinusoid function repeats every 360 degrees and there are 3 of them in Eqn [C.16], there are at least 4 possible +/− combinations when calculating θ_{Moon}. The situation is further complicated by the ranges of the angles θ_{Moon}, $(\varphi_{mer}+\varphi_{lat})$ and θ_{rot} being larger than 90 degrees, which requires choosing positive or negative values and sometimes adding 180 or 360 degrees as shown below.

Northern Hemisphere:

$0°< (\varphi_{mer}+\varphi_{lat}) < 90°$, $-180°<\theta_{rot}<-90°$, $\qquad \theta_{Moon} = -\text{asin}[\sin(\varphi_{mer}+\varphi_{lat})\sin\theta_{rot}/\cos\varphi]$ $\qquad$ [C.16a]

$-90°< \theta_{rot}< 0°$, $\qquad \theta_{Moon} = 180° + \text{asin}[\sin(\varphi_{mer}+\varphi_{lat})\sin\theta_{rot}/\cos\varphi]$ $\qquad$ [C.16b]

$0°< \theta_{rot}< 90°$, $\qquad \theta_{Moon} = 180° + \text{asin}[\sin(\varphi_{mer}+\varphi_{lat})\sin\theta_{rot}/\cos\varphi]$ $\qquad$ [C.16c]

$90°< \theta_{rot}< 180°$, $\qquad \theta_{Moon} = 360° - \text{asin}[\sin(\varphi_{mer}+\varphi_{lat})\sin\theta_{rot}/\cos\varphi]$ $\qquad$ [C.16d]

$90°<(\varphi_{mer}+\varphi_{lat})<180°$, $-180°<\theta_{rot}<-90°$, $\qquad \theta_{Moon} = -\text{asin}[\sin(\varphi_{mer}+\varphi_{lat})\sin\theta_{rot}/\cos\varphi]$ $\qquad$ [C.16e]

$-90°< \theta_{rot}< 0°$, $\qquad \theta_{Moon} = 180° + \text{asin}[\sin(\varphi_{mer}+\varphi_{lat})\sin\theta_{rot}/\cos\varphi]$ $\qquad$ [C.16f]

$0°< \theta_{rot}< 90°$, $\qquad \theta_{Moon} = 180° + \text{asin}[\sin(\varphi_{mer}+\varphi_{lat})\sin\theta_{rot}/\cos\varphi]$ $\qquad$ [C.16g]

$90°< \theta_{rot}< 180°$, $\qquad \theta_{Moon} = 360° - \text{asin}[\sin(\varphi_{mer}+\varphi_{lat})\sin\theta_{rot}/\cos\varphi]$ $\qquad$ [C.16h]

Southern Hemisphere:

$-90° < (\varphi_{mer}+\varphi_{lat}) < 0°,\ -180° < \theta_{rot} < -90°,$ $\qquad \theta_{Moon} = 180° - asin[sin(\varphi_{mer}+\varphi_{lat})sin\theta_{rot}/cos\varphi]$ $\qquad$ [C.16i]

$\qquad\qquad\qquad -90° < \theta_{rot} < 0°,$ $\qquad \theta_{Moon} = asin[sin(\varphi_{mer}+\varphi_{lat})sin\theta_{rot}/cos\varphi]$ $\qquad$ [C.16j]

$\qquad\qquad\qquad\quad 0° < \theta_{rot} < 90°,$ $\qquad \theta_{Moon} = 360° + asin[sin(\varphi_{mer}+\varphi_{lat})sin\theta_{rot}/cos\varphi]$ $\qquad$ [C.16k]

$\qquad\qquad\qquad\ 90° < \theta_{rot} < 180°,$ $\qquad \theta_{Moon} = 180° - asin[sin(\varphi_{mer}+\varphi_{lat})sin\theta_{rot}/cos\varphi]$ $\qquad$ [C.16l]

$-180° < (\varphi_{mer}+\varphi_{lat}) < -90°,\ -180° < \theta_{rot} < -90°,$ $\qquad \theta_{Moon} = 180° - asin[sin(\varphi_{mer}+\varphi_{lat})sin\theta_{rot}/cos\varphi]$ $\qquad$ [C.16m]

$\qquad\qquad\qquad -90° < \theta_{rot} < 0°,$ $\qquad \theta_{Moon} = asin[sin(\varphi_{mer}+\varphi_{lat})sin\theta_{rot}/cos\varphi]$ $\qquad$ [C.16n]

$\qquad\qquad\qquad\quad 0° < \theta_{rot} < 90°,$ $\qquad \theta_{Moon} = 360° + asin[sin(\varphi_{mer}+\varphi_{lat})sin\theta_{rot}/cos\varphi]$ $\qquad$ [C.16o]

$\qquad\qquad\qquad\ 90° < \theta_{rot} < 180°,$ $\qquad \theta_{Moon} = 180° - asin[sin(\varphi_{mer}+\varphi_{lat})sin\theta_{rot}/cos\varphi]$ $\qquad$ [C.16p]

where φ is from Eqn [C.11], $0° < \theta_{Moon} < 360°$ and true north is at $0°$.

Times of Moonrise and Moonset

Defining the rotation angles θ_{rot1} for moonrise and θ_{rot2} for moonset (where $\varphi = 0°$), from Eqn [C.11] we have $[cos\theta_{rot}sin(\varphi_{mer}+\varphi_{lat})cos\varphi_{lat} - cos(\varphi_{mer}+\varphi_{lat})sin\varphi_{lat}] = 0$ and so:

$$cos\theta_{rot} = cos(\varphi_{mer}+\varphi_{lat})sin\varphi_{lat}/sin(\varphi_{mer}+\varphi_{lat})cos\varphi_{lat}$$
$$= tan\varphi_{lat}/tan(\varphi_{mer}+\varphi_{lat})$$
$$\theta_{rot} = \pm acos[tan\varphi_{lat}/tan(\varphi_{mer}+\varphi_{lat})]$$

thus:

$$\theta_{rot1} = -acos[tan\varphi_{lat}/tan(\varphi_{mer}+\varphi_{lat})] \qquad\qquad\text{[C.17]}$$
$$\theta_{rot2} = +acos[tan\varphi_{lat}/tan(\varphi_{mer}+\varphi_{lat})] \qquad\qquad\text{[C.18]}$$

where $\theta_{rot1} < 0°$. From Eqns [C.2] and [C.4], the times (in hours) of of moonrise and moonset may be calculated as:

$$t_{Mrise} = t_{mer} + \theta_{rot1}/14.4920° \qquad\qquad\text{[C.19]}$$
$$t_{Mset} = t_{mer} + \theta_{rot2}/14.4920° \qquad\qquad\text{[C.20]}$$

and for other celestial bodies:

$$t_{rise} = t_{mer} + \theta_{rot1}/15° \qquad\qquad\text{[C.21]}$$
$$t_{set} = t_{mer} + \theta_{rot2}/15° \qquad\qquad\text{[C.22]}$$

Verification

Values from the formulas derived above are compared with those supplied for the Moon by two astronomical data sources, Tables C.1, C.4 and C.5. The same formulas also work for other planetary bodies, such as Jupiter and Saturn, Tables C.2 and C.3.

Tables C.4 and C.5 demonstrate the formulas for two southern hemisphere scenarios. Since the plane of the solar system is below the horizon for a southern hemisphere observer when looking south, the meridian is taken as due north. The rotation angle θ_{rot} still increases east to west and $\theta_{rot} = 0°$ at true north, but φ_{lat} and φ_{mer} are negative values when using the Equations derived here.

The differences in Table C.1, C.4 and C.5 are all within about 10 minutes for time (2.8% of 6 hours away from the meridian), about 3 degrees for the Moon heading angle θ_{Moon} (0.8% of a full circle) and about 0.6 degree for the altitude angle φ (0.7% of a quarter circle), which is acceptable for the current analysis. Somewhat lesser differences arise in Tables C.2 and C.3 for distant planets.

The differences are due to complexity of modelling. The Equations represent the simplest model. The TimeAndDate data takes atmospheric refraction into account but, along with the Almanac data, rounds time to the nearest minute and angles to the nearest degree. Stellarium carries the greatest precision but requires the most computational resources (about a 645 MB executable file size for version 24.2).

The output of Stellarium was obtained using the Astronomical Calculations window. The procedure is:

1) pause the clock from the pop-up task bar at the lower edge of the main window
2) set the Location from the pop-out sidebar on the left edge of the main window, also the Date&Time of the observation, also Configuration/Tools checkbox to display decimal degrees
3) open the Astronomical Calculations window from the sidebar
4) within the Calculations window, clicking the Positions icon brings up a list of visible planets
5) double click on the desired item, which moves the sky view to center on that object
6) using the RTS (Risings, Transits, Settings) icon, choose the range of dates to perform calculations for the selected object
7) click the Calculate button to get approximate times (use Date&Time + update Positions to get times to ±1 second)

	Moonrise Eqns [C.19], [C.17], [C.16e], [C.11]	Moonrise Data (Time+ Date)	Moonrise Data (Stellarium)	Observed Moon Eqns [C.2], [C.16g], [C.11]	Observed Moon Data (Time+ Date)	Observed Moon Data (Stellarium)	Moonset Eqns [C.20], [C.18], [C.16h], [C.11]	Moonset Data (Time+ Date)	Moonset Data (Stellarium)
Time	11:58	11:53	11:53:50	20:30	20:30	20:30:00	00:30	00:26	00:26:24
θ_{rot}	-90.85°	-92.09°	-91.89°	32.78°	32.78°	32.78°	90.85°	89.79°	89.88°
θ_{Moon}	88.73°	86°	86.74°	224.73°	225°	224.99°	271.27°	270°	270.23°
φ	0°	0°	0°	39.71°	39°	39.09°	0°	0°	0°

Table C.1 Terryville CT 15 June 2013 moonrise, moon at observation time and moonset values of time, θ_{rot}, θ_{Moon} and φ from the Equations compared with astronomical data sources (Data: φ_{lat} = 41.6782°, φ_{mer} = 49.2722° at t_{mer} = 18:14:16, θ_{rot}/hr = 14.492°, https://www.timeanddate.com/moon/@4844084?month=6&year=2013 and Stellarium.org).

	Jupiter rise Eqns [C.19], [C.17], [C.16e], [C.11]	Jupiter rise Data (Almanac)	Jupiter rise Data (Stellarium)	Observed Jupiter Eqns [C.2], [C.16h], [C.11]	Observed Jupiter Data (Almanac)	Observed Jupiter Data (Stellarium)	Jupiter set Eqns [C.20], [C.18], [C.16h], [C.11]	Jupiter set Data (Almanac)	Jupiter set Data (Stellarium)
Time	05:35	05:33	05:32:53	20:30	20:30	20:30:00	20:34	20:37	20:37:24
θ_{rot}	-112.41°	-113.03°	-113.06°	111.22°	111.22°	111.22°	112.41°	112.97°	113.07°
θ_{Jup}	58.19°	-	57.61°	301.02°	-	301.17°	301.81°	-	302.40°
φ	0°	0°	0°	0.76°	-	1.01°	0°	0°	0°

Table C.2 Comparison of Terryville CT 15 June 2013 Jupiter rise, Jupiter at observation time and Jupiter set values of time, θ_{rot}, θ_{Moon} and φ from the Equations with astronomical data sources (Data: φ_{lat} = 41.6782°, φ_{mer} = 71.5073° at t_{mer} = 13:05:07, θ_{rot}/hr = 15°, https://www.almanac.com/astronomy/planets-rise-and-set/CT/Terryville/2013-06-15 and Stellarium.org).

	Saturn rise Eqns [C.19], [C.17], [C.16b], [C.11]	Saturn rise Data (Almanac)	Saturn rise Data (Stellarium)	Observed Saturn Eqns [C.2], [C.16b], [C.11]	Observed Saturn Data (Almanac)	Observed Saturn Data (Stellarium)	Saturn set Eqns [C.20], [C.18], [C.16c], [C.11]	Saturn set Data (Almanac)	Saturn set Data (Stellarium)
Time	16:08	16:06	16:06:19	20:30	20:30	20:30:00	02:50	02:52	02:52:14
θ_{rot}	-80.21°	-80.82°	-80.74°	14.82°	14.82°	14.82°	80.21°	80.68°	80.74°
θ_{Sat}	104.55°	-	104.06°	161.97°	-	161.92°	255.45°	-	255.94°
φ	0°	0°	0°	35.77°	-	35.76°	0°	0°	0°

Table C.3 Comparison of Terryville CT 15 June 2013 Saturn rise, Saturn at observation time and Saturn set values of time, θ_{rot}, θ_{Moon} and φ from the Equations with astronomical data sources (Data: φ_{lat} = 41.6782°, φ_{mer} = 37.5093° at t_{mer} = 21:29:16, θ_{rot}/hr = 15°, https://www.almanac.com/astronomy/planets-rise-and-set/CT/Terryville/2013-06-15 and Stellarium.org).

	Moonrise Eqns [C.19], [C.17], [C.16j], [C.11]	Moonrise Data (Time+Date)	Moonrise Data (Stellarium)	Observed Moon Eqns [C.2], [C.16k], [C.11]	Observed Moon Data (Time+Date)	Observed Moon Data (Stellarium)	Moonset Eqns [C.20], [C.18], [C.16k], [C.11]	Moonset Data (Time+Date)	Moonset Data (Stellarium)
Time	11:11	11:14	11:14:44	20:30	20:30	20:30:00	23:23	23:24	23:24:42
θ_{rot}	-88.41°	-87.79°	-87.62°	46.50°	46.50°	46.50°	88.41°	88.53°	88.70°
θ_{Moon}	86.39°	86°	86.74°	296.06°	295°	294.89°	268.14°	272°	270.23°
φ	0°	0°	0°	36.28°	36°	36.00°	0°	0°	0°

Table C.4 Johannesburg, South Africa 15 June 2013 moonrise, moon at observation time and moonset values of time, θ_{rot}, θ_{Moon} and φ from the Equations compared with astronomical data sources (Data: φ_{lat} = -26.2056°, φ_{mer} = -60.5603° at t_{mer} = 17:17:29, θ_{rot}/hr = 14.492°, https://www.timeanddate.com/moon/@4844084?month=6&year=2013 and Stellarium.org).

	Moonrise Eqns [C.19], [C.17], [C.16m], [C.11]	Moonrise Data (Time+Date)	Moonrise Data (Stellarium)	Observed Moon Eqns [C.2], [C.16o], [C.11]	Observed Moon Data (Time+Date)	Observed Moon Data (Stellarium)	Moonset Eqns [C.20], [C.18], [C.16p], [C.11]	Moonset Data (Time+Date)	Moonset Data (Stellarium)
Time	13:35	13:39	13:41:50	20:30	20:30	20:30:00	03:21	03:31	03:29:37
θ_{rot}	-99.73°	-98.82°	-98.13°	0.45°	0.45°	0.45°	99.73°	102.14°	101.81°
θ_{Moon}	101.85°	101°	100.34°	359.39°	359°	359.39°	258.15°	255°	255.29°
φ	0°	0°	0°	41.98°	42°	41.99°	0°	0°	0°

Table C.5 Ushuala, Argentina 17 June 2013 moonrise, moon at observation time and moonset values of time, θ_{rot}, θ_{Moon} and φ from the Equations compared with astronomical data sources (Data: φ_{lat} = -54.8108°, φ_{mer} = -41.9860° at t_{mer} = 20:28:07, θ_{rot}/hr = 14.492°, https://www.timeanddate.com/moon/@4844084?month=6&year=2013 and Stellarium.org).

APPENDIX D – Stretched Angle-of-View

A formula is derived for the stretched angle-of-view $\alpha_{stretch}$ of Eqn [A.2] in Appendix A. It involves solving two sets of two simultaneous equations, including one equation obtained from differential calculus.

Since the Moon is at an angle φ above the horizon, the actual distance of wave travel across the elliptical field-of-view will be over twice the stretched semi-axial length $b_{stretch}$, Fig. D.1.

Three points are highlighted in red. The initial point of wave contact with the ellipse is at (x_1, y_1) and the terminating point of contact is on the opposite side of the ellipse. An intersection of the wavefront with the travel vector passing through the center of the circle is at (x_2, y_2). The wavefront is indicated as a grey line at three positions during its transit of the field-of-view and is oriented at a fixed angle θ_{wave} relative to the x-y reference frame.
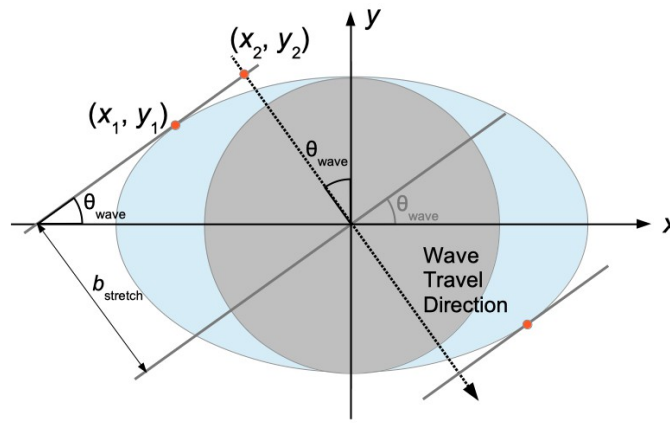

Fig. D.1 Geometry for determining the travel distance $2b_{stretch}$ of the wavefront across the ellipse. The circle has radius b. The orthogonal wave travel component (vector) is the dotted line.

Determining the Point of Contact (x_1, y_1)

An ellipse is defined by the formula $1 = X^2 + Y^2$, where $X = x/a$ and $Y = y/b$ and the ellipse semi-axial lengths are a and b, Fig. A.2 in Appendix A. In Fig D.1, the graphical curve of the ellipse in the neighbourhood of (x_1, y_1) is given by:

$$y = b[1 - (x/a)^2]^{1/2} \tag{D.1}$$

and thus, for the point of initial contact, $y_1 = b[1 - (x_1/a)^2]^{1/2}$. Also, the wavefront passing through (x_1, y_1) is defined by the line:

$$y = y_1 + (x - x_1) \tan\theta_{wave} \tag{D.2}$$

The local slope of the ellipse is the derivative from differential calculus:

$$dy/dx = -(b/2)(2x/a^2)/[1 - (x/a)^2]^{1/2} \tag{D.3}$$

33

and this is equated to the slope of the wavefront $\tan\theta_{wave}$ at (x_1, y_1). Rearranging and solving for the x-position:

$$\tan\theta_{wave}[1 - (x_1/a)^2]^{1/2} = -(b/a)(x_1/a)$$
$$\tan^2\theta_{wave}[1 - (x_1/a)^2] = (b/a)^2(x_1/a)^2$$
$$(x_1/a)^2\,[(b/a)^2 + \tan^2\theta_{wave}] = \tan^2\theta_{wave}$$

we obtain:

$$x_1 = -a\,\tan\theta_{wave}/(\sin^2\varphi + \tan^2\theta_{wave})^{1/2} \qquad\text{[D.4]}$$

where $b/a = \sin\varphi$ was used and $x_1 < 0$ for $0° < \theta_{wave} < 90°$. Eqn [D.4] may be substituted into Eqn [D.1] to get y_1 and thus (x_1, y_1):

$$y_1 = b[1 - \tan^2\theta_{wave}/(\sin^2\varphi + \tan^2\theta_{wave})]^{1/2}$$
$$= b[(\sin^2\varphi + \tan^2\theta_{wave} - \tan^2\theta_{wave})/(\sin^2\varphi + \tan^2\theta_{wave})]^{1/2}$$
$$= b\,\sin\varphi/(\sin^2\varphi + \tan^2\theta_{wave})^{1/2} \qquad\text{[D.5]}$$

Determining the Point of Intersection (x_2, y_2)

The travel vector in Fig. D.1 passes through the origin of the x-y coordinates and is shown as a line that is orthogonal to the wavefront, with the equation:

$$y = -x/\tan\theta_{wave} \qquad\text{[D.6]}$$

This line intersects Eqn [D.2] at the point (x_2, y_2), which can be determined by simultaneously solving Eqns [D.2] and [D.6]. From this, the x-position is:

$$y_2 = -x_2/\tan\theta_{wave} = y_1 + (x_2 - x_1)\,\tan\theta_{wave}$$
$$x_2\,(\tan\theta_{wave} + 1/\tan\theta_{wave}) = -y_1 + x_1\tan\theta_{wave}$$

$$x_2 = (x_1\tan^2\theta_{wave} - y_1\tan\theta_{wave})/(\tan^2\theta_{wave} + 1)$$
$$= (x_1\tan^2\theta_{wave} - y_1\tan\theta_{wave})\cos^2\theta_{wave}$$
$$= x_1\sin^2\theta_{wave} - y_1\sin\theta_{wave}\cos\theta_{wave} \qquad\text{[D.7]}$$

From Eqn [D.6], the y-position is:

$$y_2 = -x_2/\tan\theta_{wave} \qquad\text{[D.8]}$$

Determining the Stretched Angle-of-View

Using the Pythagorean theorem and Eqn [D.8] to calculate the length $b_{stretch}$, Fig. D.1:

$$b_{stretch} = [x_2^2 + y_2^2]^{1/2}$$
$$= |x_2|[1 + 1/\tan^2\theta_{wave}]^{1/2}$$
$$= |x_2/\sin\theta_{wave}|$$

where $b_{stretch} > 0$ for all x_2 values. Substituting x_2 from Eqn [D.7]:

$$b_{stretch} = |(x_1\sin^2\theta_{wave} - y_1\sin\theta_{wave}\cos\theta_{wave})/\sin\theta_{wave}|$$
$$= |x_1\sin\theta_{wave} - y_1\cos\theta_{wave}|$$

From Eqns [D.4] and [D.5], $x_1 = -a\,\tan\theta_{wave}/(\sin^2\varphi + \tan^2\theta_{wave})^{1/2}$ and $y_1 = b\,\sin\varphi/(\sin^2\varphi + \tan^2\theta_{wave})^{1/2}$, so:

$$b_{stretch} = |(a\,\tan\theta_{wave}\sin\theta_{wave} + b\,\sin\varphi\,\cos\theta_{wave})|/(\sin^2\varphi + \tan^2\theta_{wave})^{1/2}$$
$$= b\,|(\tan\theta_{wave}\sin\theta_{wave}/\sin\varphi + \sin\varphi\,\cos\theta_{wave})|/(\sin^2\varphi + \tan^2\theta_{wave})^{1/2}$$
$$= b\,|(\tan^2\theta_{wave}/\sin\varphi + \sin\varphi)\cos\theta_{wave}|/(\sin^2\varphi + \tan^2\theta_{wave})^{1/2}$$

where $a = b/\sin\varphi$ was used. Finally, creating a common denominator ($\sin\varphi$),

$$b_{stretch} = b(\tan^2\theta_{wave} + \sin^2\varphi)\,\cos\theta_{wave}/[\sin\varphi\,(\sin^2\varphi + \tan^2\theta_{wave})^{1/2}]$$
$$= b(\tan^2\theta_{wave} + \sin^2\varphi)^{1/2}\,\cos\theta_{wave}/\sin\varphi$$
$$= b(\sin^2\theta_{wave}/\sin^2\varphi + \cos^2\theta_{wave})^{1/2} \tag{D.9}$$

or, substituting $b = \alpha/2$, the wave will travel over the stretched (elliptical) angle-of-view:

$$\alpha_{stretch} = \alpha(\sin^2\theta_{wave}/\sin^2\varphi + \cos^2\theta_{wave})^{1/2} \tag{D.10}$$

Fig. D.2 shows the graphical relationship of $\alpha_{stretch}/\alpha$ versus θ_{wave} for several altitude angles φ. It is noted that Eqns [D.9] and [D.10] are positive for all wavefront angles $-180° < \theta_{wave} < 180°$.

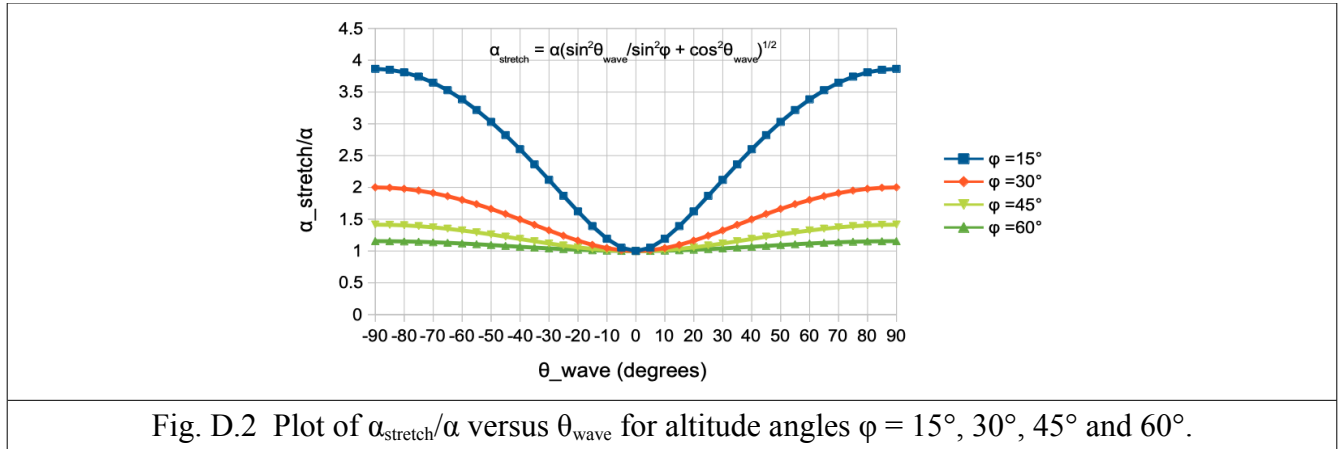Fig. D.2 Plot of $\alpha_{stretch}/\alpha$ versus θ_{wave} for altitude angles $\varphi = 15°, 30°, 45°$ and $60°$.

APPENDIX E – Refractive Index Models for Image Shift

There are two proposed models to explain the cause of the lunar wave phenomenon:
1) They are generated by the wake of a passing aircraft in the lower atmosphere (Appendix G).
2) They are generated during a plasma event in the upper atmosphere, triggered by a celestial or planetary alignment (Appendix H).

In either case, the result is a pair of nearly straight tube-like structures or vortices that can persist for several minutes and which may be observed moving across the face of the Moon or a bright planet, hence the name "lunar waves". A distinctive feature is a shift in the apparent position of well-lit background objects, such as lunar craters, as each wave passes by, Fig. E.1.
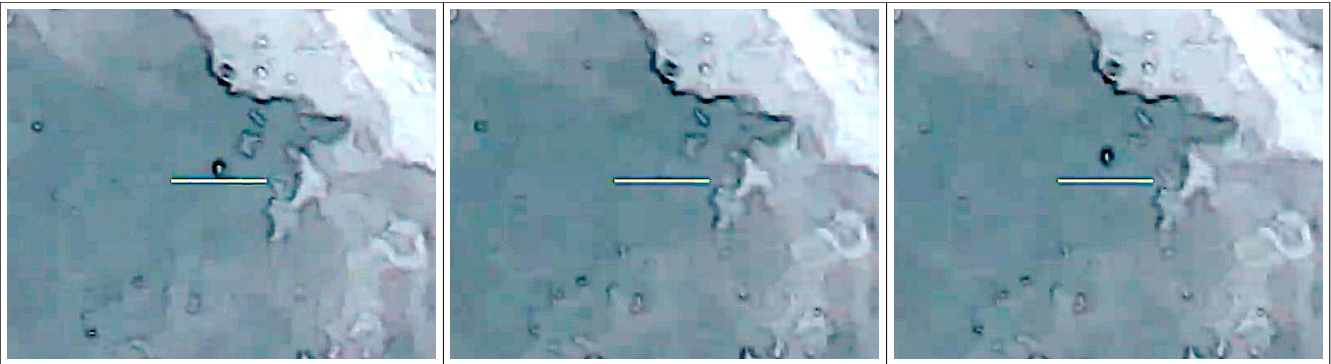
Fig. E.1 Left: the position of a crater before the wave passes by, Center: the wave is passing over the crater, Right: the crater appears to have shifted upward in the direction of wave travel
(Video: Crrow777, https://www.youtube.com/watch?v=0u5Bh5PJGuI, video time code 01:52)

Simple Model

Presuming the waves are located in Earth's atmosphere, it follows that the moving wavefronts or vortices are made of heated (or cooled) gas acting as lenses, causing a ripple effect to move over the image of background objects. To account for the double shift of the image, there must be at least three distinct regions within a layer (or in closely spaced layers) separated by two wavefronts passing by the observer. Each of the moving wavefronts would have a difference in gas density, causing two different indices of refraction to operate.
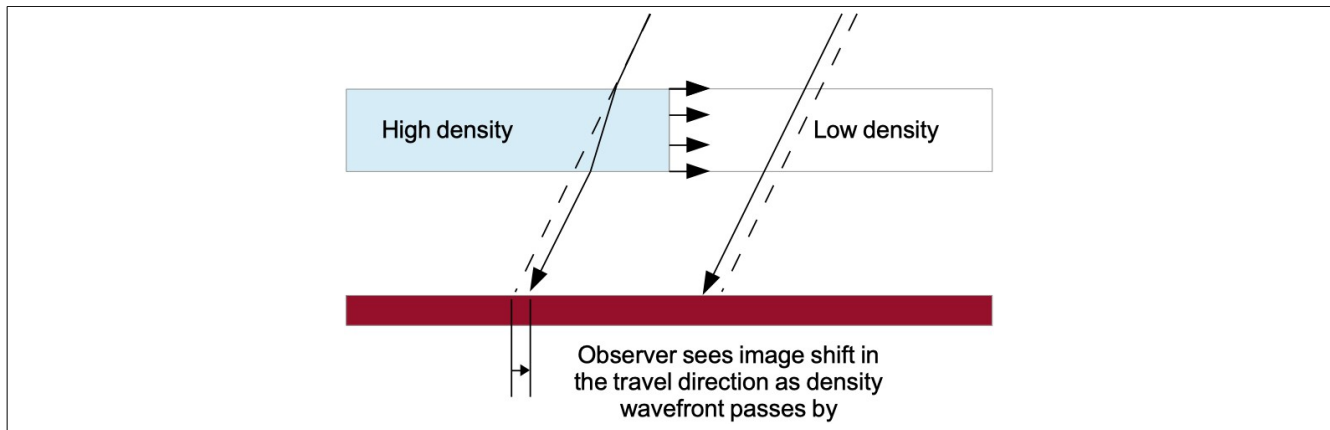

Fig. E.2 A simple refractive index model to explain the observed ripple effect where a background object appears to shift in the north-to-south direction of wave travel.

Almost all known results have been from observers in the northern hemisphere. Since the Moon and other solar system bodies are located essentially in a plane, those observers will be looking southward with either an eastward (moonrise) or westward (moonset) component.

Fig. E.2 shows light rays coming from a background celestial object and passing through the atmosphere. A single wavefront between gases of two differing densities is shown moving north to south, which is in an opposing direction to the incoming light rays from the southern sky. Due to a difference in the refractive index of the two regions, a shift in the position of the background image is observed as the wave passes by.

36

Vortex Model

For the case of a vortex trail, Fig. E.3, the observer will see two closely spaced edges straddling the vortex axis. The core of the rapidly spinning vortex has lower pressure and thus a lower density and temperature compared with the ambient air. The lower density causes the core to have a lower index of refraction, which gives rise to the mirage effect, Fig. E.4.

If the vortex is seen at a shallow angle, looking along the axis, the cross-section appears as an ellipse, Fig. E.5. The optical paths diverge strongly, causing the mirage effect to be more pronounced compared with a view looking straight across the circular cross-section.

Mirages are usually not larger than about 0.5 degrees, or about the angular diameter of the Sun and Moon (https://en.wikipedia.org/wiki/Mirage). The result is an inversion of the background image on both sides of the vortex core, which is a key observation in many lunar wave videos.
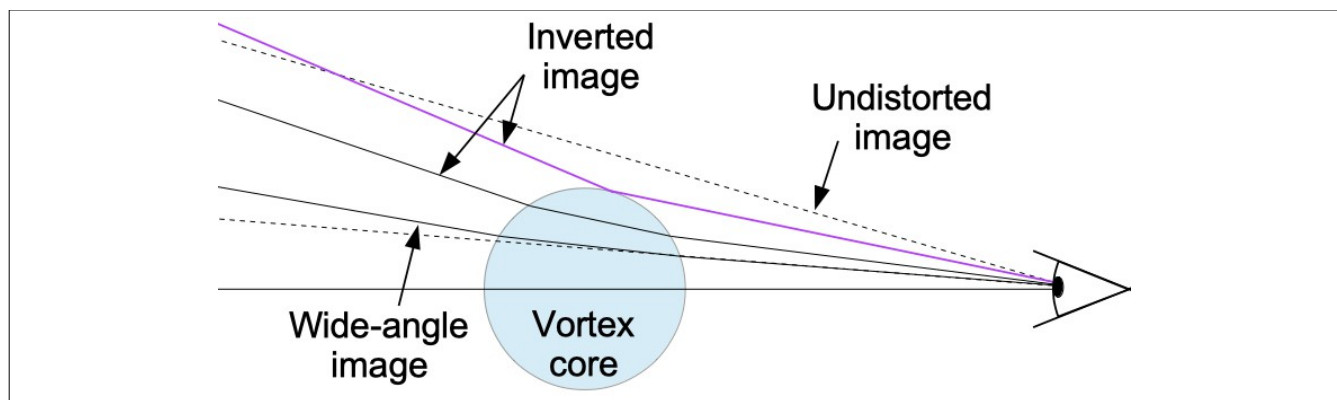

Fig. E.3 Refraction of light rays through a vortex core of circular cross-section and relatively low index of refraction. Most of the refracted background image is seen over a wider angle than normal, causing some image inversion. The purple ray indicates part of the image is inverted due to reflection.
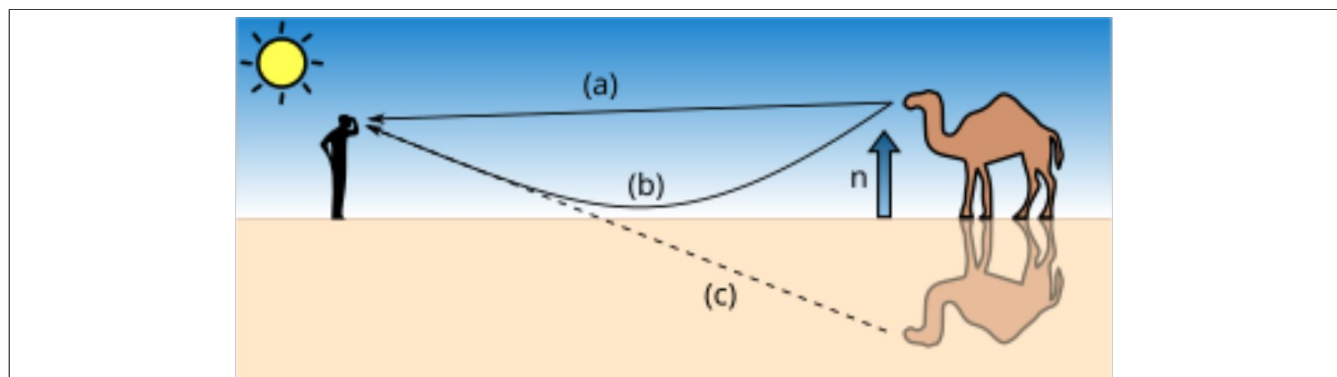

Fig. E.4 Schematic of a mirage showing a) the unrefracted line of sight, b) the refracted light path (resembling a "soft" reflection) and c) the apparent position of the refracted image
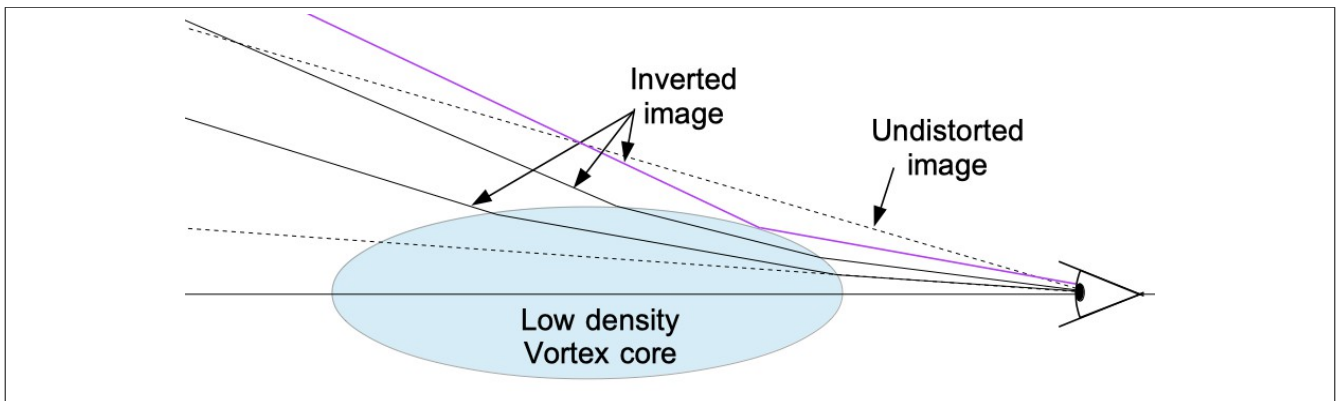(Source: https://en.wikipedia.org/wiki/Mirage).

Fig. E.5 A shallow viewing angle (close to the vortex axis) makes the mirage effect more pronounced. At an angle, the vortex cross-section appears as an ellipse.

In Fig. E.6, there is a noticeable difference between the observed images due to the angle at which the vortex core is viewed. The mirage effect is weakest for the left-hand image, since the view is orthogonal to the vortex axis. The mirage is strongest strongest for the center image, where the view is closely aligned with the vortex axis (in 3-dimensional space), giving an elliptical mirage shape. The viewing angle of the right-hand image is somewhere in between.
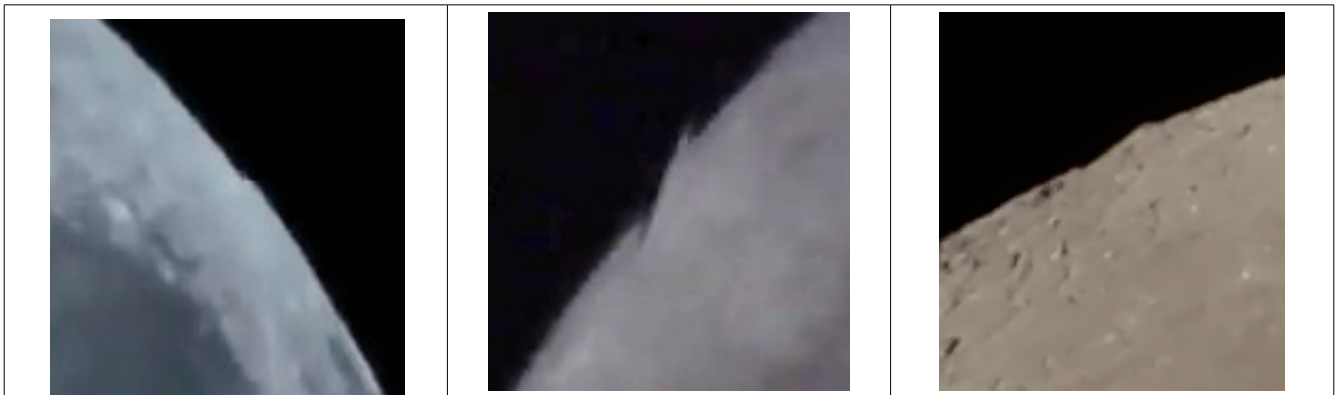

Fig. E.6 Lunar wave closeups showing an image shift, inversion or discontinuity near the lunar rim.
(Left: Crrow777, https://youtu.be/_3axPn65MGM?si=cd1HxgAep9woWlxk, video time code 00:30
Center: Take Back Space, https://www.youtube.com/watch?v=Prl5yYHKHic, video time code 00:56
Right: Jayling, https://youtu.be/XIKAJK1sNSg?si=SxXENF_SmgJ9kEJH, video time code 05:18)

Heated Zone with Dual Vortices

Combining the effects of the two models above, the situations of both an aircraft wake and a plasma-induced event may be modelled, Figs E.7 and E.8. In the first case, the heated wake moves downward as a reaction to the lift generated by the aircraft wings to maintain altitude during flight. In the second case, the rising column of heated gas causes the ring vortex to move upwards.

In both cases, there is mixing of hot and cold air at the edges of the heated zone. This, in turn, provides the range of indices of refraction needed to explain the double image shift of background objects observed in lunar wave videos.
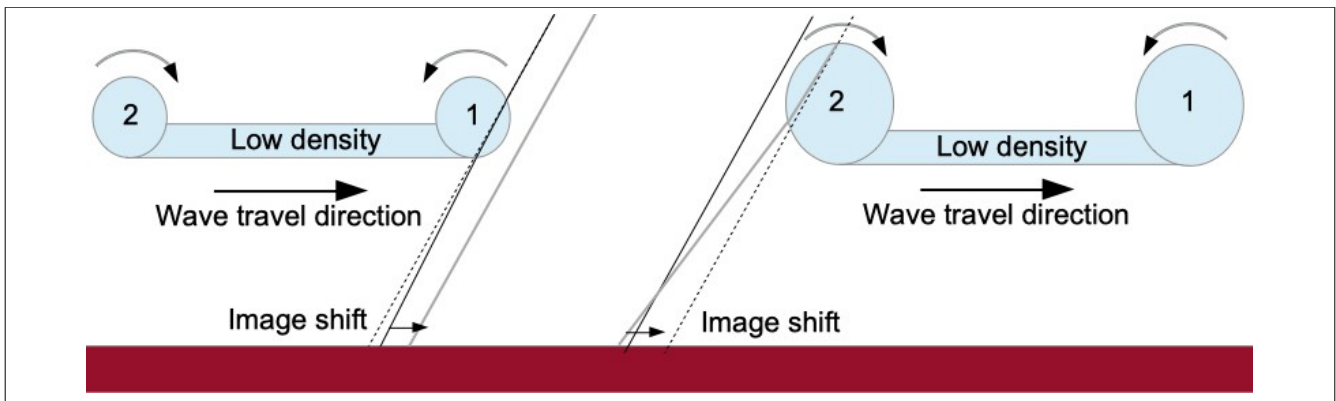
Fig. E.7 Left: refraction by the first vortex of a sinking aircraft wake, Right: the second vortex is more diffuse. The solid grey line is the light ray seen just before the vortex boundary passes the observer, the solid black line just after it passes. Both vortices cause image shift in the travel direction.
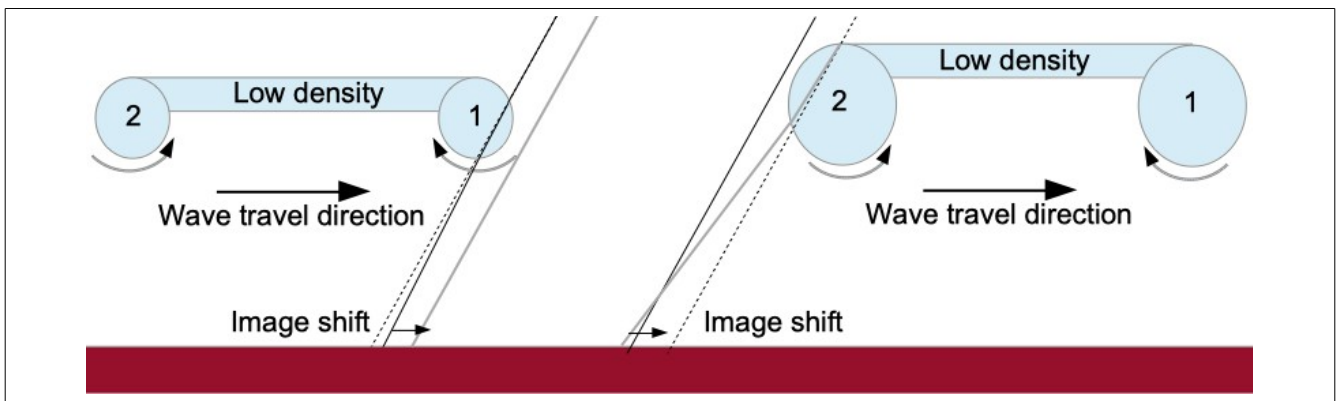

Fig. E.8 Left: refraction by the leading edge of a rising ring vortex, Right: the trailing edge is more diffuse. The solid grey line is the light ray seen just before the vortex boundary passes the observer, the solid black line just after it passes. Both vortices cause image shift in the travel direction.

Refractive Index Calculations

For a freshly generated, highly intense vortex, the core density of the air may be about 80% of the ambient value (https://en.wikipedia.org/wiki/Wingtip_vortices). Based on this value, Table E.1 indicates the difference in vortex refractive indices for air at nominal altitudes. The higher the altitude, the thinner the air and the smaller the difference between the vortex density and that of the ambient air.

From a curve-fit of air density data, Fig. E.9 and Table E.1, (U.S. Standard Atmosphere data, https://www.engineeringtoolbox.com/standard-atmosphere-d_604.html), ambient air density as a function of altitude h is approximately:

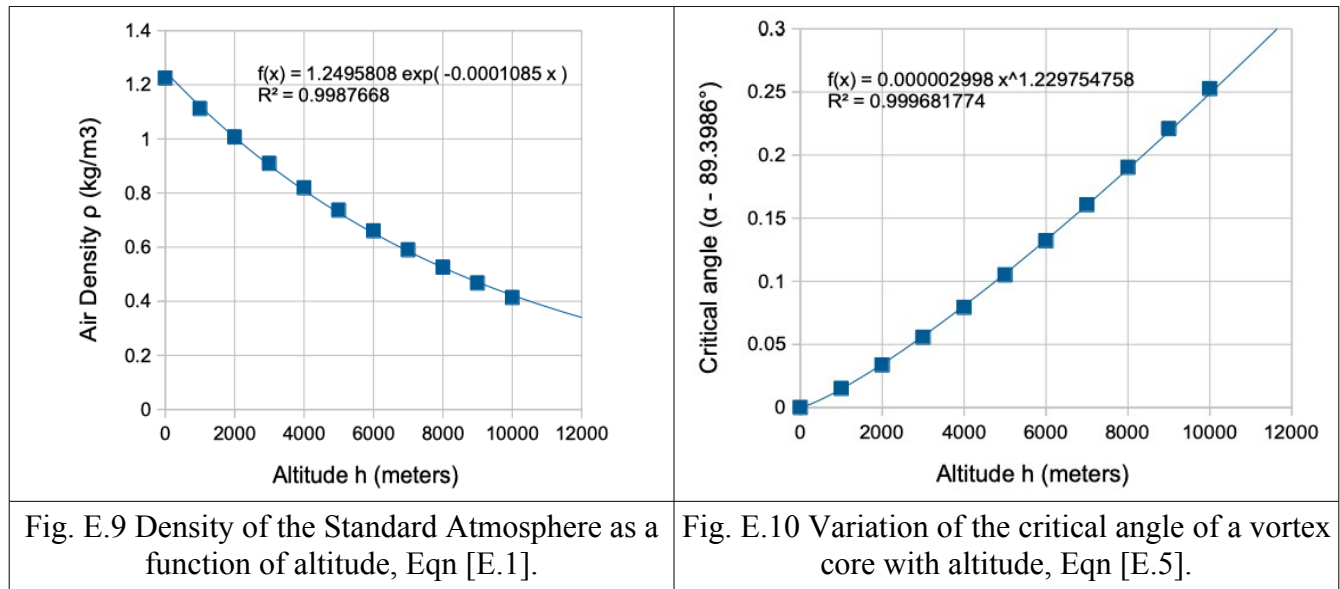$$\rho_1 = 1.250 \exp(-1.085\text{E-}4\ h) \qquad\qquad [\text{E.1}]$$

where ρ_1 is the density expressed in kg/m^3 and h is in meters. This includes the effect of temperature at the given altitude and is accurate to about 2% for $h < 11{,}000$ m (36,000 ft). Above this altitude, the stratosphere begins and the temperature becomes warmer as h increases.

A nominal value for the index of refraction for air is $n_1 = 1.000272$ at 1 atmosphere pressure and 20°C (68°F) (https://emtoolbox.nist.gov/Wavelength/Documentation.asp). This increases to $n_1 = 1.000293$ at a lower temperature of 0°C (32°F) due to an increase in density. From the ideal gas law and Eqn [E.1], a formula for the refractive index n_1 as a function of ambient air density ρ_1 may be expressed:

$$n_1 = 1 + 0.000277(\rho_1/\rho_0)$$
$$= 1 + 0.000277 \exp(-1.085\text{E-}4\ h) \qquad \text{[E.2]}$$

where $\rho_0 = 1.225$ kg/m³ at Standard Atmosphere values of 1 atmosphere pressure and 15°C (59°F). For a vacuum, $\rho_1 = 0$ and $n_1 = 1$. For a vortex core density where $\rho_2 = 0.8\rho_1$, the formula used in Table E.1 becomes:

$$n_2 = 1 + 0.000277(\rho_2/\rho_0)$$
$$= 1 + 0.0002219 \exp(-1.085\text{E-}4\ h) \qquad \text{[E.3]}$$

Fig. E.9 Density of the Standard Atmosphere as a function of altitude, Eqn [E.1].	Fig. E.10 Variation of the critical angle of a vortex core with altitude, Eqn [E.5].

Finally, the critical angle θ_c where reflection of light occurs at the interface between the ambient and the core densities, Fig. E.11, is calculated using Snell's law:

$$\theta_c = \operatorname{asin}(n_2/n_1) \qquad \text{[E.4]}$$

where $n_2 < n_1$, calculated from Eqns [E.2] and [E.3]. A curve-fit of the critical angle in degrees as a function of altitude h in meters, Fig. E.10, accurate to about 0.004 degrees is:

$$\theta_c = 89.3986° + 2.998\text{x}10^{-6}\ h^{1.230} \qquad \text{[E.5]}$$

Table E.1 lists the maximum angle $\alpha_c = 90° - \theta_c$ to obtain reflection of light from the vortex core. All values are 0.6 degrees or less, which is in the range of that observed for a mirage. Note that as the vortex fades, the density difference becomes less and so the maximum angle α_c reduces. Eventually the vortex core becomes too weak and diffuse to be seen optically.
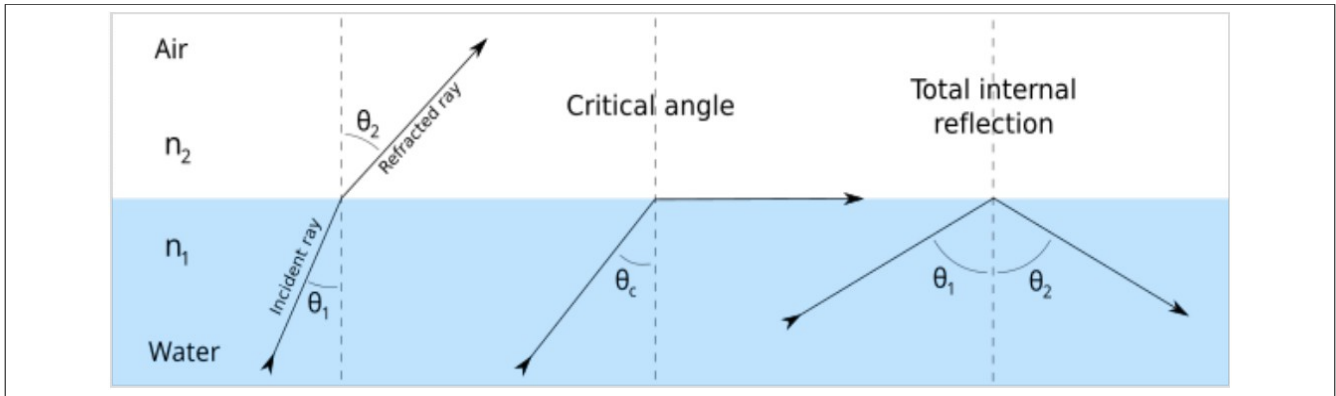
Fig. E.11 Examples of refraction or reflection of a light ray approaching a boundary between two transparent media of differing indices of refraction (Source: https://en.wikipedia.org/wiki/Snell%27s_law).

Altitude h	Ambient air density ρ_1 (kg/m³)	Ambient refractive index n_1, Eqn [E.2]	Vortex refractive index n_2, Eqn [E.3]	Critical angle $\theta_c = asin(n_2/n_1)$ (degrees)	Angle-of-reflection $\alpha_c = 90° - \theta_c$
0 m (0 ft) – sea level	1.225	1.0002770	1.0002219	89.3986	0.6014°
1,000 m (3,280 ft)	1.112	1.0002514	1.0001991	89.4137	0.5863°
2,000 m (6,560 ft)	1.007	1.0002277	1.0001786	89.4323	0.5677°
3,000 m (9,840 ft)	0.9093	1.0002056	1.0001602	89.4543	0.5467°
4,000 m (13,120 ft)	0.8194	1.0001853	1.0001438	89.4780	0.5220°
5,000 m (16,400 ft)	0.7364	1.0001665	1.0001290	89.5037	0.4963°
6,000 m (19,690 ft)	0.6601	1.0001493	1.0001157	89.5308	0.4692°
7,000 m (22,970 ft)	0.59	1.0001334	1.0001038	89.5593	0.4407°
8,000 m (26,250 ft)	0.5258	1.0001189	1.0000932	89.5889	0.4111°
9,000 m (29,530 ft)	0.4671	1.0001056	1.0000836	89.6195	0.3805°
10,000 m (32,810 ft)	0.4135	1.0000935	1.0000750	89.6513	0.3487°

Table E.1 Nominal differences in the index of refraction of air for a vortex core at 80% of the density of ambient air. The maximum angle α_c to obtain reflection from the vortex core is calculated.

Visibility Limit

For a given optical magnification, the limiting factor to see a vortex in clear air is the resolution of the camera, typically 1080 by 1920 pixels per frame for HD quality video.

The video quality of YouTube downloads is often 360 by 640 pixels per frame, which further limits the resolution of a given sighting. If the lunar size is taken as 0.5 degrees and this fills the video frame horizontally, the limit of detection is one pixel covering 0.5°/640 = 0.00078 degrees or 2.8 arcseconds.

From Appendix G, the vortex core diameter in the wake of a smaller commercial-size aircraft is nominally 0.5 meters. The maximum distance from the camera to resolve the vortex, based on Eqn

[A.7] in Appendix A, is:

$$L = 2b/\tan\alpha$$
$$= (0.5m)/\tan(0.00078°)$$
$$= 36.7 \text{ km} \quad \text{or} \quad 22.8 \text{ miles} \qquad \text{[E.6]}$$

With additional zoom magnification of 5 or 6 times, the resolution may approach 0.5 arcseconds (0.00014 degrees), which is achievable even with modest equipment and/or a 4k video camera (2160 by 3840 pixels per frame). This is sufficient for most practical situations to resolve strong lunar waves or vortices at a distance exceeding 100 miles (160 km).

APPENDIX F – Detailed Lighting Analysis

A study of moving or transient aerial light sources gives insight into the possible causes of the lunar wave phenomenon. Currently, the waves are only detected in dark sky conditions against a well-lit background area such as the Moon or a bright planet. Occasionally there may be other light sources, such as:

1) an aircraft moving near the scene
2) an atmospheric plasma discharge
3) a meteor (or meteorite) flash
4) one or more spotlights used for advertising purposes
5) a fireworks display
6) a rocket launch or space capsule reentry
7) a large-scale fire, or
8) a military weapons discharge.

A distinguishing feature for items 1), 4), 5), 6) and 7) is their relatively long duration compared with items 2), 3) and 8). Items 3) and 6) are rare, requiring a relatively large object passing through Earth's atmosphere to create a noticeably bright and rapidly moving light burst. Items 4), 5), 6), 7) and 8) would usually be newsworthy, so may easily be eliminated as sources in a given case.

That leaves items 1) and 2) as the most likely sources of light in addition to the Moon or bright planet. These are readily distinguished by their duration. Two theoretical models based on such occurrences are presented in Appendices G and H.

Recordings of Extra Light Sources

Regarding item 1), there are several videos available online that show an aircraft transiting the face of the Moon. Some of these show the aircraft navigation and landing lights. In particular, the landing lights exceed the intensity of the full Moon, Fig. F.1, and are capable of generating a moving light burst when seen through a telescope at night.

Video recordings of aircraft transits provide a baseline to evaluate other videos where an extra light source may have appeared just outside the view of the camera.

It is noted that video cameras with rectangular fields-of-view are mounted on round-barrelled

telescopes in order to capture fleeting events such as the lunar waves. The rectangular field or frame is usually zoomed-in so that the circular view of the telescope is not apparent, Fig. F.2.

In terms of a passing aircraft, the light source could move across the telescope field-of-view in an area not covered by the camera frame. In such a case, the high-intensity landing lights could indirectly illuminate the image over several video frames, Fig. F.2, causing either:
- a) a diffuse light pulse (glancing light source, indicated by the red arrow), or
- b) an internal reflection (curved waves and well-aligned light source, indicated by black arrows).

In terms of a plasma event, a light pulse lasting for just one video frame might be linked to a celestial trigger creating the waves.

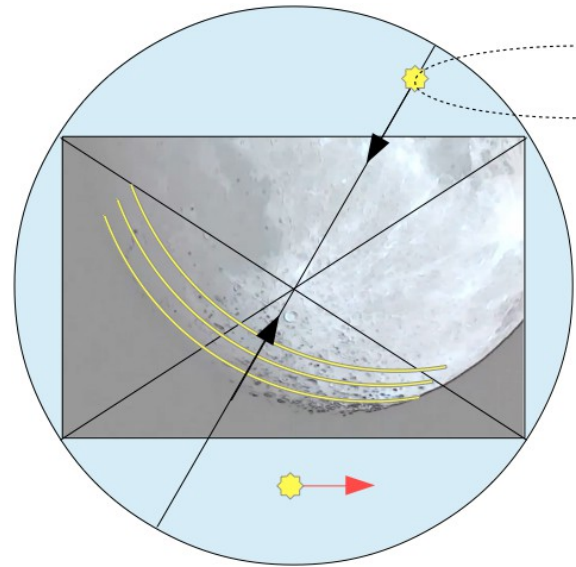|	
Fig. F.1 An aircraft during takeoff with landing lights brighter than the Moon (Video: Crosswind, https://www.youtube.com/watch?v=0i8xsxdhWkY, video time code 01:55).	Fig. F.2 A rectangular camera frame fitted within a circular telescope field-of-view. Moving light pulses could emanate from the areas not videoed (Video: Crrow777, https://www.youtube.com/watch?v=iMQTEEbtTYc, video time code 03:20).

Edge Detection Filter

While a pair of waves is directly visible in most lunar wave videos, they can be faint and difficult to see especially when the video is paused. To enhance the image, applying filters such as edge detection can improve the contrast so that subtle effects become noticeable, Fig. F.2.

The edge detection filter behaves differently under different circumstances:
1) for a static image, there is no motion blur and even the faintest edges can be rendered
2) for a panning motion, the motion blur means only the most pronounced edges are rendered
3) for a localized moving area or object, motion blur can reduce the rendering locally, thus for the Moon viewed through a shimmering atmosphere, the filtered video appears to pulsate
4) the sensitivity to subtle effects is increased so that diffuse light pulses and internal reflections are more noticeable.

First Light Pulse

The earliest (and probably the most scrutinized) lunar wave event is that of Crrow777 from 2012. In his 2015 derivative video, the waves are presented both in the original form and with various filters to obtain the maximum information possible (https://www.youtube.com/watch?v=iMQTEEbtTYc).

In the edge detection mode, a brief increase in the light level of the whole scene is seen over 4 video frames, at time codes 1:58:*06* to 1:58:*09*. This is followed by the first appearance of a wave at 1:59:*20*, just 41 frames later (1.37 seconds at 30 fps).

Since the duration of the light pulse was longer than one video frame, the close proximity of a passing aircraft would best account for the appearance of the waves. The very short delay would also explain the strong contrast of the freshly generated waves (vortices, Appendix G) against the lunar background, which has made this sighting the prime reference for the study of lunar waves.

Curved Waves

In the same case, the edge detection filter enabled observation of a curved wave simultaneously with the straight wave event, Fig. F.2. The brief appearance of the curved wavefront has been interpreted as an energy pulse apparently following the spherical lunar surface.

From a lighting perspective, even the most advanced telescope equipment is subject to internal reflections within the round barrel of the telescope and/or the smaller barrel of the eyepiece, Fig. F.3. The optics of the eyepiece in any telescope may also be subject to lens flare in the presence of a very intense light source, Fig. F.4.

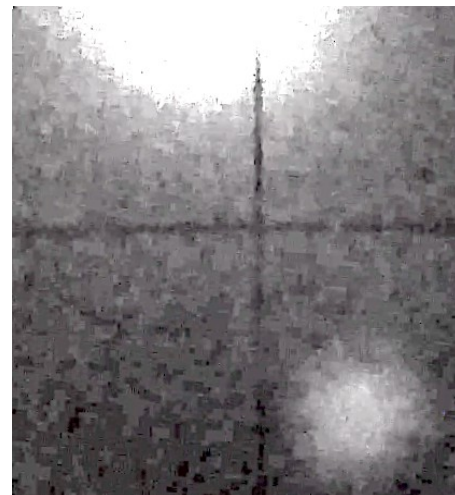|	
Fig. F.3 An enhanced and cropped video frame showing the reflection of an overexposed Moon from inside the circular telescope barrel.	Fig. F.4 An enhanced and cropped video frame showing lens flare (lower right) from an overexposed Moon.

Since the diameters of the barrels of many amateur telescopes and eyepieces are similar to the apparent

size of the Moon, it would explain the similar curvature of any internal reflections to that of the image under observation.

Furthermore, the travel direction of the curved internal reflections would point towards the moving light source, which would be approaching from the opposite direction (black arrows, Fig. F.2). This would indicate that a second aircraft was in the area, possibly executing a turn (dotted curve) to follow the first aircraft. The powerful landing lights may have pointed briefly straight at the telescope and caused internal reflections.

Recommendations

Since there was no audio track accompanying the original sighting by Crrow777, nor a second wide-angle camera to monitor the area of the sky around the Moon, there is no proof that this lunar wave event was actually caused by aircraft. The durations of the light pulses only indicate a plasma event was not responsible, so the aircraft theory becomes the most probable explanation.

It is recommended that future astronomical observations be accompanied by recordings of both ambient audio and wide-angle video, which would provide definitive proof of any nearby aircraft.

APPENDIX G – Aircraft Wake Analysis

There are two theories proposed to explain the cause of the lunar wave phenomenon. These assume either a lower atmosphere cause or an upper atmosphere cause for the waves. The first, presented here, is the more advanced theory and is based on data gained from more than a century of aerodynamic study and practice. The second theory is more speculative, presented in Appendix H, serving as a space-age alternative.

Fig. G.1 Refraction of the lunar rim by the flap-induced vortex of an aircraft at takeoff (Video: Crosswind, https://www.youtube.com/watch?v=7tLziSDYFiw, video time code 00:44).	Fig. G.2 Enhanced video still frame showing one of a pair of aircraft induced refractive waves (Video: Crosswind, https://www.youtube.com/watch?v=7tLziSDYFiw, video time code 00:49).

Observations supporting a lower atmosphere model for the lunar waves are:

1) A convincing lunar wave effect has been observed repeatedly in video recordings within a few seconds after an aircraft crosses the face of the Moon during takeoff, Figs G.1 and G.2.

2) Most modern commercial aircraft have two engines which leave a twin trail of exhaust plumes along the flight path. The plumes consist of a heated mass of exhaust gases ejected from the engines into the much colder ambient atmosphere.

3) The aircraft wake also includes a pair of wingtip vortices during normal flight, Fig. G.3, and flap-induced vortices during takeoff or landing, Fig. G.1. The lingering trail of these intense vortices presents a significant hazard to closely following aircraft (https://mms-safetyfirst.s3.eu-west-3.amazonaws.com/pdf/safety+first/wake-vortices.pdf, https://pilotinstitute.com/wingtip-vortices/, https://www.faa.gov/air_traffic/publications/atpubs/aim_html/chap7_section_4.html).
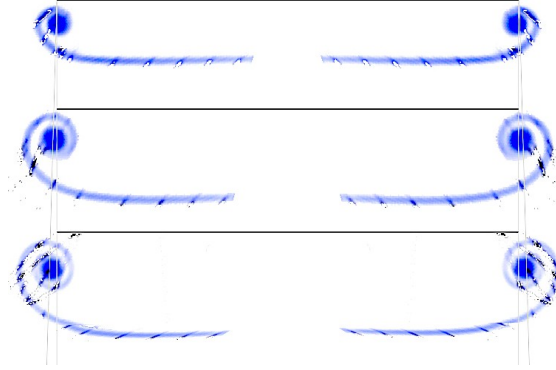

Fig. G.3 Successive downstream cross-sections of the wingtip vortices in an aircraft wake. The opposing spins of the twin vortices causes the wake to move slowly downward
(Source: https://en.wikipedia.org/wiki/Wingtip_vortices).

4) The vortices circulate in opposite rotations, causing the heated air mass as well as each other to move downward. The vortex motion causes mixing of gases, producing a range of values in the local index of refraction, which supports the image shift models of Appendix E.

5) As the wake evolves over time, it spreads slowly outwards, Fig. G.4. The visible plume at the highest altitudes consists of ice crystals that form out of the water vapour produced by combustion of the jet fuel. The non-uniform profile explains why the vortex pairs are not quite parallel and why they can move at slightly different speeds, as each vortex belongs to a different position along the wake.

6) From the Fig. G.4 curve-fit $y = 0.089x^{0.5}$, a formula to estimate the location x of a section of the wake behind the generating aircraft (in aircraft lengths) is based on the angle between the vortices θ_{wake} (in degrees) as seen in the wave layer. Equating this to the slope dy/dx from differential calculus:

$$\theta_{wake} = 2\,atan(dy/dx)$$
$$= 2\,atan(0.0445/x^{0.5}) \qquad\qquad [G.1]$$

and rearranging gives:
$$x = [0.0445/\tan(\theta_{wake}/2)]^2 \qquad\qquad [G.2]$$

which is closely approximated by $x = 26.00/(\theta_{wake})^2$ for small values of θ_{wake}. The results are plotted in Fig. G.5.

7) Noting that an aircraft at cruising speed travels about 2 to 3 times its own length per second, the time t_{pass} since the aircraft passed near the Moon can be estimated as:

$$t_{pass} = x/2 \qquad\qquad [G.3]$$

A maximum time of perhaps 150 seconds will elapse before the vortices lose their identity, hence Eqn [G.3] is valid for x up to about 300 aircraft lengths ($\theta_{wake} > 0.3$ degrees). Since the wake is spreading with time, the aircraft direction of travel is indicated towards where the extended lines of the two vortices (wavefronts) intersect.

8) In addition, if an aircraft is rolling into (or out of) a turn, the vortex trail will appear twisted to a ground-based observer. This would result in strongly differing wave travel directions.
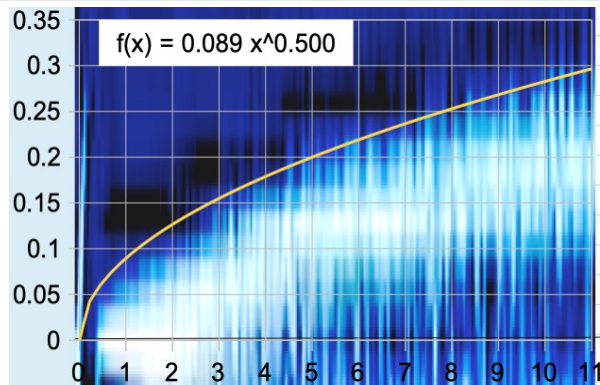

Fig. G.4 Curve-fit applied to the 20:1 stretched image of an aircraft engine exhaust plume seen from directly underneath. The scale units are aircraft lengths (Photo: Shutterstock/contrails).
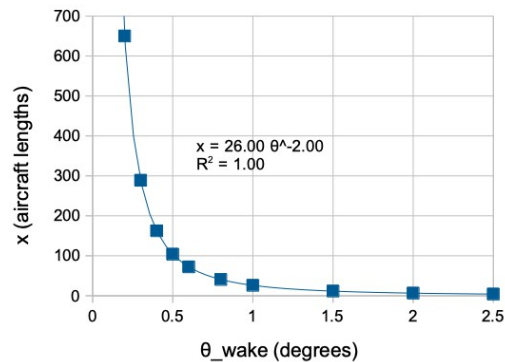

Fig. G.5 Predictions for the wake distance x (in aircraft lengths) behind the generating aircraft as a function of the local angle θ_{wake} (in degrees) between the twin wingtip vortices, Eqn [G.2].

Fig. G.6 Twin exhaust plumes behind a Boeing 757-200 aircraft with 4 wavefronts seen against the lunar background (Video: Brennan Clark, https://www.youtube.com/watch?v=dwkB8_gWpPM).

Fig. G.7 Twin exhaust plumes of an aircraft during takeoff seen shortly after sunset (Photo: https://www.faa.gov/air_traffic/by_the_numbers updated September 9, 2024).
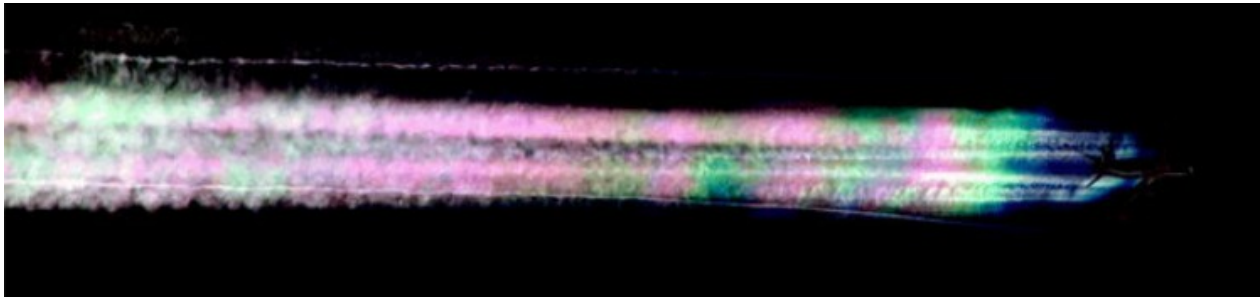
Fig. G.8 Enhanced daytime photograph of the wake of an Airbus A340 at a cruising altitude of 9600 m (31,500 ft) seen from another aircraft 1200 m (4000 ft) below it. The thread-like wingtip vortices are made visible by the iridescent sheet of micro-crystalline ice particles shed by the A340 wings (Photo: Jeff Well, https://journals.ametsoc.org/view/journals/atsc/66/2/i1520-0469-66-2-217-f01.jpg).

9) At lower altitudes where there is no condensate trail, Fig. G.1, the model predicts the vortices are made visible because of the different indices of refraction of the ambient air and the colder low pressure air inside the wingtip vortex. The drifting vortex causes an optical ripple effect similar to that of a lens moving across background objects (Appendix E).

10) In addition, the hot exhaust plume emerging from each engine has a different index of refraction from the ambient air. The edges of the exhaust plume may be observed to distort the background lunar image, causing up to 4 wavefronts to appear simultaneously behind a twin engined aircraft, Figs G.6 and G.7. This may be seen, for instance, in a Crrow777 video with a clip by Gustav in Germany (https://www.youtube.com/watch?v=0mi0w8bLtUM, video time code 07:25 to 07:32).

11) The vortices may not be detectable by some telescopes in the thinner air at the highest cruising altitudes, particularly for a weak and faded portion of the wake. The difference in density may be too small, resulting in very small differences in the index of refraction that cannot be resolved by the recording system at the distance of observation (Appendix E).

12) One notable exception to item 11) is shown in Fig. G.8 where, under specific weather conditions, the wingtip vortices of an Airbus A340 at cruising altitude are made visible by a sheet of micro-crystalline ice particles shed from the wings. There is a complex 3-dimensional rearranging of the wake in the first few aircraft lengths behind the wings.

13) The model predicts the separation between the pair of vortices during normal flight is essentially the aircraft wingspan (about 30-60 m or 100-200 ft for many commercial craft). The wavefronts are predicted to be parallel to the flight path, consistent with the orientation of the exhaust plumes.

14) Older aircraft without the energy-saving winglets, sharklets or fences on each wingtip will generate a stronger pair of vortices in their wake. Newer aircraft will exhibit weaker vortices, Fig. G.8.

Fig. G.9 Rear view of a Boeing 737 aircraft approaching landing with intense flap vortices (and no visible wingtip vortices) as seen under high humidity conditions
(Photo: https://www.boldmethod.com/learn-to-fly/weather/contrails/).

15) There are also intense vortices shed by the flaps extended from the wing trailing edge briefly during takeoff and for a few minutes on the approach to landing. These can exceed the strength of the wingtip vortices, Fig. G.9. The vortices usually fade into obscurity after about 1-3 minutes (https://skybrary.aero/articles/wake-vortex-propagation-and-decay).

16) The flap-span may be taken as 2/3 of the wingspan for most commercial aircraft (about 20-40 m or 65-130 ft).

17) From Fig. G.9, the known wingspan of the Boeing 737 is 34.3 m (113 ft) and the flap-span 20.3 m (67 ft). From this scale, the vortex core diameter is about 45 cm (18 inches).

Supersonic Objects

The model presented above assumes the waves are the twin vortex wake of a subsonic aircraft. It has been suggested that lunar waves are the pair of shockwaves generated from a supersonic object. From Schlieren photography of supersonic bullets, Fig. G.10, there are indeed two main shockwaves observed. The leading wave is generated by the nose of the bullet and the trailing wave is connected to the tail of the bullet.

There are two reasons this cannot be an explanation for the lunar wave phenomenon:

a) The rate of travel of the shock front (shockwave) is at the speed of sound, which in air at high altitudes is roughly 320 m/s (1050 ft/s). In the majority of available records of lunar waves, the pair of waves are separated by at least 3 seconds, meaning an associated supersonic object would have to have been at least 3000 feet long. However, the largest rocket launched so far is only about 400 feet tall and thus could only generate a pair of shockwaves about 0.4 seconds apart, at most.

b) The lunar waves are typically observed to take about 5 to 50 seconds to transit an angle-of-view equal to that observed for the lunar surface – about 0.47 degrees. If moving at the speed of sound, the waves would travel between 1 mile (1.6 km) and 10 miles (16 km) in that time. From trigonometry,

cot(0.47°) ≈120 and so the distance of such waves from the observer would be 120 to 1200 miles (190 to 1900 km). This greatly exceeds the thickness of the atmosphere (no more than about 62 miles or 100 km) and outside of an atmosphere, neither sound nor sonic shockwaves can exist.
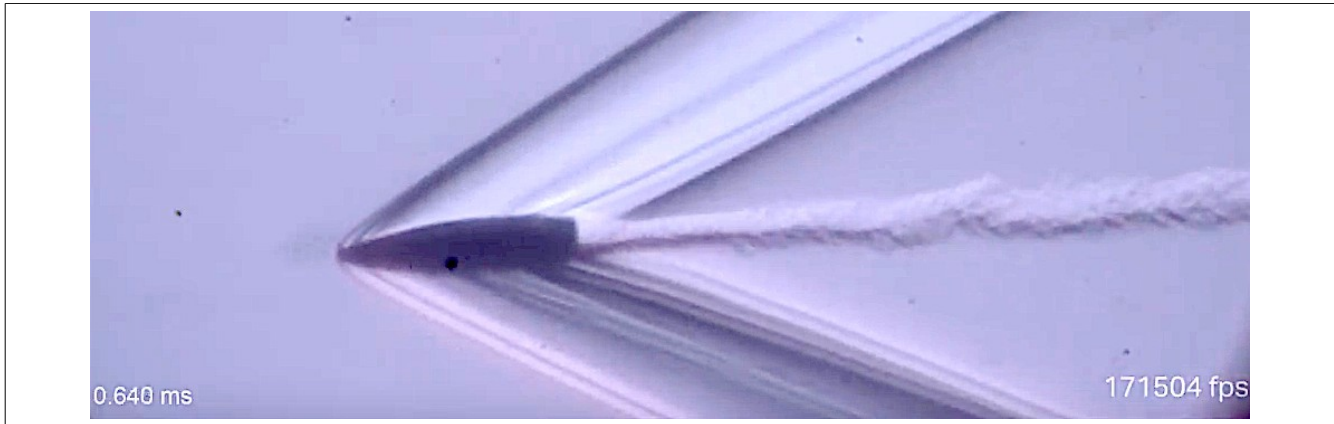

Fig. G.10 Still frame from high-speed Schlieren videography of a supersonic bullet. The Mach cone angle is 29 degrees, so the speed was Mach = 1/sin(29°) = 2.06 times the speed of sound (720 m/s, 2360 ft/sec) (video: Smarter Every Day, https://www.youtube.com/watch?v=BPwdlEgLn5Q, video time code 01:34).

APPENDIX H – Celestial Barkhausen Analysis

An alternative theory to explain the lunar wave phenomenon links their occurrence with the timing of celestial alignments, such as sunsets, sunrises, planetary conjunctions and eclipses.

It is well known to radio astronomers that a significant change is detected in the electrodynamics of the upper atmosphere shortly after sunset and again shortly before sunrise. As may be verified by the casual radio listener, the nighttime situation permits certain terrestrial radio broadcast frequencies to travel much farther than during daytime, bringing distant radio stations within range of the receiver. It is almost always under these nighttime conditions that the lunar wave phenomenon has been observed.

Furthermore, as early as the solar eclipse of June 30, 1954 the effect of an eclipse on the behaviour of a Foucault pendulum has been documented (https://en.wikipedia.org/wiki/Allais_effect). Normally, the freely swinging pendulum acts similarly to a gyroscopic inertial guidance system and thus precesses at a rate and in a direction determined by Earth's rotation and the latitude of the observation. However, the pendulum will precess at a different rate than normal during an eclipse, apparently due to an unexplained torque (or torsion) generated during the celestial event.

Accutron

An electronic version of this instrument is based on the Accutron timepiece first marketed by Bulova in 1960 (https://www.watchonista.com/articles/bulova-accutron-tuning-fork-revolution). The original design used a miniature tuning fork oscillating at 360 Hz as the time reference, Fig. H.1. Note that the tips of a tuning fork actually rotate back and forth over a very small angle relative to the base, hence are susceptible to the same unexplained torque (torsion) as the Foucault pendulum.

The Accutron was designed to be accurate to ±1 minute per month or to 1 part in 43,200 and so the maximum frequency deviation should be less than 0.00833 Hz. However, the frequency has been documented to deviate between 326 Hz (-34 Hz) and 856 Hz (+496 Hz) in a series of pulses coinciding with a nearby celestial alignment, Fig. H.2.

Similarly, during an alignment much farther away, Fig. H.3, the Accutron registered deviations as large as +4.5 Hz.

Such excursions have yet to be thoroughly explained, but they do indicate that a complex cosmic and/or quantum mechanics cause may exist for the lunar wave phenomenon.
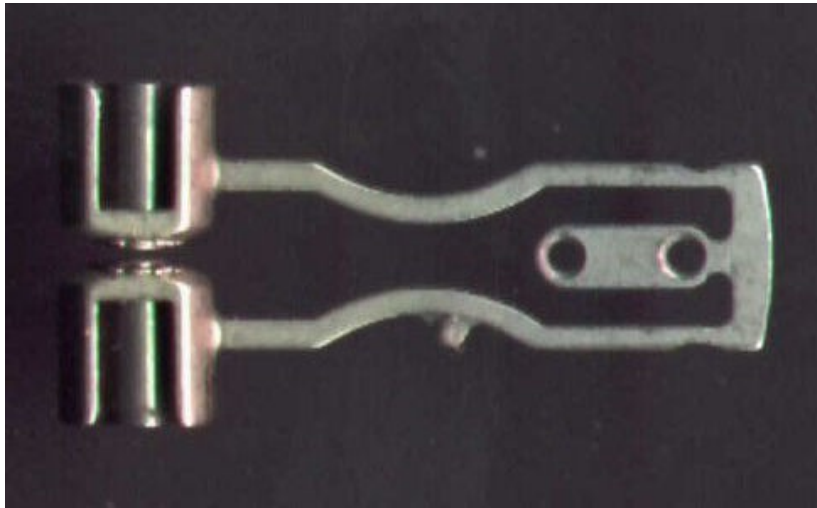

Fig. H.1 Accutron tuning fork with tip-mounted magnetic cores
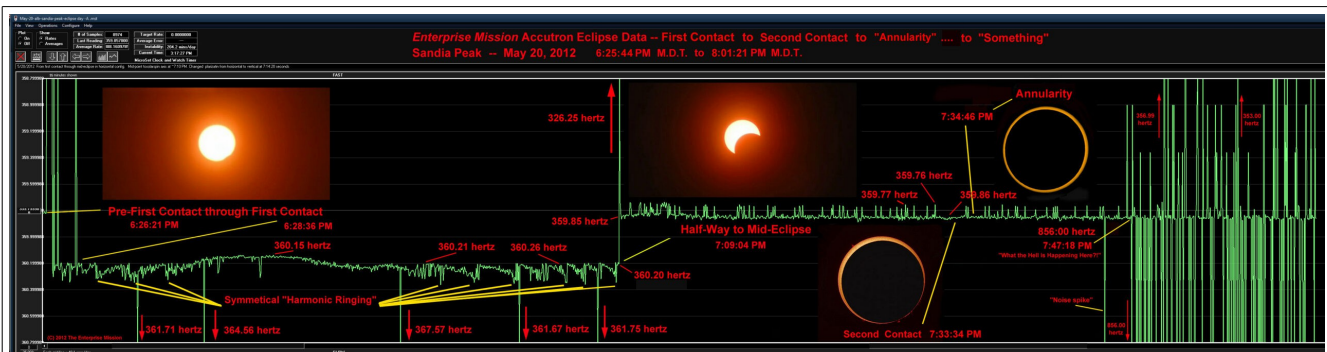(Source: EnterpriseMissions.org, "Accutron Tuning Fork.jpg").

Fig. H.2 Time trace of Accutron 360 Hz tuning fork frequency deviations compared with a conventional quartz oscillator during the 20 May 2012 solar eclipse
(Source: EnterpriseMissions.org, "Eclipse-Day-Sandia-Accutron-Data 2-FIRST-CONTACT-to-SECOND-CONTACT-to-Annularity-to-Something-dup-scaled.jpeg").
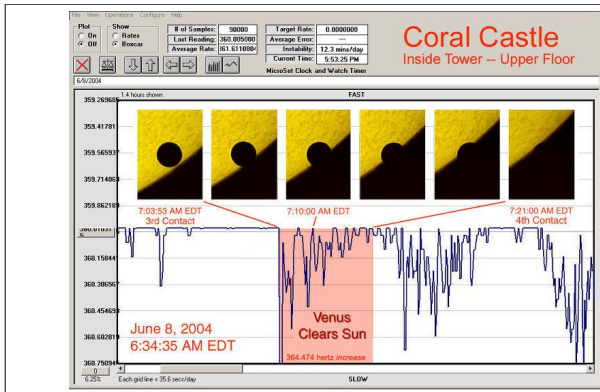
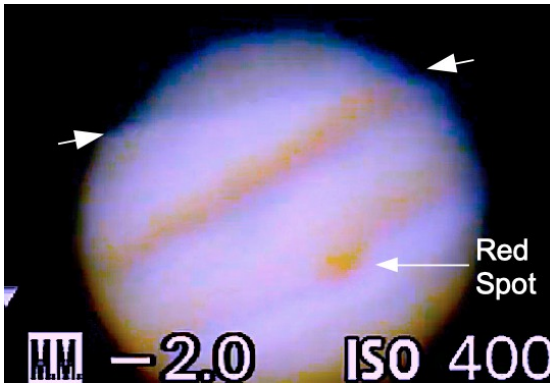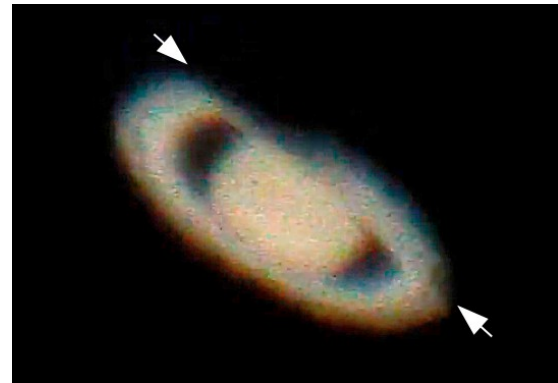|	
Fig. H.3 Time trace of Accutron 360 Hz tuning fork frequency deviations compared with a conventional quartz oscillator during the 8 June 2004 Venus transit (Source: EnterpriseMissions.org, "Accutron-Venus Third Contact.jpg").	Fig. H.4 Enhanced video frame from a live stream of the start of the Jupiter-Io transit 23 May 2018 at 20:47 EDT (00:47 UT) (Video: Take Back Space, https://www.youtube.com/watch?v=tenGuBoNVis, video time code 00:20 to 00:27).
Fig. H.5 Enhanced video frame from a live stream of 16 June 2020 at 00:49 EDT (04:47 UT) as the Red Spot rear edge passes the axis of Jupiter (Video: Take Back Space, https://www.youtube.com/watch?v=IzXroCOcmzg, video time code 38:35 to 38:41).	Fig. H.6 Enhanced video frame from a live stream of Saturn 2 September 2019 at 00:00:51 EDT (04:00 UT) with the ring outer edge aligned with the planet rim (Video: Take Back Space, https://www.youtube.com/watch?v=OxiJS4pYVG4, video time code 00:08 to 00:19).

In the astronomical observations of Figs H.4, H.5 and H.6, the passing refractive waves are indicated by arrows:

1) The double wave phenomenon crossing the face of Jupiter has coincided with first contact of the moon Io as it began a transit of Jupiter, Fig. H.4.
2) In a separate sighting, the waves occurred as the rear edge of the Red Spot passed the axis of Jupiter, Fig. H.5.
3) The waves have been observed at a time when the outer edge of the rings of Saturn aligned with the rim of the planet, Fig. H.6.

Since the waves in these examples do not align with the scan direction of the digital video recording, nor do they jump, fragment or display other digital artifacts, it is certain that they were not generated by the camera.

Barkhausen Effect

A tentative model begins with the Barkhausen effect (https://en.wikipedia.org/wiki/Barkhausen_effect), whereby a moon or large body moving through the magnetic field of a distant planet or the sun causes a sudden adjustment in the location of a magnetic line of force. A list of candidate events is in Table H.1

When the resulting Barkhausen pulse reaches Earth, it would possibly cause a plasma-related electrical event in the upper atmosphere. At present, it is assumed that the double wave phenomenon would be the immediate aftermath (persisting 2 or 3 minutes) of a complex process amplifying the original pulse. A plausible mechanism is outlined below.

Since the pulse would travel at light speed, such an event would happen very quickly in Earth-received time. The pulse direction would come straight from the planetary alignment and thus the lunar waves may be expected to emanate from where the pulse makes first contact with the nighttime atmosphere.

Plasma Events

Over the past 35 years, the list of known plasma phenomena in Earth's atmosphere has expanded, assisted by advances in video recording technology (https://en.wikipedia.org/wiki/Upper-atmospheric_lightning). With the launch of specialized satellites to detect such phenomena (https://ghrc.nsstc.nasa.gov/lightning/overview_ssle.html, https://en.wikipedia.org/wiki/Lightning), a better understanding of possible causes for the lunar waves may emerge in the near future.

Current data suggests a powerful upper atmospheric discharge, such as a columniform sprite (C-sprite, Fig. H.7) or blue jet (Fig. H.8), could generate the double waves. Sprites and jets are a form of very high altitude vertical lightning, reaching from about 10 km (33,000 feet) at the top of the troposphere to over 50 km (165,000 feet). These discharges are estimated to be at least an order of magnitude more powerful than regular lightning.

Fig. H.7 A red sprite as seen from the ISS (Source: https://en.wikipedia.org/wiki/Upper-atmospheric_lightning).	Fig. H.8 A blue jet as seen from Hawaii (Source: https://en.wikipedia.org/wiki/Upper-atmospheric_lightning).

The sudden heating of a vertical column of gas by the electrical discharge will cause that mass to rise rapidly, creating a ring vortex circling the base of the column (Fig. E.7, Appendix E). The effect is akin to the rising gas in the stem of a mushroom cloud, but with the base at an elevated location. Note that

high altitude lightning is strongly vertical, thus the circular ring will tend to lie in a horizontal plane.

If the ring is sufficiently large, perhaps hundreds of meters across, the circular edge will appear to be nearly straight to a ground-based observer as the vortex structure transits the Moon. If the Moon is relatively low on the horizon, the ring may also appear as an ellipse with nearly parallel sides, giving the illusion of parallel double waves.

A known condition for the occurrence of these plasma events is an impulse supplied by thunderstorm activity, although the storm may be hundreds of kilometers away from an observer. The present model assumes the Barkhausen pulse would be of planetary scale, hence possibly of sufficient power to trigger a suitable upper atmosphere event.

A Space Shuttle experiment of 25 February, 1996, (https://pwg.gsfc.nasa.gov/Education/wtether.html, https://en.wikipedia.org/wiki/STS-75) launched a tethered satellite downward from orbit to measure electrical energy at the top of the atmosphere. The results confirmed abundant energy was stored, generating enough current to cause melting of the 20 km-long tether. Thus, the present model does not require the nearby presence of a thunderstorm to energize the plasma event, only a sufficiently powerful pulse to trigger it.

Due to the thin air of the upper atmosphere and the relatively great distance from the observer, no thunder would be audible after such plasma discharges.

Testable predictions

The predictions of:
1) a precise planetary alignment
2) precise timing and
3) creation of a near-circular large ring vortex

may all be tested in the current context.

For item 3), an assumed altitude of $h = 10,000$ meters allows prediction of the ring diameter based on the angular spacing between the two waves α_{wsep}, Appendix A. From this, the elliptical appearance of the ring can be calculated from the known altitude angle φ of the Moon at the time of observation, Eqns [A.15] and [A.16]. Rearranging yields:

$$L = h/\sin\varphi \qquad \text{[H.1]}$$
$$d_{wsep} = L \tan(\alpha_{wstretch}) \qquad \text{[H.2]}$$

where $\alpha_{wstretch} = \alpha_{wsep}[\sin^2\theta_{wave}/\sin^2\varphi + \cos^2\theta_{wave}]^{1/2}$ is from Eqn [A.14] and $\theta_{wave} = \text{atan}[\sin\varphi \tan\theta_{wtel}]$ is from Eqn [A.8]. From Eqn [A.13], the scaled ring size α_{wsep} compared with the Moon size α is:

$$\alpha_{wsep} = \alpha(t_{1wsep}/t_{1Moon} + t_{2wsep}/t_{2Moon})/2 \qquad \text{[H.3]}$$

The ring is scaled to the apparent size of the Moon and superimposed on a stretched (elliptical) still frame from the video recording of the waves. A mismatch of the curvatures would mean the ring model is not a good explanation for that particular sighting.

Magnetically Active Bodies

A list of the most magnetically active bodies in the solar system and their largest moons, surface-spots and rings is presented in Table H.1 along with the frequency of potential conjunctions per year as seen from Earth. Even without grand celestial alignments such as sunrises, sunsets, moonrises, moonsets and eclipses, there are between ten thousand and twenty thousand occurrences per year.

Magnetic Parent	Moon or Dependant Body	Period of Alignments	Conjunctions per Year
Jupiter	Callisto	16.690 days	175
	Europa	3.5255 days	828
	Ganymede	7.1556 days	408
	Io	1.7627 days	1657
	Red Spot (main spot only)	9.93 hours	3529
Saturn	Dione	2.7 days	1007
	Enceladus	1.4 days	2086
	Iapetus	79 days	37
	Mimas	0.9 days	3244
	Rhea	4.5 days	649
	Tethys	1.9 days	1537
	Titan	16 days	183
	White Spot (sporadic)	10.66 hours (radio)	Up to 3290 if active
	Rings	29.4 years	0.068
Sun	Earth horizon	24 hours	730
	Earth (lunar eclipse)	241 per 100 years	9.65
	Moon (solar eclipse)	224 per 100 years	8.96
	Mercury (transit/eclipse)	13 per 100 years	1.04
	Venus (transit/eclipse)	4 per 243 years	0.132
	6 Outer planets (eclipse)	Up to 1 per year each	Up to 24
Earth horizon	Moon	24.74 hours	708
			TOTAL 20,111

Table H.1 Magnetically active bodies and their largest moons or dependent bodies, with frequency of possible alignments with Earth. Each time period counts for up to 8 conjunctions, namely the first contact and last contact as the rim of each moon or dependant body appears to move past the rim (or horizon) of the magnetic parent as seen in both forward and reverse directions. Even more occurrences may be possible when an edge aligns with the magnetic parent axis (eg., 20 May 2012 eclipse at 7:09pm MDT (01:09 UT) Fig. H.2; Red Spot crossing Jupiter's axis Fig. H.5).
(Data: https://en.wikipedia.org/wiki/Moons_of_Jupiter, https://en.wikipedia.org/wiki/Moons_of_Saturn, https://en.wikipedia.org/wiki/Transit_of_Mercury, https://en.wikipedia.org/wiki/Transit_of_Venus, https://www.britannica.com/science/eclipse/The-frequency-of-solar-and-lunar-eclipses, https://eclipse.gsfc.nasa.gov/LEsaros/LEperiodicity.html).

The large number of possible occurrences translates into at least a dozen events per 12-hour night of observation by terrestrial astronomers or at least one per hour on average. If the conditions of precise alignment and adequate triggering power are fulfilled by only a few percent of occurrences, there are still potentially hundreds of celestially triggered lunar wave events per year. If these events are relatively localized, this would help explain why they are so rarely observed and recorded (an average of 3 per year since 2012, mostly in the United States).

As a final note, while the Barkhausen effect is detected electromagnetically, there may be a scalar aspect, thus linking the model to aetheric or hyper-dimensional (HD) torsion-field physics and the Accutron measurements.